Structure-function Studies of Fibroblast Growth Factors (FGFs)

Thesis by

Xiaotian Zhu

Partial Fulfillment of the Requirements

for the Degree of

Doctor of Philosophy

California Institute of Technology

Pasadena, California

1993

(submitted February 16, 1993)

Dedicated to my family

Acknowledgments

I would like to thank my advisor Professor Doug Rees for his support, encouragement and invaluable guidance during my stay in graduate school. In addition to showing me the beauty of macromolecular crystallography, Doug has been fully involved in my research project and has always been of great help whenever I encountered difficulties. Also, my research project has been carried along with his encouragement and understanding. By working closely with him in the past few years, I have been constantly inspired by his enthusiastic attitude towards science as well as his correct but simple ways of attacking scientific problems.

I am deeply indebted to Barbara Hsu who has been giving me enormous help since I joined this research group. With her breadth of scientific knowledge, she has helped me in each stage of my research. I also cherish the friendship that has developed between us in all these years.

I also owe many thanks to Art Chirino. Art not only has taught me the basic crystallographic theories and experimental manipulations when I first came to the field of crystallography, but has helped me all the way along. His patience and contributions are greatly appreciated.

Thanks also go to Salem Faham for his participation and contribution to this project. I would also like to thank Hiromi Komiya, Millie Georgiadis, Debbie Woo, Michael Stowell, Mike Day and Larry Henleig as well as other members of Rees' group for their help.

Special thanks go to Kam Zhang for his help with the CCP4 programs and many stimulating discussions.

I am grateful to Drs. T. Arakawa and G. M. Fox of Amgen who have provided us with large amounts of protein samples for the structural studies of FGFs.

I would like to thank Professors Sunney Chan and Pamela Bjorkman for their help and advice.

Finally, thanks to my parents and my sister for their love and encouragement. I wish to thank my wife, Hongying Xie for her companionship, understanding and great support during these years. Many discussions with her about my research have been truly stimulating.

Abstract

The fibroblast growth factor (FGF) family exhibits mitogenic, chemotactic and angiogenic activity in a variety of cell types. The first three-dimensional structures of two members of the FGF family, bovine acidic FGF (aFGF) and human basic FGF (bFGF), have been crystallographically determined by multiple isomorphous replacement (MIR), and refined to 2.7 Å and 1.9 Å respectively. The structures of both aFGF and bFGF consist of twelve antiparallel β strands which are arranged in a folding pattern with approximate three-fold internal symmetry. A striking feature of the FGF structures is the overall similarity to the structures of soybean trypsin inhibitor and interleukins-1α and 1β, in spite of the low sequence homology between these proteins.

FGF stimulates cellular proliferation and differentiation through the interactions with both the cell surface FGF receptor and heparin. In the FGF structures, the two putative receptor binding sites are located on different sides of FGF. Also, a region rich in positively charged amino acids that is likely involved in heparin binding has been found in the FGF structures. It is further shown that the putative heparin and receptor binding regions occupy distinct locations on the protein surface.

Because heparin is required for FGF binding to its receptor, the interactions between FGF and sucrose octasulfate, a heparin analog, have been studied. The crystal structure of the complex between aFGF and sucrose octasulfate has been determined to 2.7 Å resolution by a combination of MIR and molecular replacement methods. Sucrose octasulfate binds to the aFGF positive patch mentioned above as a potential heparin binding site. Based on the structure of aFGF and sucrose octasulfate

complex, a possible FGF receptor binding mechanism in the presence of heparin is proposed.

Other crystallographic studies of FGF include the structural determination of the two FGF mutants; the complex of aFGF and 1,3,6-naphthalene trisulfonate, a close analog of the FGF inhibitor suramin; and the bFGF-copper complex.

Contents

LIST OF FIGURES

CHAPTER 4.

CHAPTER 5.

LIST OF TABLES

Chapter 1

General Introduction to Fibroblast Growth Factors (FGFs)

Growth is a fundamental process in all living organisms. It is not only associated with the early stages of development, but remains a general feature in many tissues. It has long been known that cell proliferation and differentiation are strictly modulated by hormones. Hormones can be amino acid derivatives, or cholesterol based steroid, or polypeptide growth factors (1). The knowledge about polypeptide growth factors is relatively scarce compared to that of other hormones due to the difficulty of protein purification. But with the rapid development of protein purification and molecular biology techniques, more and more polypeptide growth factors have been recognized, isolated and cloned and their biological functions have been further investigated (2). The knowledge of how these polypeptide growth factors are triggered and interact with their target cells is critical for understanding the origin, development and maintenance of life.

Fibroblast growth factors (FGFs), belong to the polypeptide growth factor family that can stimulate and regulate cellular growth and development. Although it was originally purified from fibroblast cells (3, 4), FGF has been revealed to be mitogenic, chemotactic and angiogenic to a wide spectrum of cells (5, 6, 7). In addition, FGF is also an important neurotropic effector which can influence the proliferation and differentiation of neuroectoderm derived cells (7). The FGF family contains at least seven homologous proteins. This includes the two original members: acidic and basic FGF (8, 9), the four oncogene products: int-2/KS3/K-fgf, hst, FGF5, FGF6 (10-16) and keratinocyte growth factor (17). As a consequence of their strong affinity for heparin, FGF is also often referred to as heparin-binding growth factor (HBGF). The FGF family members have quite high sequence homology and similar biological activities (Figure 1.1). For instance, the two original members of the FGF family, aFGF and bFGF, share 55% sequence identity over the 140 amino acid length and have been shown to display similar activities to most cell types (18). On the other hand, functional differences between these growth factors definitely exist. For

example, while normal members of the FGF family lack the leader signal peptides in their sequences, all the proto-oncogene FGF products possess a hydrophobic peptide sequence at their amino terminus. Another example supporting the unique roles of each FGF family member is that KGF has been demonstrated to be much more potent than acidic and basic FGF in stimulating the growth of epithelial cells (19) and further, bFGF appears to lack binding affinity for KGF receptors (20).

The mitogenic response initiated by FGF is, in common with most peptide growth factors, mediated through cellular FGF receptors (7). Kinetic studies indicate there are two types of receptors on the cell surface which participate in FGF binding. One is a high affinity receptor (Kd = 10^{-11} M) (21-23) and the other one is a low affinity receptor (Kd = 10^{-9} M) (24, 25). Both aFGF and bFGF have been cross-linked to one high affinity FGF receptor which has an approximate molecular weight of 130 kD (26). At present, at least four high affinity FGF receptors have been identified and cloned, each encoding a receptor that responds to one or more of the FGFs (27). The first FGF receptor, FGFR1, was purified from chicken embryos and the corresponding gene was identified as the chicken *cek1* gene and human *flg* gene. The derived amino acid sequence from the isolated gene reveals that the FGF receptor belongs to the class of membrane tyrosine kinase (28). It consists of two or three extracellular immunoglobulin-like domains, one transmembrane helix and one intracellular tyrosine kinase domain. FGFR1 has been shown to have equal binding affinity for aFGF and bFGF but with about 10 times lower affinity for KGF (29, 30). The second member of the FGF receptor family, FGFR2, is homologous to FGFR1. Being encoded by the related genes *bek, ck3, K-sam* and TK14 (29, 31-33), FGFR2 binds aFGF and bFGF equally well but has little binding affinity for FGF-5 (29). With the structural similarity in the primary sequence with FGFR1 and FGFR2, FGFR3 responds to both aFGF and bFGF (34). Recently FGFR4 has been identified (35) and it exhibits the highest affinity for aFGF followed by K-fgf and bFGF (36). In

addition, the FGF receptor is complicated by the fact that each FGF receptor gene may give rise to three or more different forms as a result of alternative mRNA splicing (37). Therefore, FGF receptors with either two or three extracellular immunoglobulin-like domains and different lengths of the intracellular tyrosine kinase domains have been observed (37)

After binding of FGF to the tyrosine kinase receptor, the high affinity receptors are dimerized and subsequently the intracellular tyrosine kinase activity is switched on via an autophosphorylation mechanism (38, 39). Although the signal from FGF is known to be ultimately transduced into the nucleus to induce DNA synthesis, the detailed signal pathway remains unclear. A cascade of phosphorylation could be involved because it is reported that incubation of FGF with 3T3 cells results in phosphorylation of a series of proteins (40). Recently, phospholipase C-γ (PLC-γ) has been suggested to be a major substrate of FGFR1 (41). Furthermore, calcium concentration also appears to be connected with the level of expression of FGF receptors (42).

In addition to the high affinity receptors, low affinity FGF binding sites have been characterized and shown to be heparin or heparin-like proteoglycans which are located on the cell surface or in the extracellular matrix (43-46). Binding of FGF to heparin not only provides a convenient way for the protein purification but also stabilizes and potentiates FGF activities (47). Recent studies have further demonstrated that binding of FGF to the receptor absolutely requires the presence of heparin-like molecules (48-50). Neither aFGF nor bFGF can bind high affinity FGF receptor in heparin or heparan sulfate deficient cells, while the mutant phenotype has been shown to be inverted if heparin is added. Furthermore, heparin is suggested to be possibly directly attached to the FGF receptor by the identification of a proteoglycan which has been shown to be the high affinity FGF receptor (51). Treatment of this proteoglycan with heparinase resulted in a receptor with lower molecular weight and

less binding affinity for FGF (51).

To identify the specific functional domains on FGF that may bind the FGF receptor and heparin, a series of peptides derived from the bFGF sequence were synthesized (52). These bFGF derived peptides were tested for their abilities to inhibit bFGF binding to the receptor as well as their binding affinity for heparin. Peptides related to the sequences of FGF-(21-41) and bFGF-(107-116) were demonstrated to compete for bFGF binding to the receptor. In addition, these two peptides were also shown to inhibit thymidine incorporation into 3T3 fibroblasts when stimulated by bFGF, which further suggests the importance of these regions in receptor binding. In fact, more evidence supports the idea that the region of bFGF-(107-116) is very likely to be directly involved in interacting with the FGF receptor. For example, Thr 113 of bFGF, which is located in this region can be phosphorylated by protein kinase A, and the phosphorylated bFGF displays an enhanced binding affinity for the FGF receptor (53). Additionally, although the members of the FGF family are highly homologous, a high frequency of sequence insertions or deletions have been observed in the region of bFGF-(107-116) (Figure 1.1). For example, between bFGF amino acids 112 and 115, aFGF and KGF have two and four more residues than bFGF. Because various FGFs exhibit different binding affinities for the FGF receptors, it is likely that receptor binding specificity is related to these insertions and deletions.

Since heparin plays a necessary role in FGF binding to its receptor (48-50), understanding the interactions between FGF and heparin is also critical for understanding the receptor binding mechanism by FGF. Chemical modification and thrombin digestion (54-56) studies have implicated that lysine 118 and Arg 122 of aFGF may be involved in heparin binding. Further, bFGF related peptides from this region containing the residues after 94 have been shown to bind heparin (52). A similar result supporting the importance of the carboxyl terminal region in heparin binding was obtained by using a series of genetically truncated bFGF (57). In

addition, the primary sequence of FGF reveals that there is a region in the C-terminus rich in positively charged amino acids. There are five lysines and arginines clustered around lysine 126 in bFGF whereas there are seven lysines and arginines in aFGF. It is very likely that these positively charged residues may play an important role in heparin binding.

In addition to facilitating FGF binding to the tyrosine kinase receptor, heparin as well as other polyanions reveal the ability to protect FGF from thermal, acidic and proteolytic degradations (58, 59). FGF has been found to be surprisingly unstable at physiological temperatures but appears to be more stable *in vivo*, probably because of complexation to polyanionic molecules such as heparin or heparin-like molecules (60). The stabilization effect of polyanions on FGF has further been shown by the observation that aFGF appears to require lower energy for refolding in the presence of polyanionic molecules such as heparin, inositol hexasulfate and ATP (61). Heparin is primarily present on the cell surface and in the extracellular matrix (ECM). Indeed, endogenous bFGF has been found associated with heparin and heparin-like molecule such as heparan sulfate in the ECM (62-64), and addition of heparinase to ECM results in the release of FGF from ECM (65). Furthermore, the ECM has been implicated as a source of FGF for long-term stimulation of DNA synthesis for a variety of cells (66). These findings suggest that the ECM may serve as a reservoir of stored FGF. Because aFGF and bFGF are not secreted due to the lack of signal peptide sequences, the storage and release of FGFs from the ECM may be an important regulatory mechanism of FGF activity.

Based on these observations, various mechanisms have been proposed to explain the partition of heparin or heparin-like molecules in regulating FGF activities. These include that 1) heparin may function to stabilize the tertiary structure of FGF; 2) binding of heparin may trigger a conformational change in FGF so that FGF can bind the FGF receptor with high affinity; 3) binding of FGF to heparin may facilitate FGF

oligomerization which is necessary for FGF receptor dimerization. In fact, evidence has been observed for all these possible models. While it has been discussed that FGF can be stabilized by heparin as described above, the binding of heparin to bFGF but not aFGF has been reported to induce a small but highly reproducible conformational change as observed in the amide I region of the protein's infrared spectrum (67, 68). Furthermore, FGF dimerization has also been demonstrated recently by a cross-linking experiment with the presence of heparin (69). For further examination of these possibilities, a three-dimensional structure of FGF complexed with heparin is really necessary.

After binding of FGF to the receptor, FGF is internalized by receptor-mediated endocytosis (43, 70). The detection of translocation of intact FGF into the cell nucleus led to the discovery that the amino terminus of FGF is a nuclear translocation sequence (71). A truncated form of FGF without the N-terminus fails to stimulate DNA synthesis and cell proliferation, though tyrosine kinase activity is observed to be induced after FGF binding to the receptor. It was further shown that when the FGF N-terminus is replaced with another nuclear translocation sequence such as that of yeast histone 2B, the chimeric FGF exhibits a comparable activity to the native protein (71). After nuclear translocation, FGF is involved in the transcriptional regulation of at least two genes (72). Although the detailed interaction of FGF with the genes awaits further investigation, this is the first time that a peptide growth factor has been reported to be directly involved in the gene-specific transcription.

To better understand the signal process triggered by FGF, crystallographic studies of FGF have been carried out by us since 1989. A three-dimensional structure of FGF can provide not only a structural understanding of the receptor binding mechanism by FGF and other similar peptide growth factors, but also can provide a solid basis for the rational designs of drugs to either promote or inhibit FGF activities. It has been demonstrated that the oncogenes int-2, hst, FGF-5 and FGF-6 are expressed in many

transformed cells such as those of lung cancer and breast cancer (73) and the significance of the FGF family for malignant transformation is further indicated by the finding that, after genes from the *ras* family, the *hst* gene is the most frequently encountered oncogene in transfection assays (16). More efficient anti-tumor strategies should possibly be devised based on the active site structure of FGF. On the other hand, FGF is a potential drug for tissue repair of burnt skin and stomach or duodenal ulcers (74). If FGF is used as a tissue growth promoting therapy, the stability of FGF inside cells is a crucial factor. Without disrupting FGF activities, this can be achieved either by changing FGF *per se* such as proper site-directed mutagenesis or by designing accessory molecules that can stabilize FGF by protecting it from acidic and enzymatic degradation. All those approaches rely heavily on an accurate three-dimensional structure of FGF. Furthermore, recent studies have revealed that bFGF can prevent the death of lesioned cholinergic neurons (75), and Alzheimer's disease is connected with an increased level of expression and abnormal distribution of bFGF in brains (76). We anticipate our structural and functional studies of FGF will also help to find either novel or improved therapies aginst the FGF related diseases.

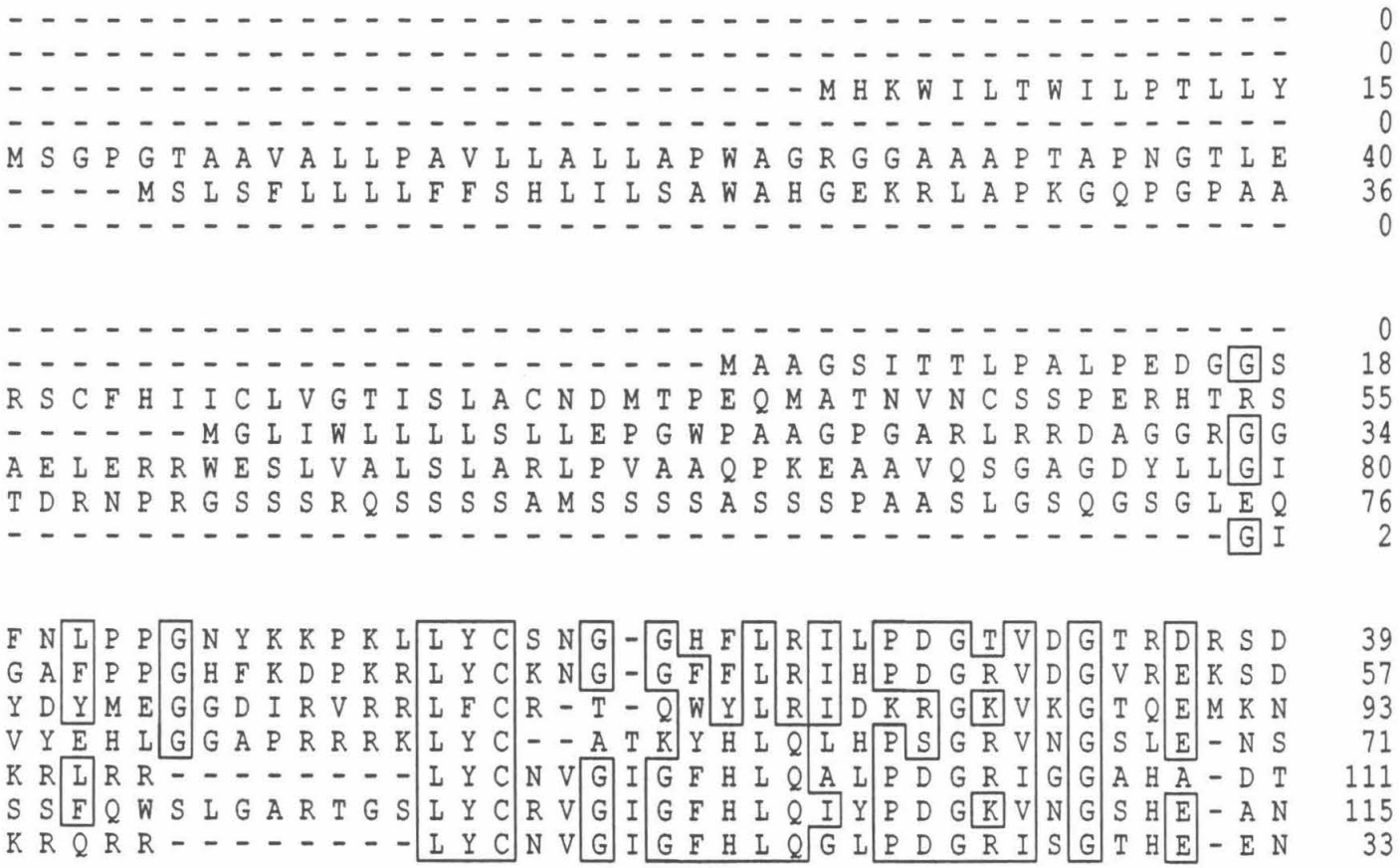

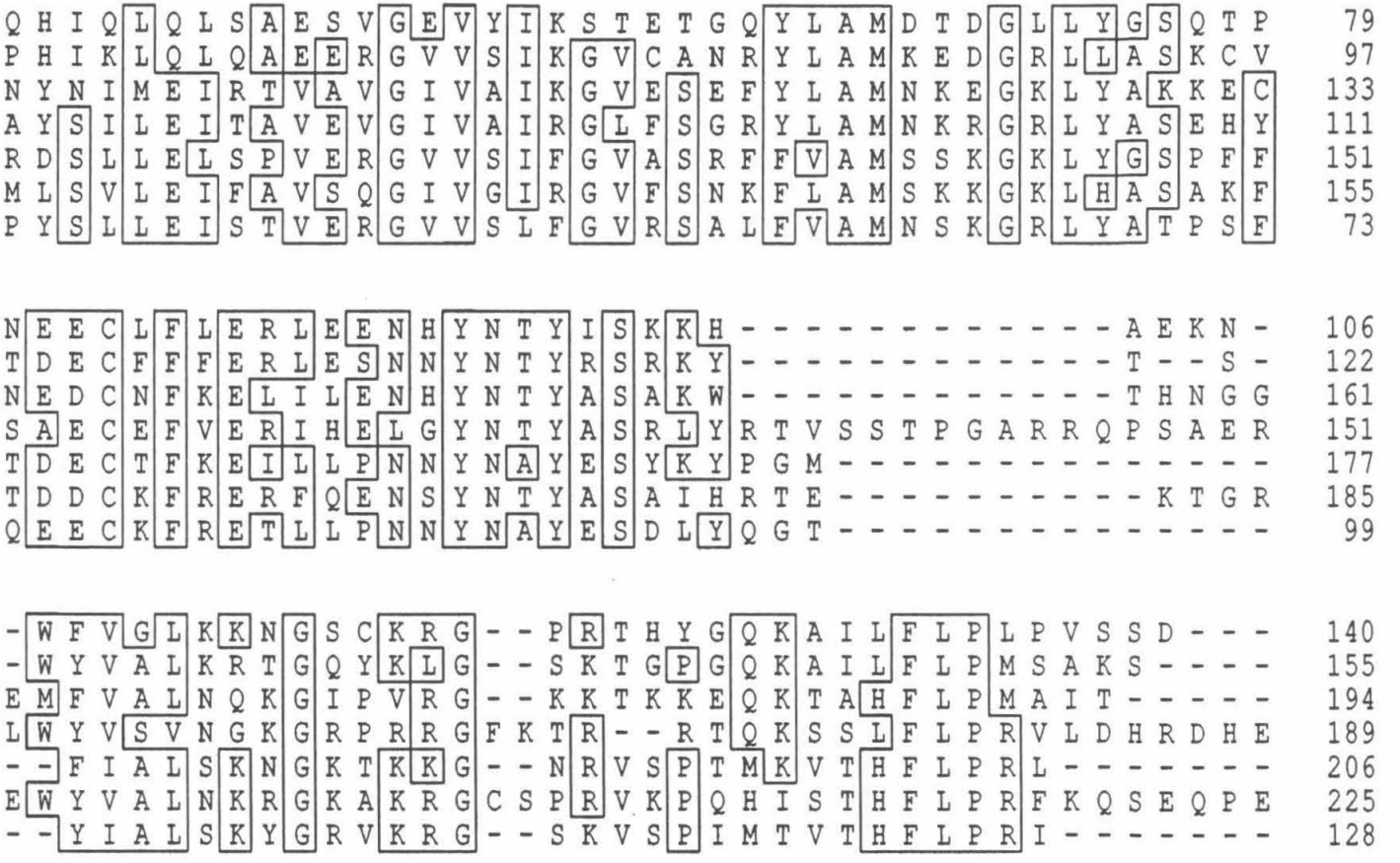

```
- - - - - - - - - - - - - - - - - - - - - - - - - - - - - - - - - - - - - - - -   140
- - - - - - - - - - - - - - - - - - - - - - - - - - - - - - - - - - - - - - - -   155
- - - - - - - - - - - - - - - - - - - - - - - - - - - - - - - - - - - - - - - -   194
M V R Q L Q S G L P R P P G K G V Q P R R R R Q K Q S P D N L E P S H V Q A S R   229
- - - - - - - - - - - - - - - - - - - - - - - - - - - - - - - - - - - - - - - -   206
L S F T V T V P E K K N P P S P I K S K I P L S A P R K N T N S V K Y R L K F R   265
- - - - - - - - - - - - - - - - - - - - - - - - - - - - - - - - - - - - - - - -   128

- - - - - - - - - -                                                               140
- - - - - - - - - -                                                               155
- - - - - - - - - -                                                               194
L G S Q L E A S A H                                                               239
- - - - - - - - - -                                                               206
F G - - - - - - - -                                                               267
- - - - - - - - - -                                                               128
```

Figure 1.1. Sequence alignment of human FGFs. (1): aFGF; (2): bFGF; (3): KGF; (4): int-2; (5): hst; (6): FGF-5 and (7): FGF-6.

References

1. L. Stryer, *Biochemistry* (W. H. Freeman and Company, New York, 1988), pp. 975.

2. K. Arai, M. B. Sporn, A. B. Roters, J. F. Battey, *Peptide Growth Factors and Their Receptors* (Springer-Verlag, New York, 1991).

3. D. Gospodarowicz, *J. Biol. Chem.* **250,** 2515 (1975).

4. D. Gospodarowicz, H. Bialecki, G. Greenberg, *J. Biol. Chem.* **253,** 3736 (1978).

5. J. Folkman and M. Klagsbrun, *Science* **235,** 442 (1987).

6. D. Gospodarowicz, N. Ferra, L. Schweigerer, G. Neufeld, *Endocrinol. Rev.* **8,** 95 (1987).

7. W. H. Burgess and T. Maciag, *Annu. Rev. Biochem.* **58,** 575 (1989).

8. G. Gimenez-Gallego, J. Rodkey, C. Bennett, M. Rios-Candelore, J. Disalvo, K. Thomas, *Science* **230,** 1385 (1985).

9. J. A. Abraham *et al., Science* **233,** 545 (1986).

10. R. Moore, G. Casey, S. Brookes, M. Dixon, G. Peters, C. Dickson, *EMBO J.* **5,** 919 (1986).

11. C. Dickson and G. Peters, *Nature* **326,** 833 (1987).

12. R. Smith, G. Peters, C. Dickson, *EMBO J.* **7,** 1013 (1988).

13. D. G. Wilkinson, G. Peters, C. Dickson, A. P. McMahon, *EMBO J.* **7,** 691 (1988).

14. M. Taira, T. Yoshida, K. Miyagawa, H. Sakamoto, M. Terada, T. Sugimura, *Proc. Natl. Acad. Sci. USA* **84,** 2980 (1987).

15. X. Zhan, B. Bates, X. Hu, M. Golfarb, *Mol. Cell. Biol.* **6,** 3541 (1986).

16. I. Marics *et al., Oncogene* **4,** 335 (1989).

17. P. W. Finch, J. S. Rubin, T. Miki, D. Ron, S. A. Aaronson, *Science* **245,** 752 (1989).

18. R. R. Lobb, *Eur. J. Clin. Invest.* **18,** 321 (1988).

19. S. Werner, K. G. Petters, M. T. Longaker, F. Fuller-Pace, M J. Banda, L. T. Williams, *Proc. Natl. Acad. Sci. USA* **89,** 6896 (1992).

20. D. P. Bottaro, J. S. Rubin, D. Ron, P. W. Finch, C. Florio, S. A. Aaronson, *J. Biol. Chem.* **266,** 12767 (1990).

21. T. A. Libermann *et al.*, *EMBO J.* **6,** 1627 (1987).

22. M. Moenner, J. Badet, B. Chevallier, M. Tardieu, J. Courty, D. Barritault, *Current Communications in Molecular Biology,* pp. 52-57.

23. M. Kan, D. DiSorbo, J. Hou, H. Hoshi, P. E. Mansson, W. L. McKeehan, *J. Biol. Chem.* **263,** 11306 (1988).

24. J. Moscatelli, *J. Cell. Physiol.* **131,** 123 (1987).

25. M. C. Kiefer, J. C. Stephans, K. Crawford, K. Okino, P. J. Barr, *Proc. Natl. Acad. Sci. USA* **87**, 6985 (1990).

26. G. Neufeld and D. Gospodarowicz, *J. Biol. Chem.* **261,** 5631, 1986.

27. A. Yayon, Y. Zimmer, G. H. Shen, A. Avivi, Y. Yarden, D. Givol, *EMBO J.* **11,** 1885 (1992).

28. P. L. Lee, D. E. Johnson, L. S. Cousens, V. A. Fried, L. T. Williams, *Science* **245,** 57 (1989).

29. C. A. Dionne, G. Crumley, F. Bellot, J. M. Kaplow, G. Searfoss, M. Ruta, W. H. Burgess, M. Jaye, J. Schlessinger, *EMBO J.* **9,** 2685 (1990).

30. A. Manshukani, P. Dell'Era, D. Moscatelli, S. Kornbluth, H. Hanafusa, C. Bailico, *Proc. Natl. Acad. Sci. USA* **89,** 3305 (1992).

31. E. B. Pasquale, *Proc. Natl. Acad. Sci. USA* **87,** 5812 (1990).

32. S. Kornbluth, K. E. Paulson, H. Hanafusa, *Mol. Cell. Biol.* **8,** 5541 (1988).

33. E. Houssaint, P. R. Blanquet, P. Champion-Arnaud, M. C. Gesnel, A. Torriglia, Y. Courtois, R. Breathnach, *Proc. Natl. Acad. Sci. USA* **87,** 8180 (1990).

34. K. Keegan, D. E. Johnson, L. T. Williams, M. J. Hayman, *Proc. Natl. Acad. Sci. USA* **88,** 1095 (1991).

35. J. Paranen, T. P. Makela, E. Eerola, J. Korhonen, H. Hirvonen, L. Claesson-Welsh, K. Alitalo, *EMBO J.* **10,** 1347 (1991).

36. S. Vainikka, J. Partanen, P. Bellosta, F. Coulier, C. Basilico, M. Jaye, K. Alitalo, *EMBO J.* **11,** 4273 (1992).

37. J. Hou, M. Kan, K. McKeehan, G. McBride, P. Adams, W. L. McKeehan, *Science* **251,** 665 (1991).

38. E. Amaya, T. J. Musci, M. W. Kirschner, *Cell* **66,** 257 (1991).

39. H. Ueno, M. Gunn, K. Dell, A. Tseng, L. T. Williams, *J. Biol. Chem.* **267,** 1470 (1992).

40. S. R. Coughlin, P. J. Barr, L. S. Cousens, L. J. Fretto, L. T. Williams, *J. Biol. Chem.* **263,** 988 (1988).

41. W. H. Burgess, C. A. Dionne, J. Kaplow, R. Mudd, R. Friesel, A. Zilberstein, J. Schlessinger, M. Jaye, *Mol. Cell. Biol.* **10,** 4770 (1990).

42. K. Sakaguchi, *J. Biol. Chem.* **267,** 24554 (1992).

43. D. Moscatelli, *J. Cell Biol.* **107,** 753 (1988).

44. I. Vlodavsky *et al.*, *Proc. Natl. Acad. Sci. USA* **84,** 2292 (1987).

45. M. C. Kiefer, J. C. Stephans, K. Crawford, K Okino, P. J. Barr, *Proc. Natl. Acad. Sci. USA* **87,** 6985 (1990).

46. M. Kan, D. Disorbo, J. Hou, H. Hoshi, P. E. Mansson, W. L. Mckeehan *J. Biol. Chem.* **263,** 11306 (1988).

47. S. C. Thornton, S. N. Mueller, E. M. Levine, *Science* **222,** 623 (1983).

48. A. Yayon, M. Klagsbrun, J. D. Esko, P. Leder, D. M. Ornitz, *Cell* **64,** 841 (1991).

49. K. Sakaguchi *et al.*, *J. Biol. Chem.* **266,** 7270 (1991).

50. A. C. Rapraeger, A. Krufka, B. B. Olwin, *Science* **252,** 1705 (1991).

51. K. Sakaguchi, M. Yanagishita, Y. Takeuchi, G. D. Aurbach, *J. Biol. Chem.* **266,** 7270 (1991).

52. A. Baird, D. Schubert, N. Ling, R. Guillemin, *Proc. Natl. Acad. Sci. USA* **85,** 2324 (1988).

53. J-T. Feige and A. Baird, *Proc. Natl. Acad. Sci. USA* **85,** 3174 (1989).

54. J. W. Harper and R. R. Lobb, *Biochemistry* **27,** 671 (1988).

55. R. R. Lobb, *Biochemistry* **27,** 2572 (1988).

56. W. H. Burgess, A. M. Shaheen, M. Ravera, M. Jaye, P. J. Donohue, U. A. Winkes, *J. Cell Biol.* **111,** 2129 (1990).

57. M. Seno, R. Sasado, T. Kurokawa, K. Igarashi, *Eur. J. Biochem.* **188,** 239 (1990).

58. D. Gospodarowicz and J. Chen, *J. Cell Physiol.* **128,** 475 (1886).

59. O. Saksela, D. Moscatelli, A. Sommer, D. B. Rifkin, *J Cell Biol.* **107,** 743 (1988).

60. M. Klagsbrun, *Curr. Opinion Cell Biol.* **2,** 857 (1990).

61. J. M. Dabora, G. Sanya, C. R. Middaugh, *J. Biol. Chem.* **266,** 23637 (1991).

62. I. Vlodavsky, J. Flokman, R. Sullivan, R. Fridman, R. Ishaimichaili, J. Sasse, M. Klagsbrun, *Proc. Natl. Acad. Sci. USA* **84,** 2292 (1987).

63. J. Folkman, M. Klagsbrun, J. Sasse, M. Waszinski, D. Ingber, I. Vlodavsky, *Am. J. Pathol.* **130,** 393 (1988).

64. A.-M. Gonzalez, M. Buscaglia, M. Ong, A. Baird, *J. Cell Biol.* **110,** 753 (1990).

65. R. Ishai-Michaeli, A. Eldor, I. Vlodavsky, *Cell Regu.* **1,** 833 (1990).

66. S. Rogelj, M. Klagsbrun, R. Atzmon, M. Kurokawa, A. Haimovitz, Z. Fuks, I. Vlodavsky, *J. Cell. Biol.* **109,** 823 (1989).

67. S. J. Prestrlsi, G. M. Fox, T. Arakawa, *Arch. Biochem. Biophys.* **293,** 314 (1992).

68. R. A. Copeland *et al., Arch. Biochem. Biophys.* **289,** 53 (1991).

69. D. M. Ornitz, A. Yayon, J. G. Flanagan, C. M. Svahn, E. Levi, P. Leder, *Mol.& Cell. Biol.* **12,** 240 (1992).

70. R. Frisel and T. Maciag, *Biochem. Biophys. Res. Comm.* **151,** 957 (1988).

71. T. Imamura *et al., Science* **249,** 1567 (1990).

72. Y. Nakanishi, K. Kihara, K. Mizuno, Y. Masamune, Y. Yoshitake, K. Nishikawa, *Proc. Natl. Acad. Sci. USA* **89,** 5216 (1992).

73. J. Marx, *Science* **249,** 1376 (1990).

74. J. Folkman *et al., Annals of Surgery* **214,** 414 (1991).

75. K. J. Anderson, D. Dam, S. Lee, C. W. Cotman, *Nature* **332,** 360 (1988).

76. E. G. Stopa *et al., Biochem. and Biophys. Research Communications* **171,** 690 (1990).

Chapter 2

Structure Determination of Acidic and Basic FGF

2.1. Crystallization and preliminary diffraction studies of FGF

The recombinant analogs of bovine aFGF (Ala47Cys, Gly93His) and human bFGF (Ser70Cys, Ser88Cys), which were expressed in *E. coli,* have comparable or even higher biological activities than the native forms (1, 2) and were used in our structural and functional studies. The factorial method (3) was employed for crystallization trials. The protein samples of 10 mg/ml aFGF in 20 mM Na Citrate (pH 5.6) and 13 mg/ml bFGF in 20 mM Na Citrate (pH 5.0) were used.

Crystals of aFGF were obtained by vapor diffusion against 0.2 M $(NH_4)_2SO_4$, 2 M NaCl, 0.02 M sodium potassium phosphate and 0.1 M sodium citrate at pH 5.6 (Figure 2.1). The protein droplet contained equal volumes (3 μl) of the reservoir solution and a 10 mg/ml protein solution. The typical aFGF crystal is about 0.5 x 0.5 x 0.5 mm^3 in size and diffracts to approximately 2.5 Å resolution. The crystals stop growing after about one month with fresh protein samples, but it takes much longer for old protein samples to grow to the optimal size. This may be due to an increased amount of dimeric arising from formation of intermolecular disulfide bonds. Precession photographs showed that the crystals are trigonal with space group $P3_121$ (or its enantiomorph $P3_221$) with unit cell edges of a = b = 78.6 Å, c = 115.9 Å (Figure 2.3). The Matthews coefficient calculation (4) indicated that there may be three aFGF molecules per asymmetric unit.

Crystals of bFGF were also obtained by S. Faham using the hanging drop method. The precipitant solution contained 25% polyethylene glycol 8000 and 0.1 M Hepes at pH 7.6 (Figure 2.3). The crystals grow in the triclinic space group P1, with unit cell dimensions of a = 31.1 Å, b = 33.5 Å, c = 37.0 Å, $\alpha = 64.2^o$, $\beta = 106.4^o$, $\gamma = 103.3^o$ and diffract to about 1.9 Å (Figure 2.2). Crystals of bFGF used for data collection are typically larger than 1 mm x 0.4 mm x 0.4 mm.

2.2. Heavy atom derivative search for aFGF crystals

The multiple isomorphous replacement (MIR) method was used to obtain phase information. Heavy atom derivatives were screened by soaking aFGF crystals in different heavy atom reagents at various concentrations. Because no satisfactory synthetic mother liquor was found for the aFGF crystals, heavy atom reagent solutions were injected directly into the hanging drop with a 10 μl syringe. Typical volume was about 0.3 μl of heavy atom solution added to 6 μl crystallization drop. The screening of heavy atom compounds was carried out by comparing diffraction intensities on precession photographs of the soaked crystals with precession photographs of the native crystals. Table 2.1 lists the heavy atom compounds that were screened for aFGF.

2.3. Area detector data for aFGF

All diffraction data for the aFGF structure determination were collected at room temperature on a Siemens area detector mounted on a Siemens rotating anode generator operating at 50 KV x 90 mA. CuKα radiation (λ = 1.54 Å) was used for the diffraction studies. Crystals were sealed in the capillaries in equilibrium with several microliters of a high salt synthetic mother liquor (1000 μl of such a solution consists of 750 μl 4 M NaCl, 80 μl $(NH_4)_2SO_4$, 8.0 μl 4 M $NaKPO_4$, 150 μl 1.0 M Na Citrate at pH 5.6 and 12 μl H_2O) in which crystals can survive for several days. The crystals were mounted with a random orientation in capillaries. Data collection for these crystals started at a random Ω angle and stopped after scanning 100°. The Ω scan was repeated after phi was changed by 90°. The collected data sets were autoindexed, integrated, scaled and reduced with the XENGEN software package (5, 6). Table 2.2 lists the data statistics for the native and the derivative crystals which were soaked in 4 mM EMTS and 3.3 mM K_2PtCl_4 for 12 hours and 3 days, respectively.

2.4. Heavy atom binding sites in aFGF

After both native and derivative data sets are available, heavy atom sites can be located by the difference Patterson function if the derivatives are isomorphous with the native crystal. All the derivative data sets were locally scaled to the native with the ROCKS program (7) before the difference Patterson maps were calculated. The difference Patterson for EMTS was very clear as illustrated for the Harker section w = 1/3 (Figure 2.4A). Similar results were obtained for the anomalous difference Patterson (Figure 2.4B). The difference Patterson for K_2PtCl_4 is noisy and the anomalous signal can barely be observed (Figure 2.5).

In either space group $P3_121$ or $P3_221$, the asymmetric unit is one sixth of the unit cell and by convention it is located between x = (0, 1), y = (0, 1) and z = (0, 1/6). But because of the origin ambiguity on z, only x = (0, 1), y = (0, 1) and z = (0, 1/12) needs to be searched for self vectors while z = (0, 1/6) is needed for cross vectors because of the fixed origin. In order to find the heavy atom binding sites of EMTS and K_2PtCl_4, half of the Patterson function unit cell was searched with PSP (program written by B. T. Hsu). The peak height output by PSP does not take symmetry into account, which means in $P3_121$ or $P3_221$, all points on the two fold axis will be doubled. After these factors were considered, one and two binding sites for EMTS and K_2PtCl_4 derivatives were found, respectively (Table 2.3). One binding site (0.53, 0.35, 0.023) was found to be the same for the two derivatives, implying that a common origin is used.

2.5. Phase calculations and phase extensions for aFGF

With the heavy atom binding sites available, the multiple isomorphous replacement phases were calculated and refined with PHARE (8). The phase possibilities for centric reflections in space group of $P3_121$ are shown in Table 2.4.

With anomalous scattering information of the EMTS derivative incorporated, the refinement showed an increased phasing power of the anomalous derivative, confirming that the space group is $P3_121$ instead of the enantiomorph $P3_221$. The

difference Fourier map showed additional minor binding site for the K_2PtCl_4 derivative after 8 cycles of heavy atom site refinement (Table 2.5). The overall figure of merit is 0.68 to 3.0 Å (Table 2.6).

To improve the quality of the MIR electron density map, two phase extension methods were applied: solvent flattening and noncrystallographic symmetry averaging. For solvent flattening, programs from the CCP4 suite were used (9). The sphere radius for generating the envelope was chosen as 10 Å. The solvent content was initially set to 40% due to the uncertainty about how many molecules were in one asymmetric unit. The protein envelope was generated automatically by B. C. Wang's method (10) and then applied to the MIR electron density map. Solvent flattening converged after six cycles. The solvent-flattened phases combined with MIR phases were used to generate another molecular envelope and applied to the MIR map again. This was repeated until convergence was achieved. After solvent flattening, the electron density map showed that there may be two molecules in one asymmetric unit. Using the value of 1 dalton/$Å^3$ for protein density, it was predicted that the solvent content of the unit cell was 60%. Using a solvent content of 55% (instead of 60% to be sure that no protein electron density was cut off), solvent flattening of the original MIR map was repeated. The final phase angle changes of noncentric and centric reflections at 3 Å were 34.9° and 12.2°, respectively.

Although the solvent flattened map clearly shows the molecular boundaries, it was still not possible to trace the backbone of the protein. To further improve the map, molecular averaging was carried out. Because the self-rotation function did not show how the two molecules in the asymmetric unit are related to each other, two P1 cells were made to include each molecule from the solvent flattened map. Cross rotation functions (11) were then calculated based on the structure factors converted from these two P1 cells. The resultant peak shows these two molecules are related to each other by a general transformation with the three spherical polar angles of 45.0°,

82.0° and 165.0°. Using these angles, the relative translation between the two molecules was determined by skewing the density of one molecule to the same orientation as the second, followed by calculation of a real-space translation function with the use of Fourier coefficients $\sum_h [F_o(-h)F_s(h)]\exp(-2\pi ihu)$ where F_o and F_s are the complex structure factors for the observed and skewed structures. The non-crystallographic symmetry was further refined by maximizing the density correlation coefficient (12).

With the refined noncrystallographic transformation matrix, initial electron density averaging between the two molecules was carried out (13) using the molecular envelopes generated by B. C. Wang's method (10). Due to the close contacts between the two molecules, the molecular envelopes generated by this method overlapped with each other in space and therefore were adjusted manually. After averaging, the R factor between F_{obs}s and F_{calc}s which were calculated from the symmetry averaged electron density map, dropped from 43.0% to 19.8%. The electron density map calculated with $2F_o - F_c$ coefficients and the averaged phases was obviously much improved and chain tracing became possible (Figure 2.6).

2.6. Model building and refinement of aFGF

The positions of the alpha carbon atoms were initially determined from sections of the averaged map stacked on acetate slabs. Ninety one C_αs were roughly located and displayed on a Silicon Graphics workstation using the TOM/FRODO program (14). After polyalanine models of the two aFGF molecules were built, refinement of the model with PROLSQ (15) and phase recombination of the model phases with the averaged phases was carried out. The initial aFGF model was built based on the averaged maps. Because the averaged map had some loop regions truncated due to the size of the initial molecular envelope, averaging was carried out again with a

molecular envelope generated by putting 3 Å spheres on each atom of the initial model. Using the new envelope, averaging converged at an R factor of 18.3% to 3 Å resolution. After more cycles of model building, refinement and phase combination, residues 1-137 and 10-137 for the two aFGF molecules in the asymmetric unit were built into the electron density map. The last three carboxyl terminal residues are disordered in both molecules and the amino terminus of one aFGF is also disordered. Refinement of this model between 8 - 2.7 Å resolution yielded an R factor of 20.9% , with root-mean-square deviations from ideal bond distances and angles of 0.02 Å and 3.8° respectively. A total of 35 water molecules were located by difference Fourier calculations and added to this aFGF model. Refinement with XPLOR (16) of this model which has 2009 nonhydrogen atoms progressed to the final R factor of 17.7% with r.m.s. deviations from the ideal bond distances and angles of 0.012 Å and 2.3° respectively. The structure coordinates have been deposited in the Protein Data Bank (1BAR_AFGF.PDB). The two aFGF molecules have about 98% and 91% complete structures respectively.

2.7. Structure determination and refinement of bFGF

The same heavy atom derivatives, EMTS and K_2PtCl_4, were used in the bFGF structure determination by S. Faham and B. T. Hsu. Crystals of bFGF were soaked in a synthetic mother liquor (30% PEG8K, 0.1 M Hepes, pH 7.5), containing either 3 mM EMTS or 5 mM K_2PtCl_4 for 2 days (Table 2.7). Using the aFGF model, the heavy atom binding positions in bFGF crystals were located by difference Fourier map with the molecular replacement phases of aFGF. There is one EMTS binding site and 4 K_2PtCl_4 binding sites on bFGF. Isomorphous replacement phases were calculated to 2.8 Å with an overall figure of merit of 0.62. The MIR map revealed similar molecular folds with aFGF and residues 20 to 144 of bFGF were subsequently fitted into the electron density map by A. J. Chirino. The first 19 and the last 6 bFGF

residues are disordered. Refinement of the bFGF model with a total of 40 water molecules with XPLOR programs by A. J. Chirino led to the final R factor of 17.0% between 5 - 1.9 Å resolution. The r.m.s. deviations of bond length and bond angle are 0.015 Å and 2.3° respectively (1BAS_BFGF.PDB).

Table 2.1. Heavy Atom Compounds Tested

Compound	Concentration	Soaking time
EMTS	4 mM	12 hrs
K_2PtCl4	3.3 mM	7 days
K_2IrCl_6	20 mM	7 days
$K_2Pt(CN)_4$	1.6 mM	14 days
Pt POP	1.5 mM	14 days
$K_2UO_2F_5$	4 mM	4 days
$Hg(Ac)_2$	*	12 days
$Pb(Ac)_2$	1.6 mM	16 days
$Hg(Ph)_2$	2.9 mM	9 days
NaI	12.5 mM	3 days
PCMBS	**	6 days
Meurbromin	***	3 days
EMP	0.8 mM	3 days
$AuCl_3$	1.0 mM	3 days

* 0.3 µl of 1/4 saturated $Hg(Ac)_2$ solution was added to the hanging drop.

** 0.3 µl of 1/2 saturated PCMBS solution was added to the hanging drop.

*** 0.5 µl 2% Murbromin solution was added to the hanging drop

EMTS: Ethyl Mercuri thiosalicylate

PTPOP: $K_4[Pt_2(P_2O_5H_2)]2H_2O$

EMP: Ethyl Mercury Phosphate

Table 2.2. Summary of the aFGF Area Detector Data

	resolution	reflections unique	reflections collected	completeness	R-factor
Native	2.7 Å	12,574	25,107	85%	4.4%
EMTS	3.2 Å	7638	25675	93%	6.7%
K_2PtCl_4	3.2Å	7179	23836	88%	7.9%

Table 2.3. Heavy Atom Binding Sites Located by Patterson' s Function

	x	y	z
EMTS	0.53	0.35	0.015
K_2PtCl_4	0.12	0.87	0.046
	0.56	0.37	0.015

Table 2.4. Centric Zones for $P3_121$

l	0kl	h0l
3n	0° or 180°	0° or 180°
3n-1	60° or -120°	120° or -60°
3n+1	120° or -60°	60° or -120°

Table 2.5. Refined Heavy Atom Sites

	X	Y	Z	Occupancy	B ($Å^{-2}$)
EMTS	0.545	0.343	0.0147	0.475	27.5
K_2PtCl_4	0.873	0.116	-0.0458	0.381	37.2
	0.557	0.353	0.0179	0.248	36.4
	0.150	0.548	0.145	0.115	51.1

Table 2.6. Phasing Power of the Derivatives

Resolution	11.7Å	8.3Å	6.4Å	5.2Å	4.4Å	3.8Å	3.4Å	3.0Å	overall
EMTS	2.13	2.07	2.53	2.07	1.79	1.75	1.74	1.47	1.88
$EMTS_{anom}$	2.43	1.94	1.50	1.53	1.06	0.89	0.73	0.42	0.90
K_2PtCl_4	1.08	1.66	1.75	1.71	1.27	1.08	0.87	0.66	1.17

Table 2.7. bFGF Heavy Atom Refinement Statistics

Data	Reso-lution	Concen-tration	measured reflection	comp-lete	R_{sym} (%)	Refined Sites	f_H/E
Native	1.9 Å	--	8,462	89%	4.8	--	--
EMTS	2.8 Å	3 mM	2,745	87%	5.8	1	2.0
K_2PtCl_4	2.8 Å	5 mM	2,877	91%	8.2	4	2.2

$$R_{sym} = \sum |I - \langle I \rangle| / \sum I$$

$$f_H / E = [\sum f_H^2 / \sum (F_{deriv,obs} - F_{deriv,calc})^2]^{\frac{1}{2}}$$

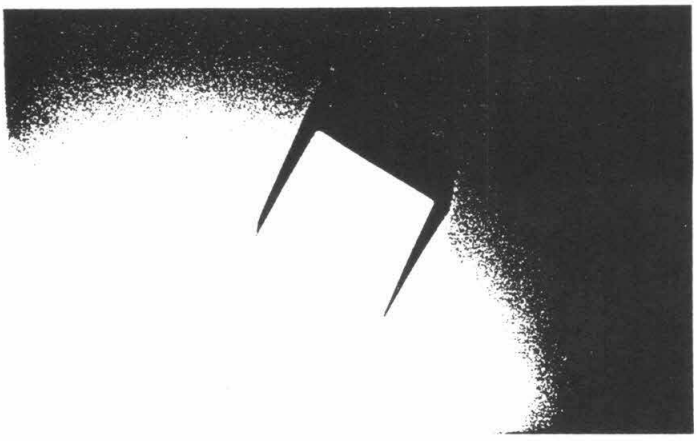

Figure 2.1. An aFGF crystal grown under the high salt condition.

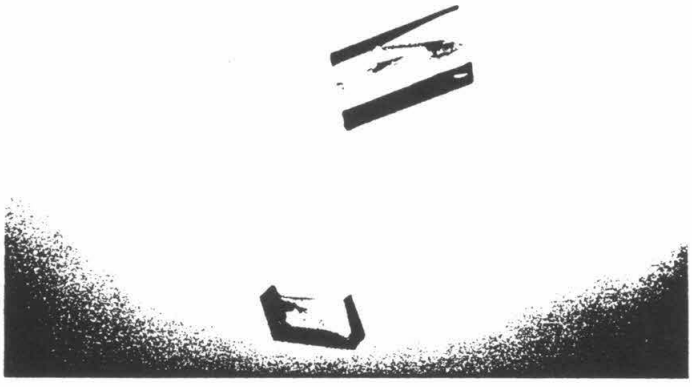

Figure 2.2. bFGF crystals grown with the condition found by S. Faham (17).

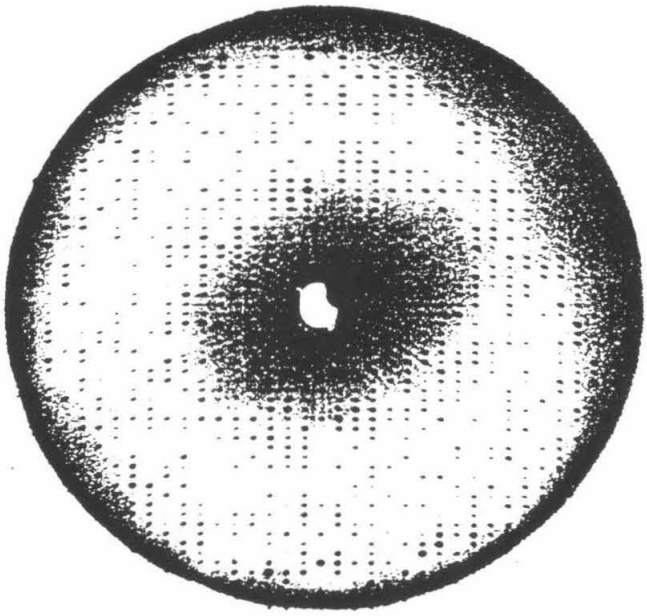

Figure 2.3. Precession photograph (μ = 12°) of the h0l zone of aFGF crystals.

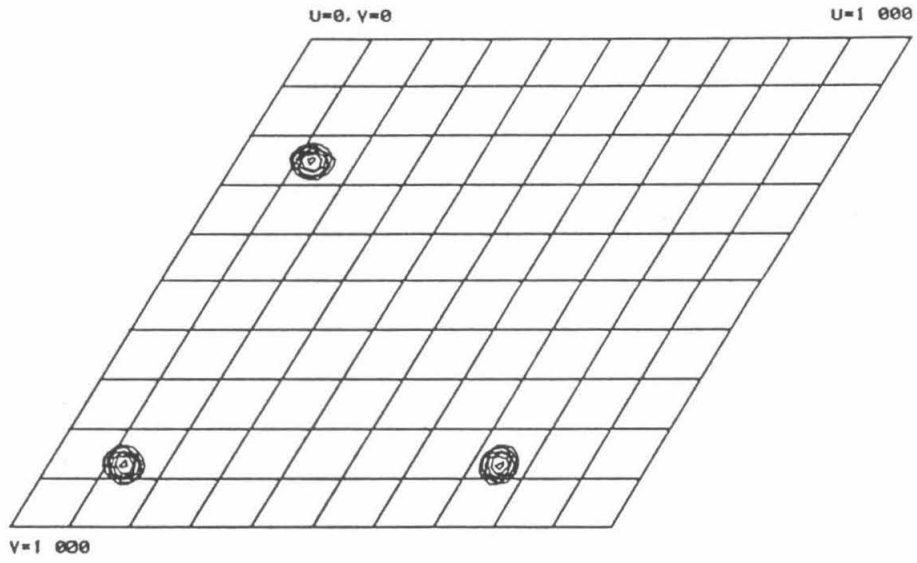

(A)

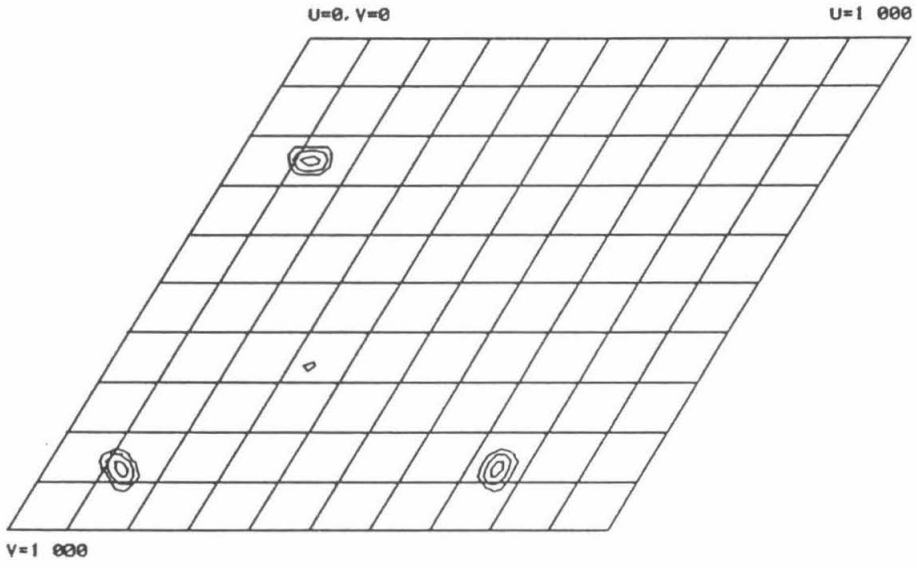

(B)

Figure 2.4. The difference Patterson (**A**) and difference anomalous Patterson (**B**) maps of EMTS in the Harker section w = 1/3.

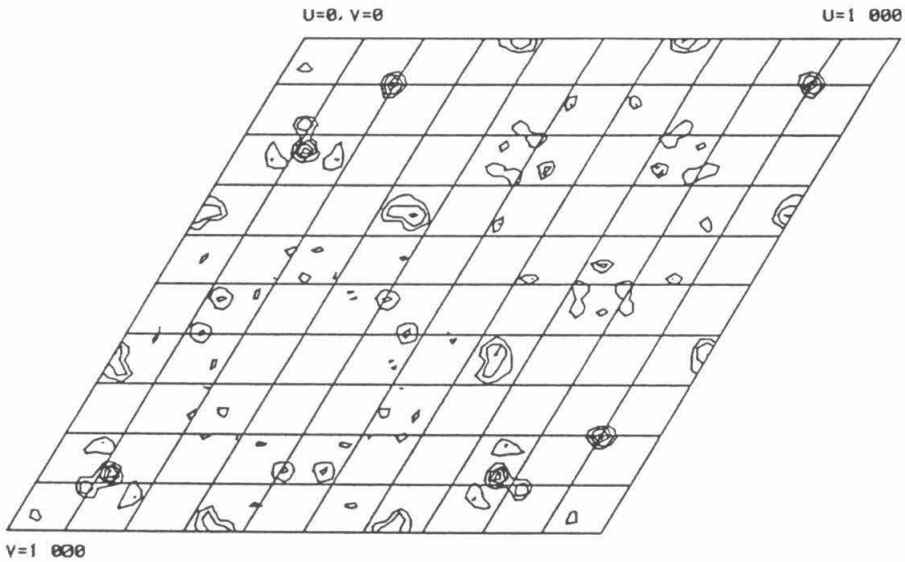

Figure 2.5. The difference Patterson map of K_2PtCl_4 in the Harker section w = 1/3.

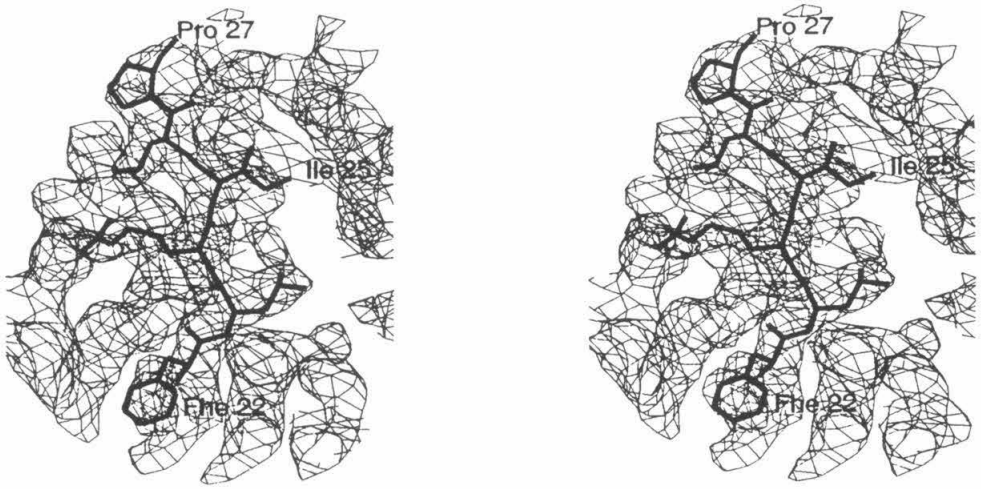

Figure 2.6. The 3 Å averaged electron density map in the region of β strand 2.

References

1. T. Arakawa, T. P. Horan, L. O. Nahri, D. C. Rees, S. G. Schiffer, P. L. Holst, S. J. Prestrelski, L. B. Tsai, G. M. Fox (submitted).

2. G. M. Fox, S. G. Schiffer, M. F. Rohde, L. B. Tsai, A. R. Banks, T. Arakawa, *J. Biol. Chem.* **263**, 18452 (1988).

3. C. W. Carter, *Methods, A Companion to Methods in Enzymology* **1,** 12 (1990).

4. B. W. Matthews, *Meth. Enzymol.* **114**, 176 (1985).

5. A. J. Howard *et al., J. Appl. Cryst.* **20**, 383 (1987).

6. Comparison between different data sets showed that indexing of h and k were not always consistent and it was found h and k needed to be switched if the R factor was unreasonably high.

7. G. N. Reeke, *J. Apply. Cryst.* **17**, 125 (1984).

8. J. L. Grawford and J. E. Lander, Phare-phase and refinement program (1982).

9. A. G. W. Leslie, *CCP Newsletter* **55 (17)** (1985).

10. B. C. Wang, *Meth. Enzymol.* **115**, 90 (1985).

11. M. G. Rossmann and D. M. Blow, *Acta Cryst.* **15**, 24 (1962).

12. J. M. Cox, *J. Mol. Biol.* **28**, 152 (1967).

13. G. Bricogne, *Acta Cryst.* **32**, 832 (1976).

14. T. A. Jones, *Meth. Enzymol.* **115**, 157 (1985).

15. W. A. Hendrickson, *Meth. Enzymol.* **115**, 252 (1985).

16. A.T. Brunger, *J. Mol. Biol.* **203**, 803 (1988).

17. X. Zhu, H. Komiya, A. Chirino, S. Faham, G. M. Fox, T. Arakawa, B. T. Hsu, D. C. Rees, *Science* **251,** 90 (1991).

Chapter 3

FGF Structures and their Relationship to Biological Function

3.1. Architectural overview of the FGF structure

The crystal structures of aFGF and bFGF reveal a very similar fold for the two proteins. With a roughly spherical shape of approximate 30 Å in diameter, FGF contains 12 antiparallel β strands that are arranged in a pattern of approximate three-fold internal symmetry as shown in Figure 3.1. Six of the strands form an antiparallel β barrel, consisting of strands 1, 4, 5, 8, 9 and 12, numbered sequentially from the amino terminus. One end of the barrel is covered by the remaining six β strands, coupled in pairs so that the axis of the β barrel coincides with the molecular pseudo 3-fold axis relating every 4 β strands (strands 1-4, 5-8 and 9-10).

A striking feature of the aFGF and bFGF structures is the overall similarity to the folding pattern observed for the interleukin -1α and -1β (IL-1α and 1β), two growth factors that mediate the immune response (1-4). Despite the fact that IL-1β has several more extended loops compared to FGF, superposition of FGF and interleukin-1β α-carbon atoms of the 12 strands reveals a root-main-square deviation of only 1.5 Å (Figure 3.2). Recently, hisactophilin, which is an actin-binding protein (5), and a Kunitz-type trypsin inhibitor from *Erythrina caffra* seeds (6) have been found to also consist of 12 antiparallel β-strands. This unusual fold was first observed in the structure of soybean trypsin inhibitor determined about twenty years ago (7, 8). Interestingly, although they possess quite different biological functions ranging from growth factors to protease inhibitor, these similarly folded polypeptides have the common feature of being involved in recognition of other proteins.

In spite of the structural similarity, sequence comparison of these proteins with 12 antiparallel β strands reveals very low sequence homology. For instance, human aFGF and interleukin-1β are only 12% identical and 33% similar. In addition, the protein internal sequence symmetry correspondent with the pseudo three-fold axis can not be detected using the programs in the University of Wisconsin GCG package. Nevertheless, when the sequences of these proteins are aligned based on the three-

dimensional structures, it is found that the hydrophobic character of residues at nine positions in the β sheets (residues 14, 23, 31, 56, 65, 73, 97, 109 and 117 of aFGF) is quite well conserved (Table 3.1). The crystal structures further demonstrate that the conserved residues form a compact core inside the protein, suggesting a unique role of these conserved amino acids in the protein folding (Figure 3.3).

3.2. Structural comparison of the two aFGF molecules in one asymmetric unit

Because the aFGF structure was determined using the crystals containing two aFGF molecules in one asymmetric unit, these two protein molecules were built and refined independently (9). An obvious difference between the two structures is that the first nine residues of one aFGF is disordered whereas the amino terminus of the second aFGF has well defined structure. Except that, superposition of the two aFGFs shows that they have quite similar backbone and side chain conformations, with an r.m.s. deviation of less than 0.56 Å for the 126 common α-carbons (Figure 3.4). The quantitative comparison of the two structures illustrated in Figure 3.6 further indicates that there are only three local regions where the structural discrepancy is over 1.0 Å. The most structurally variable region is around aFGF glutamine 77 where the difference is as large as 1.6 Å. Located on one of the longest FGF loops between β strands 7 and 8, glutamine 77 and its adjacent residues are fairly exposed to a large solvent channel inside the crystal. Usually protein loops are flexible and the different conformations observed here may reflect a dynamic picture of FGF in solution.

The second largest structural difference occurs near glutamate 91 of the β turn between strands 8 and 9. Unlike Gln 77, this is due to a lattice contact in the crystal. One aFGF has two amino acids located adjacent to Glu 91, Asn 92 and Tyr 94, which are in contact with Glu 49 of a neighboring molecule. For the other aFGF, the main chain carbonyl groups of Glu 91 and Gly 93 are hydrogen bonded to the neighboring residues Arg 88 and Lys 101, respectively. Lastly, the third site of a relatively large

structure variance is also caused by a lattice contact, where the aFGF residue glutamate 49 forms an intermolecular hydrogen bond to tyrosine 94 of the neighboring molecule .

Molecular packing inside crystals can affect the main chain conformations as well as the side chain conformations. For example, superposition of the two aFGFs shows that the side chains of tyrosine 55 are quite different (Figure 3.5). Lattice contact analysis shows that while Tyr 55 of one aFGF does not interact with its neighboring molecules, Tyr 55 of the second aFGF in the asymmetric unit is however situated at an intermolecular interface and interacts with its neighboring molecule. Consequently, the two residues Phe 75 and Pro 65, which are adjacent to Tyr 55 and have hydrophobic interactions with Tyr 55, also display different conformations in the two structures.

For further structural comparison, temperature factor analysis was performed for the two aFGFs. The temperature factor plot for the two molecules illustrated in Figure 3.7 shows that although the rough trends of the temperature factor for the two molecules are similar, one molecule has generally higher temperature factors than the other, and further, several local regions display large fluctuations. This is consistent with the calculated average temperature factors, which are 26.7 $Å^2$ and 22.7 $Å^2$ for the two aFGFs respectively. Systematic analysis of the intermolecular contacts within 4 Å between symmetry related molecules shows that the aFGF molecule with lower average temperature factor has 13 residues involved in non-covalent contacts with its neighboring molecules. In contrast, none of the amino acids of the aFGF with a higher average temperature factor interacts with adjacent protein molecules. This suggests that lattice contacts are probably responsible for the overall temperature factor difference. Also, in addition to the overall temperature factor difference, local regions near residues 49 and 72 are shown to have relatively large difference in temperature factors. These differences are also mainly due to the lattice contact effect

(Figure 3.7). The Glu 49 region, which displays structural differences in the two aFGFs, has been discussed above. And one of the two leucines 72 in the two structures is also seen interacting with residue 126 of a neighboring molecule inside the crystal.

Because the aFGF structure has been determined to 2.7 Å, only 37 water molecules have been located for the two aFGFs in the asymmetric unit. These thirty seven water molecules are nevertheless unevenly distributed between the two protein molecules. Thirteen and twenty-four water molecules are bound to the two aFGFs respectively. Superposition of the two aFGFs further showed that while most interior water molecules were at common positions in both structures, the exterior water molecules are often different. Among the 7 common water molecules in both structures, five of them are located inside the protein and only two are bound on the protein surface. Furthermore, the four buried water molecules are found to bind the main chain amino and carbonyl groups from different β strands, whereas one buried water molecule is found to form a hydrogen bond with the buried side chain of Ser 99 (Table 3.2).

In general, the two aFGF molecules in the asymmetric unit have very similar three dimensional structures and the few observed local structural differences are mainly due to the lattice contact effect. In addition, interactions between the neighboring molecules packed inside the crystal may also be responsible for the overall temperature factor difference in the two structures. The structural similarity of the different molecules in one asymmetric unit is further supported by the commonly situated interior water molecules which have been independently located. The close conformations of the two aFGFs not only assures the correctness of the structure, but also simplifies the structural comparison between acidic and basic FGF.

3.3. Structural comparison between aFGF and bFGF

With 55% sequence identity and 70% similarity, it is not surprising that acidic and basic FGF have very similar three dimensional structures. Superposition of aFGF and bFGF shows an overall r.m.s. difference of 0.74 Å between the corespondent 126 Cα atoms (Figure 3.8). Furthermore, the structure similarity of aFGF and bFGF is not only contained in the β strands but also in virtually all the loops. In addition, despite the different resolutions, many of the bound water molecules are commonly observed in the two structures (9). Although forty ordered water molecules are located in bFGF, only thirteen and twenty four water molecules are found for the two aFGFs in the asymmetric unit respectively. Yet seven water molecules, that are common in the two aFGF structures in one asymmetric unit, have also common positions in bFGF. Similar to aFGF, four out of the five interior water molecules function to mediate the interaction between different β strands (Table 3.2) while one buried water molecule interacts with bFGF Ser 109.

In spite of the overall structure similarity of aFGF and bFGF, there are several local regions that do display conformational difference between the two structures (Figure 3.8). The most variant region is around Ser 114 of bFGF or Glu 104 of aFGF where the α-carbon position difference is as large as 4 Å. The crystal structures reveal that bFGF Ser 114 is located at the end of the long loop between β strands 9 and 10 while at the same region aFGF has two more inserted residues (Lys 105 and His 106) than bFGF before β strand 10. Thus it leads to the dramatic conformational change of aFGF Glu 104 as shown in the Figures 3.8 and 3.9.

Besides the large conformational difference revealed in this amino acid insertion site, there are three additional regions that have obviouly structural differences. They are localized around bFGF residues Pro 37, Ser 70 and Ser 101 (Figure 3.9). Unlike the regions of aFGF Glu 104 or the homologous residue of Ser 114 in bFGF, which have intrinsic structural differences, the conformational difference of these three regions are all due to lattice contact effects. For example, while aFGF Glu 28 is in

contact with Arg 128 of a neighboring molecule, its corresponding amino acid Asn 38 in bFGF nevertheless interacts indirectly with Asn 105 of an adjacent bFGF through another residue Arg 40. Also, Asn 72 and Ser 101 of bFGF are both located at the molecular interface and interact with Leu 131 and Tyr 125 respectively. In contrast, aFGF Gly 62 is not involved in any lattice contacts and aFGF Glu 91 interacts with Glu 187 from a neighboring molecule.

Therefore when lattice contact effects are excluded, aFGF and bFGF do have quite close three-dimensional conformations, except for the loop between strands 9 and 10 in which the sequence insertion occurs in aFGF. The structural similarity of acidic and basic FGF demonstrated here is in agreement with the biochemical studies that a similar but slightly different activity profile for aFGF and bFGF has been reported. This will be discussed further in the following sections.

3.4. The cysteine locations revealed in the FGF structures

There are three cysteines in aFGF and four in bFGF, with two of them conserved in all species of aFGF and bFGF (aFGF Cys 16, Cys 83 and bFGF Cys 26, Cys 93). While alkylation of aFGF after reduction was reported to have no effect on mitogenic activity (13), a contrasting result was obtained by Harper *et al.* suggesting that a disulfide bond between Cys 16 and Cys 83 could be formed in aFGF (14). For bFGF, substitution of cysteine -70, -88 and -93 with serines by site-directed mutagenesis was reported to result in unaltered FGF activities, which implies that the disulfide bridge in bFGF is not functionally important (15-17).

The double mutant Ala47Cys, Gly93His aFGF analog has been shown to possess a comparable or slightly higher mitogenic activity than the native (18). The locations of cysteines -16 and -83 as well as alanine 47, the substitution for cysteine-47, are explicitly defined in the three dimensional structure of this analog (9) (Figure 3.10). Cys 16 is located on the loop between β strands 2 and 3 while Ala 47 and Cys 83 are

located on the β strands 4 and 8 respectively. Interestingly, the cysteine localized on the loop structure is totally buried whereas the cysteine or the cysteine substitution located on the β strands are exposed. The exposure of Cys 83 in the three dimensional structure of aFGF is in agreement with the observation that EMTS binds aFGF near Cys 83. Furthermore, it is shown in the crystal structure that the distance between residues 47 and 83 is about 11 Å while Cys 16 is situated relatively further away from these two residues by an approximate distance of 20 Å. It is clearly indicated here that no pair of cysteine residues are in close enough proximity to one another to form an intramolecular disulfide bond.

For bFGF, the structure of bFGF Ser70Cys and Ser88Cys analog, which has an equal activity to the native (15, 16), shows that residues -70, -88 and -93 are located on one side of the protein while cysteine-26 is buried at the other end (Figure 3.11). The shortest distance between these four residues is about 6.5 Å, which is between amino acids 88 and 93. Residue 70 is situated about 18 Å from 88 and 93 while Cys 26 is located at least 20 Å away from all the three residues. Therefore, like aFGF, it is quite certain that no intramolecular disulfide bridge can be possibly formed between these cysteines in bFGF. However, based on literature reports (20) as well as our observations that dimeric FGF can be detected with SDS-PAGE and HPLC, intermolecular disulfide bonds in both aFGF and bFGF appear to be possibly formed gradually between the exposed cysteines (i. e., cysteines-70, 88 and 93 in bFGF and cysteines-47 and -83 in aFGF).

Since two disulfide bridges are observed in some structures of twelve antiparallel β strands such as Kunitz-type trypsin inhibitor (5-7), the FGF cysteine positions are compared to that of trypsin inhibitor DE-3 from *Erythrina caffra* (ETI) (7). As revealed in the proteinase inhibitor structure, one disulfide bond is formed between the two loop residues cysteine-39 and -83 while the other disulfide bridge is between cysteines-131 and -139 located at the end of strand 9 and the beginning of strand 10.

Superposition of bFGF and ETI shows that the four cysteines in bFGF are neither overlapped with or close to the cysteines forming the disulfide bridges in ETI (Figure 3.12). In general, the disulfide bonds of ETI, which has larger molecular dimensions (44 x 40 x 40 $Å^3$) (7) than FGFs, are located on the protein surface.

3.5. Receptor binding studies

Interest in FGFs have centered on the molecular details of the receptor-mediated pathways by which their diverse physiological activities are expressed. The knowledge of the interactions between FGFs and FGF receptors could provide valuable insights into the design of therapeutically useful agents which can either mimic or inhibit the action of the growth factor. In general, hormones can be classified into two groups based on their target receptors. The first class of hormone enters cells and binds a cytosolic receptor that is a transcription factor. Examples of this class of receptors are the steroid and thyroid receptors. The second class of hormone binds a receptor which is a transmembrane protein and a second messenger is usually coupled to the hormone and receptor interaction. Most peptide growth factors belong to the second class. Furthermore, some of these peptide growth factor receptors have seven transmembrane helices (such as the β-adrenergic receptors and rhodopsin) and G proteins, cyclic AMP and ultimately protein kinases are involved in the signal transduction pathway. Others have a single transmembrane helix (such as PDGF and IL-2 receptors) and signal transduction is mediated through autophosphorylation of the intrinsic tyrosine kinase or the kinase associated with the receptors (19, 20). While many receptors of cytokines coordinating immune and inflammatory responses are non-tyrosine kinase proteins (such as the receptors of IL-2, IL-3, IL-5, IL-6, GM-CSF, G-CSF and etc.) (20), other peptide growth factor receptors such as FGF receptors contain intrinsic tyrosine kinase domains. On the basis of their structural characteristics, tyrosine kinase receptors can be further

classified into three subclasses (20). These include the cysteine-rich monomeric receptor (class I), the cysteine-rich heterotetrameric $\alpha_2\beta_2$ receptor (class II) and the receptor with several extracellular immunoglobulin-like domains (class III). For instance, EGF receptors belong to class I while insulin receptors and FGF receptors belong to class II and III respectively.

Binding of growth factors to their receptors often leads to receptor dimerization or oligomerization either by the binding of one monomeric ligand to two receptors simultaneously (such as human growth hormone (21)), or by binding of two monomeric ligands to two receptors (such as EGF (20)), or by binding of one bivalent ligand to two receptors (such as PDGF (20), NGF (22), TGF-β (23), M-CSF (24)). For FGF, although it is a monomeric ligand, the receptor binding and dimerization mechanism has not yet been elucidated and some possibilities will be further discussed in chapter 4.

The first FGF receptor cDNA was reported to be isolated in 1989 by using an oligonucleotide probe of a purified FGF receptor fragment (25). The amino acid sequence derived from this cDNA clone, which is a *fms*-like gene called *flg* (26), revealed that the receptor is composed of three extracellular Ig-like domains, one transmembrane helix and an intracellular tyrosine kinase domain with an approximate molecular weight of 130 kD. After this pioneering work, at least four more FGF receptors have been identified and cloned (25-36). Although these receptors are all encoded by *flg* and the related gene *bek* (26, 27), alternative RNA splicing has been shown to be possibly responsible for the observed multiple forms of FGF receptors, which can possess either two or three Ig-like domains, and different lengths of cytoplasmic tails (37). Furthermore, it appears that different FGF receptors have different binding specificities for the various members of the FGF family. For example, the KGF receptor, encoded by a gene closely related to *bek* (27), can bind with high affinity to KGF and aFGF but not bFGF (27). Sequence comparison shows

that the C-terminal 50 amino acids of the extracellular Ig-like domain closest to the membrane are quite diversified in KGF and bFGF receptors (27). These 50 amino acids have now been further confirmed to be the major ligand binding specificity determinant by an elegant ligand-receptor binding study with chimeric receptors in which the last 50 amino acids are interchanged between different receptors (28). While details of the binding interactions between FGF and the last 50 carboxyl terminal amino acids of FGF receptor remain obscure, the crystal structure of FGF and the putative receptor binding sites allocated on this "3-D map" of FGF may provide some clues.

Before the three-dimensional structure of FGF was determined, the possible receptor binding sites on bFGF had been explored with a series of bFGF derived peptides (38). On the basis of their ability to inhibit radiolabeled bFGF binding to the receptor and to stimulate thymidine incorporation, two functional subdomains were identified, which were bFGF-(25-69) and bFGF-(94-121). Shorter peptides contained within these sequences, 31-51 and 107-116, were less effective but still exhibited similar activities. Interestingly, these two peptides however showed inconsistent mitogenic results in different cell lines. While bFGF-(31-51) had weak growth stimulation ability to 3T3 fibroblast cells, the same peptide was observed to inhibit the growth of vascular and capillary endothelial cells. For bFGF-(107-116), although it showed quite potent agonist effects on 3T3 fibroblast cells, it had little effects on vascular and capillary endothelial cell growth.

As demonstrated by the bFGF structure (9), bFGF-(31-51) covers from the beginning of β strand 2 to the end of the loop between β strand 3 and 4. Strands 2 and 3 are adjacent, and are stabilized by interstrand hydrogen bonds (Figure 3.13). While most amino acids of β strand 2 are buried inside the protein in both aFGF and bFGF, β strand 3 and the two β turns in this region are relatively more exposed on the protein surface (Figure 3.15B). Since a longer peptide of bFGF-(25-69) was shown to

have more potent mitogenic activity than bFGF-(31-51) (38), the conformations of the two peptides are therefore compared. Surprisingly, most additional residues in the longer peptide (residues 25-30 and 52-69) are not in contact with bFGF-(31-51) (Figure 3.14). The only interactions between residues after 51 and the region of 31-51 are reflected in a hydrophobic core formed by Leu 33, Ile 35 from bFGF-(31-51) and Leu 54, Leu 56, Leu 64, Ile 66 from bFGF-(52-69). The additional six amino acids before 31, on the other hand, are observed to form a β turn which could stabilize the conformation of bFGF-(31-51) by forming two hydrogen bonds through the interactions of residues 26-31 and 29-45 respectively.

The second putative receptor binding peptide, bFGF-(107-116) is located on a different face of bFGF from 31-51 as illustrated in Figure 3.16. Much evidence has strongly suggested that the region of bFGF-(107-116) is very likely to be directly involved in interacting with the FGF receptor. For example, in addition to the peptide mapping experiment which revealed the importance of bFGF-(107-116) in receptor binding (38), Thr 113 located in this region can be phosphorylated by protein kinase A, and the phosphorylated bFGF displays an enhanced binding affinity for the FGF receptor (39). Further, between bFGF amino acids 112 and 115, aFGF and KGF have two and four more residues than bFGF respectively, and the two oncogenes int2 and FGF5 have an additional 7 to 14 amino acids at the same region (Figure 3.17). In general, the FGF family is a highly homologous protein family with very rare sequence deletions and insertions. The high frequency of sequence insertion occurring here strongly suggests the functional importance of this region.

Spanning β strands 9 and 10, bFGF-(107-116) and aFGF-(97-108) reveal a generally similar structural framework, but with a slightly different conformational loop. The two inserted residues in aFGF occur on the long loop which connects strands 9 and 10 so that the overall tertiary structure of 12 anti-parallel β strands is maintained (Figure 3.18). The β strands at this region are almost buried except the

partially exposed bFGF Trp 115. The long loop connecting the two strands is however quite exposed (Figure 3.19). The two adjacent basic residues located at the beginning of the loop, which are Lys 100, Lys 101 in aFGF and Arg 110, Lys 111 in bFGF, have perpendicular side chain conformations with the first basic residue relatively distant from the rest of the loop. The following residue in the sequence is a histidine in aFGF, but a tyrosine in bFGF. With both similar main chain and side chain positions, bFGF Tyr 112 is exposed to solvent while His 102 of aFGF is buried under the side chain of the inserted aFGF Lys 115. A very different solvent accessibility is observed again on the next residue in the two structures, which is an alanine in aFGF but a threonine in bFGF. The solvent exposure of bFGF Thr 113 is consistent with the result that this residue can be phosphorylated by protein kinase A. Following Thr 113 is Ser 114 in bFGF which is located at the end of the loop between strands 9 and 10 where a dramatic change of the backbone conformation occurs on the corresponding residue of Glu 104 in aFGF. aFGF Glu 104 is observed to swing out of the loop so that the two inserted aFGF residues Lys 105 and His 106 can be accommodated at the end of the loop. The more extended loop in aFGF leads to a 4 Å deviation in the Cα positions at this place.

Due to the overall architecture of the β-stranded protein, there are many β turns connecting adjacent strands in the FGF structure. However the loop between β strands 9 and 10, which is likely to interact with the FGF receptors, does not belong in a typical β hairpin classification. Strands 9 and 10 do not have interactions with each other except near the loop region. Two hydrogen bonds are formed between the main chain amino and carbonyl groups on β strand 9 and 10 and form the narrow end of the Ω loop. There are five bFGF residues and seven aFGF residues located in this loop. In both structures, these amino acids are demonstrated to have such geometry that three sharp turns are formed inside this loop, resulting in a stable conformation where multiple polar interactions and hydrogen bonds are formed between the main chain

amide and carbonyl groups. The two additional aFGF residues are inserted in the third turn of the loop so that the overall geometry of the loop is maintained. The stability of the loop between β strands 9 and 10 shown here supports the observation that the peptide of bFGF-(107-116) alone can possess strong inhibitory activity to the receptor binding by FGF. Because most residues on β strands 9 and 10 are buried, the loop between the two strands is very likely to play an important role in receptor binding. To further confirm and characterize this receptor binding region, more biological studies, such as the site-directed mutagenesis of the amino acids located on the loop, need to be carried out.

3.6. Nuclear translocation of FGF

After binding of FGF to the receptor, the FGF and FGF receptor complex is internalized into cells by receptor-mediated endocytosis. Intact aFGF has been identified for up to six hours after it enters cells and degradation products of 10-KD and 15-KD can be detected inside the cell up to 24 hours (40, 41). Further, the presence of FGF in the cellular nucleus has been recently shown by immunohistochemical localization studies within mesenchymal cells (42). Nuclear import of polypeptides occurs by binding of the peptides to a nuclear pore complex that facilitates the translocation process. Specific sequences containing basic residues usually accelerate targeting of proteins to the nucleus (43). Based on the sequence characteristics of nuclear translocation of proteins, a peptide of aFGF-(7-13) containing the sequence NYKKPKL was identified to be similar to the nuclear translocation sequence of other nuclear proteins (44). It was further shown that a mutant aFGF lacking the putative nuclear translocation sequence failed to stimulate cellular DNA synthesis and cell proliferation, although it could still induce receptor tyrosine kinase activities. In addition, when the aFGF N-terminus was replaced by other nuclear translocation sequence such as that of yeast histone 2B, the chimeric

aFGF was reported to exhibit comparable mitogenic activities to the native protein (44). The significance of the presence of FGF in the nucleus was further investigated in a cell-free system of nuclear extract from Ehrlich ascites tumor cells. In this experiment, bFGF was demonstrated to regulate phosphoglycerate kinase gene transcriptions (45) and a 5' upstream region of the *pgk* gene was further demonstrated to be required for gene activation induced by bFGF. Therefore, it is likely that FGF may have direct interactions either with this DNA sequence or with other unknown *cis*-elements.

The FGF crystal structure shows that the nuclear translocation peptide of FGF appears not to have a stable three-dimensional conformation. Of the two independently-determined aFGF molecules and the bFGF structure (9), the FGF amino terminus can only be observed in one aFGF molecule (Figure 3.20). The structure reveals that the peptide of aFGF-(1-9) possesses a rather extended form and does not specifically interact with the remainder of the molecule. Instead, it is stabilized by contacting neighboring molecules which are packed inside the crystal around it mainly through hydrophobic interactions. For example, Phe 1, Leu 3 and Pro 4 are clustered on one side of the amino terminal peptide and form a hydrophobic core by interacting with Phe 22, Tyr 15, Leu 133 and Leu 135 of a neighboring molecule. On the other side of the peptide, the side chain of Leu 5 is stabilized by interacting with Leu 55, Pro 64, Pro 79 and Leu 84 from another neighboring molecule. There are three closely located basic residues in the nuclear translocation peptide, lysines 9, 10 and 12. Both lysines 9 and 12 appear to be quite flexible and are disordered in the crystal structure, whereas the next basic amino acid, Lys 12, has defined side chain density, although it is quite exposed to solvent and has barely any interactions with other residues. As demonstrated here, the overall independence of the aFGF nuclear translocation sequence from the rest of the structure is consistent with the observation that the chimeric aFGF fused with other nuclear translocation

sequence maintains mitogenic activity.

3.7. FGF binding to heparin

FGF is a unique member of the peptide growth factor family in the sense that FGF is so far the only growth factor known to absolutely require heparin or heparin-like molecule to bind its receptor (46-48). While many other growth factors such as GM-CSF, IL-3, pleiotrophin, platelet factor 4, amphiregulin and heparin-binding-EGF are known to be able to interact with heparin, and some of these including IL-3 and GM-CSF, are active only in the presence of heparin (49), the significance of heparin binding to these growth factors is still unclear. However for FGF, a series of recent biochemistry experiments have demonstrated that heparin is involved in modulating FGF activity in the first step of FGF action by facilitating FGF binding to its receptor. Yayon *et al.* showed that the binding ability of FGF to the FGF receptor was lost in the heparan-sulfate deficient cells while the mutant phenotype could be inverted if heparin or heparan sulfate was added (47). In addition, it was further pointed out by Sakaguchi *et al.* that heparin could be directly attached on the FGF receptor by the identification of a 150-kD heparan sulfate proteoglycan as a high affinity FGF receptor (46). They also showed that treatment of the heparan sulfate proteoglycan with heparinase resulted in a reduced molecular size of the receptor and decreased binding affinity of FGF for the proteoglycan, which further suggests that heparin-like molecules may play an obligatory role in the regulation of receptor binding of FGF.

Besides regulating FGF binding to receptor, heparin also functions as a stabilizer of FGF and protects FGF from acid and enzymatic degradation (50,51). In addition, it also serves as a reservoir for storage of FGFs in the extracellular matrix (ECM) and release of FGF from ECM can be observed when heparinase or extra heparin is added (52). The size and the degree of sulfation in heparin, shown by many *in vitro* and *in*

vivo experiments, are the critical factors for heparin binding to FGF. Depolymerized heparin containing as little as 8-10 sugar units were demonstrated to be as effective as the whole heparin molecule for binding FGF or releasing FGF from ECM (53, 54). The sufficiency of a heparin octasaccharide for regulating FGF binding to the receptor is further supported by the recent FGF-receptor binding study with a soluble form of FGF receptor and a series of small heparin oligosaccharides of different lengths (55). For the sulfate groups, N-sulfate groups have been shown to be crucial for heparin binding to FGF while the presence of O-sulfate groups appears to have an increased but not critical effect on heparin binding to FGF (53).

Correspondent with the highly negatively changed groups on heparin (Figure 3.21), a region rich in positively charged and polar amino acids is found in both aFGF and bFGF crystal structures (9-12). Lys 112, Lys 113, Asn 114, Arg 116, Lys 118, Arg 122, Gln 127, Lys 128 are clustered around Lys 118 in aFGF while Asn 28, Arg 45, Lys 120, Arg 121, Lys 126, Lys 130 and Gln 135 are centered around Lys 126 in bFGF. Lys 118 of aFGF and Arg 126 of bFGF are located on β strand 11, which is adjacent but distinct from the putative carboxyl terminal receptor binding site (Figure 3.22). The importance of the residues after Asn 103 for heparin binding in bFGF has been demonstrated in many biochemistry experiments. For example, in agreement with the studies with a series of genetically truncated FGFs (56), peptide bFGF-(103-146) was demonstrated to possess binding affinity to radiolabeled heparin (38). Furthermore, reductive methylation, site-direct mutagenesis and thrombin digestion experiments have all implicated the importance of aFGF Lys 118 as well as its adjacent residue Arg 122 in heparin binding (57-59).

To elucidate the exact binding site of heparin on FGF, we have been working on the crystal structure of FGF and heparin oligomer complex. The structure of FGF and heparin complex is also necessary to prove the hypothesis proposed by Yayon *et al.* that a vital conformational change of FGF induced by heparin is probably required for

FGF binding to the FGF receptor (47). Crystals of aFGF obtained in the presence of low molecular weight heparin by using the old aFGF crystallization conditions (9) appeared to exclude heparin from the crystals since the "cocrystal" morphology remained the same and no obvious peaks could be observed in the difference Fourier map. The reason that heparin is not included in the crystal is probably due to the heterogeneity of the heparin sample used in crystallization. Therefore, a homogenous heparin analog, sucrose octasulfate, was used for these studies and will be further discussed in Chapter 4.

Table 3.1. Structural Aligment of β Strands in aFGF, bFGF and IL-1β

	1	2	3	4
	*	*	*	*
AFGF/I	11 PKLLYC	21 YFLRIL	30 TVDGT	42 IQLQLAA
II	53 EVYIKS	63 QFLAMD	72 LLYGS	83 CLFLERL
III	94 YNTYIS	107 WFVGLK	116 RSKLG	130 ILFLPLP
BFGF/I	21 PKRLYC	31 FFLRIH	40 RVDGV	52 IKLQLQA
II	63 VVSIKG	73 RYLAMK	82 RLLAS	93 CFFFERL
III	104 YNTYRS	115 WYVALK	124 QYKLG	138 ILFLPMS
IL1β/I	7 NCTLRDS	16 KSLVMS	25 ELKAL	40 VVFSMSF
II	57 PVALGLK	67 LYLSCV	79 TLQLE	99 FVFNKIE
III	109 KLEFESA	120 WYISTS	131 PVFLG	144 TDFTMQF

Table 3.2. Interactions between aFGF and the Buried Water Molecules

Water	Residue	Strand	Residue	Strand
H_2O 504	NH_2 56	β 5	CO 83	β 8
H_2O 505	NH_2 97	β 9	CO 109	β 10
H_2O 515	NH_2 110	β 10	CO 118	β 11
H_2O 520	NH_2 23	β 2	CO 14	β 1
H_2O 517	Ser 99	β 9		

*. Water molecules are numbered as in 1BAR_AFGF. PDB.

**. NH_2 and CO are main chain amide and carbonyl groups that bind the water molecule.

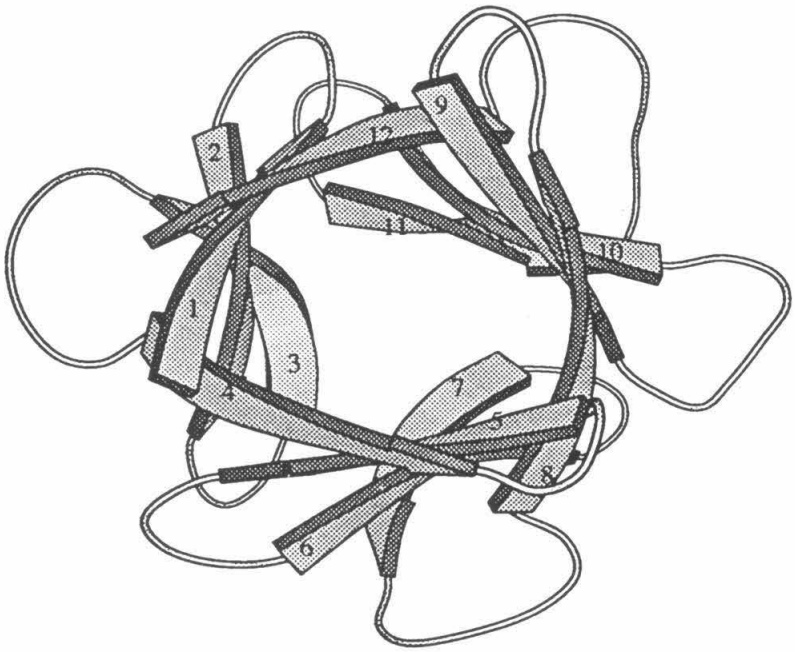

Figure 3.1. A Ribbons representation of the aFGF structure.

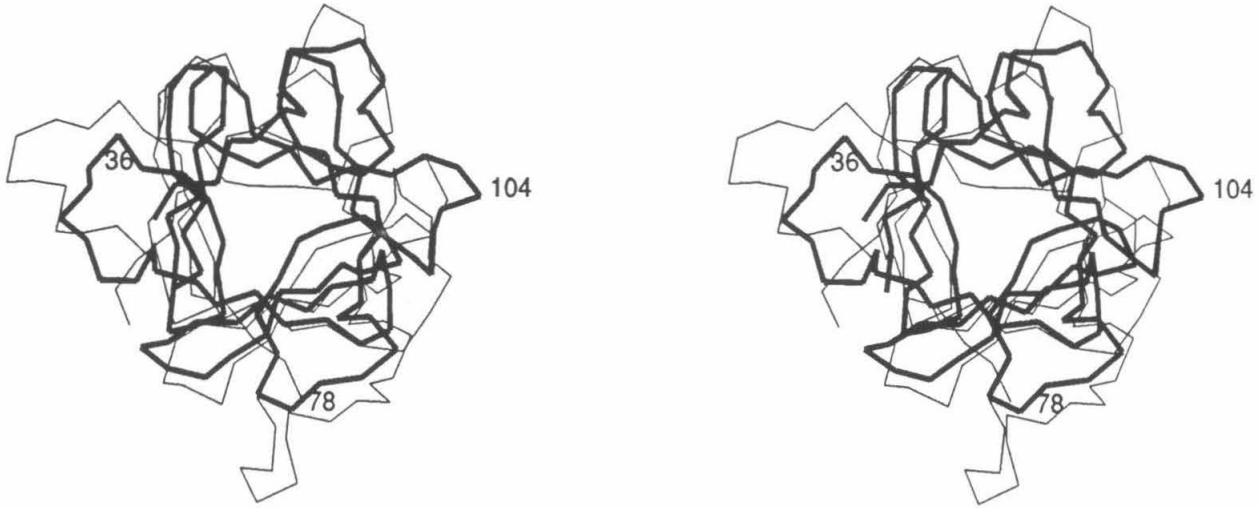

Figure 3.2 (A). Cα stereoview of superimposed aFGF (thick line) and interleukin-1β (thin line) structures.

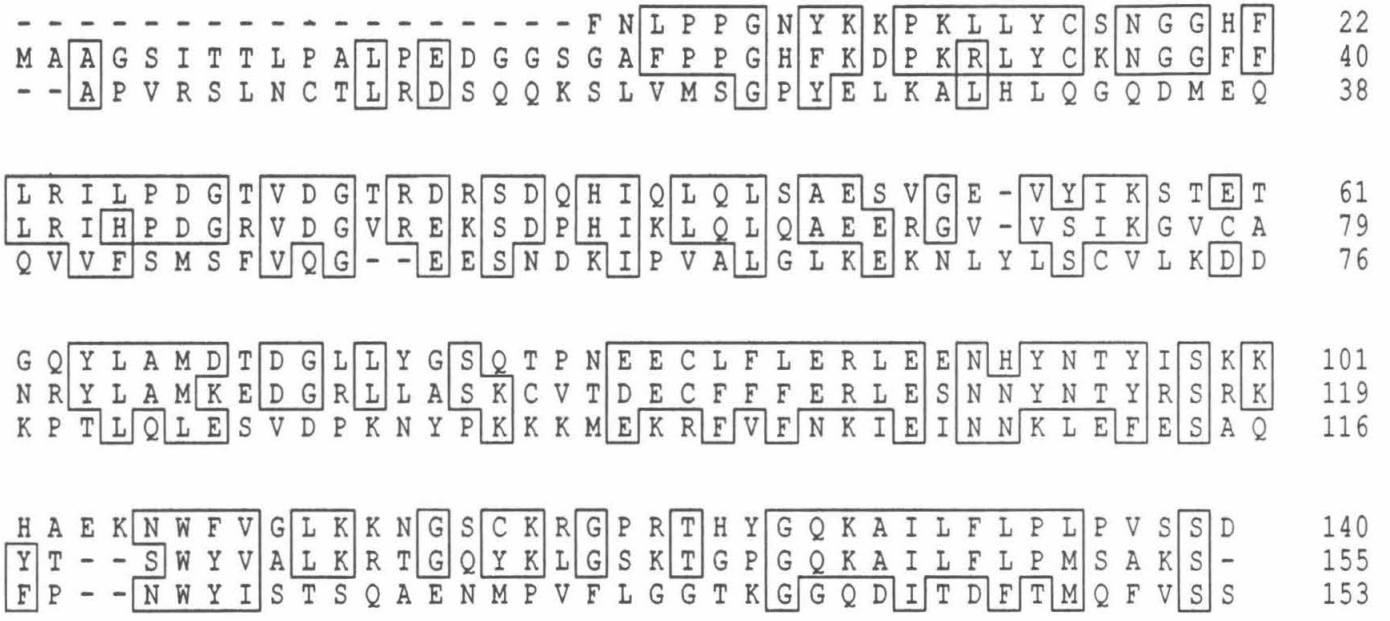

Figure 3.2 (B). Sequence alignment of human aFGF, bFGF and IL-1β.

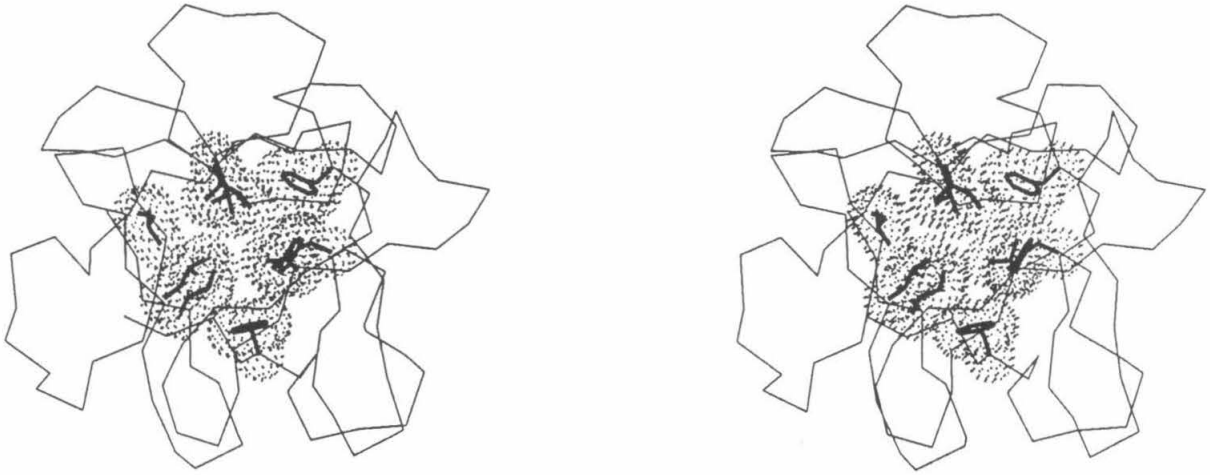

Figure 3.3. Stereoview of the Cα trace of aFGF. The van der Waals surface of the core hydrophobic residues is shown with dots.

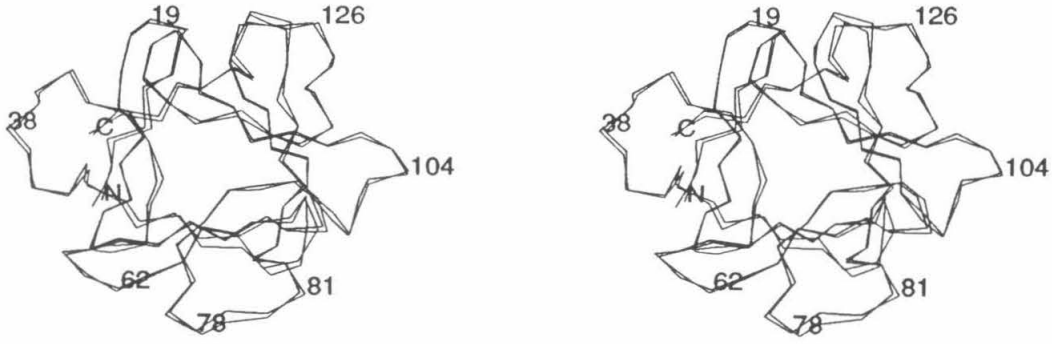

Figure 3.4. The Cα backbone superposition of the two aFGF molecules in one asymmetric unit.

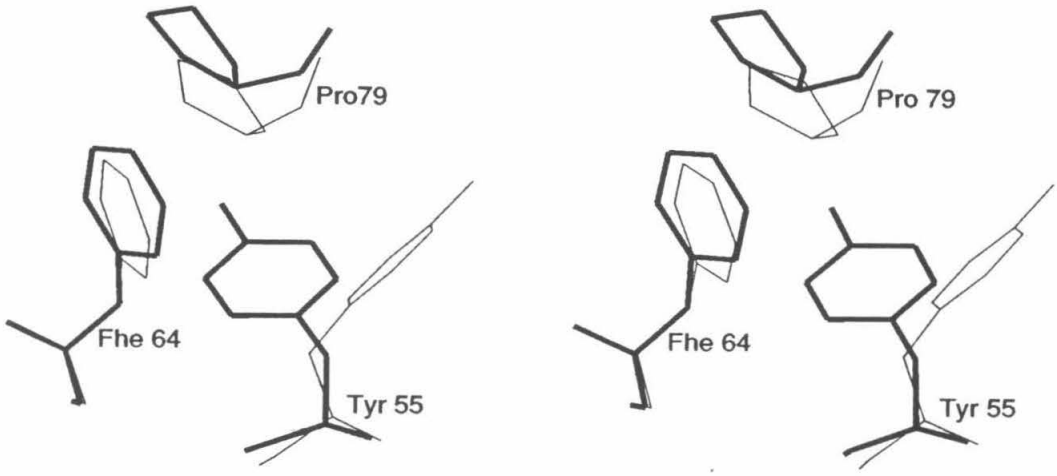

Figure 3.5. An example of side chain conformational difference caused by lattice contacts in the aFGF crystal. Residues with thick and thin lines are from the two aFGFs in one asymmetric unit after superposition.

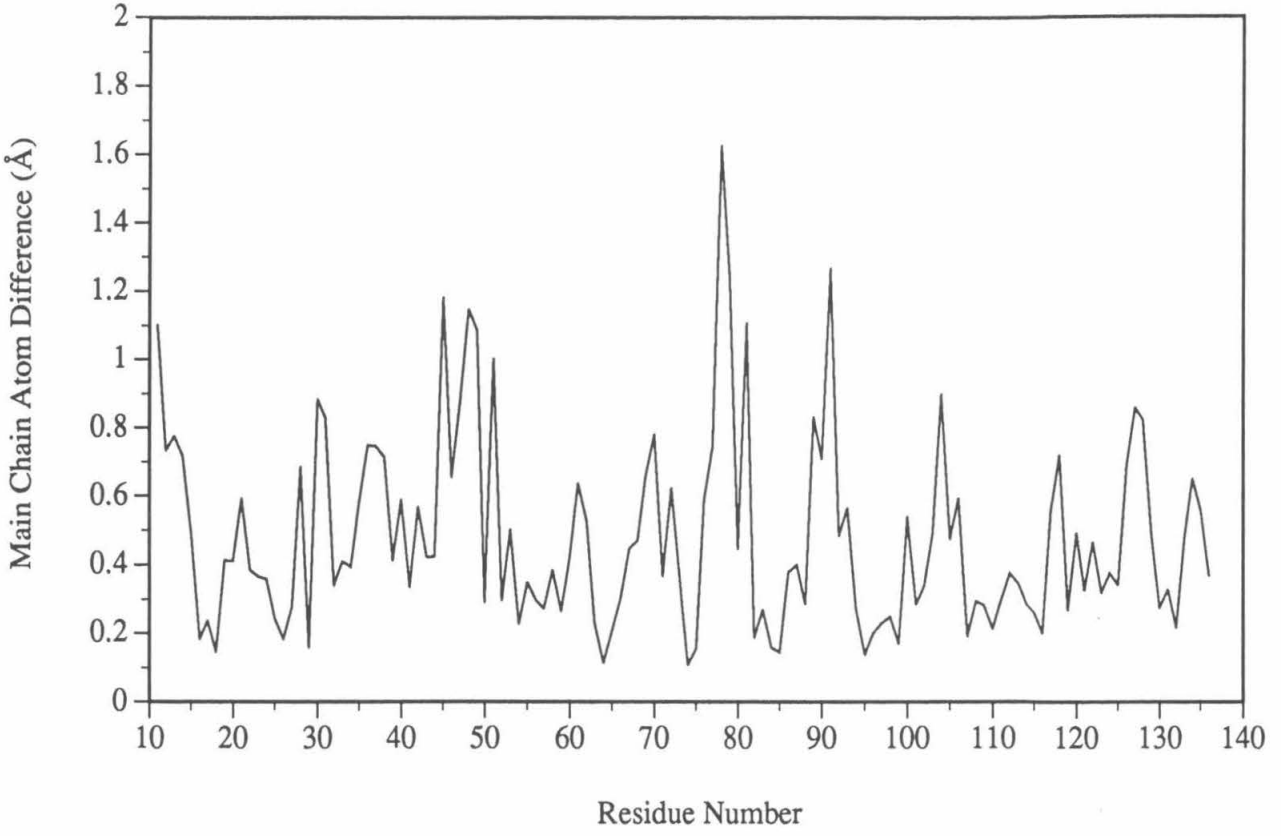

Figure 3.6. Difference in Cα position after superposition of the two aFGF molecules in the asymmetric unit.

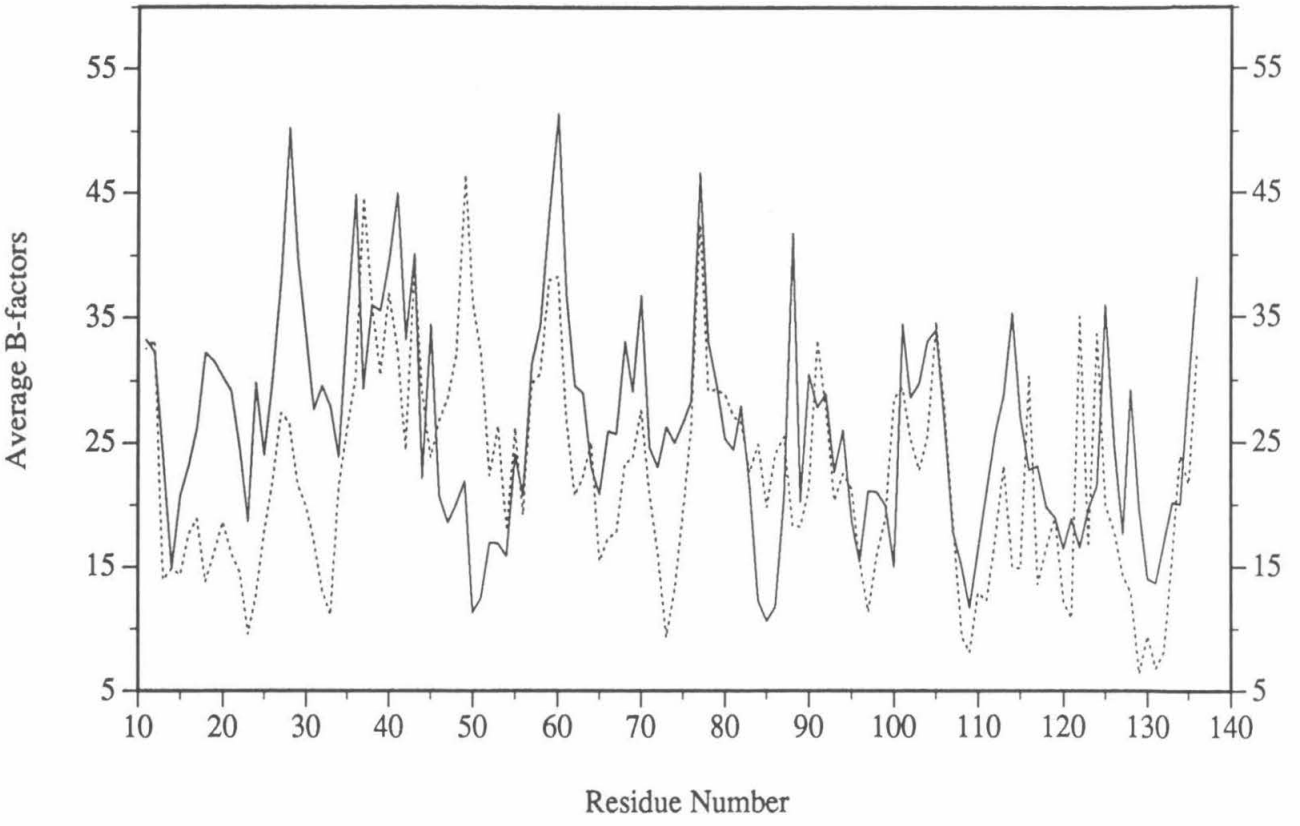

Figure 3.7. Temperature factor comparison between the two aFGFs in one asymmetric unit.

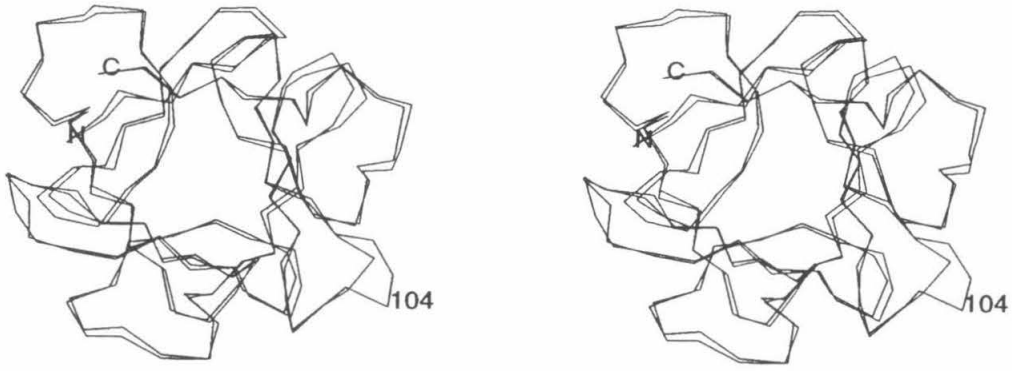

(A)

```
- - - - - - - - - - - - - - - - - - - - F N L P L G N Y K K P K L L Y C S N G G Y F    22
M A A G S I T T L P A L P E D G G S G A F P P G H F K D P K R L Y C K N G G F F    40

L R I L P D G T V D G T K D R S D Q H I Q L Q L C A E S I G E V Y I K S T E T G    62
L R I H P D G R V D G V R E K S D P H I K L Q L Q A E E R G V V S I K G V C A N    80

Q F L A M D T D G L L Y G S Q T P N E E C L F L E R L E E N H Y N T Y I S K K H   102
R Y L A M K E D G R L L A S K C V T D E C F F F E R L E S N N Y N T Y R S R K Y   120

A E K H W F V G L K K N G R S K L G P R T H F G Q K A I L F L P L P V S S D       140
T S - - W Y V A L K R T G Q Y K L G S K T G P G Q K A I L F L P M S A K S -       155
```

(B)

Figure 3.8. (**A**). Stereoview of backbone structures of superimposed aFGF and bFGF. aFGF residue 104 is labeled. (**B**). Sequence alignment of bovine aFGF (top) and human bFGF (bottom).

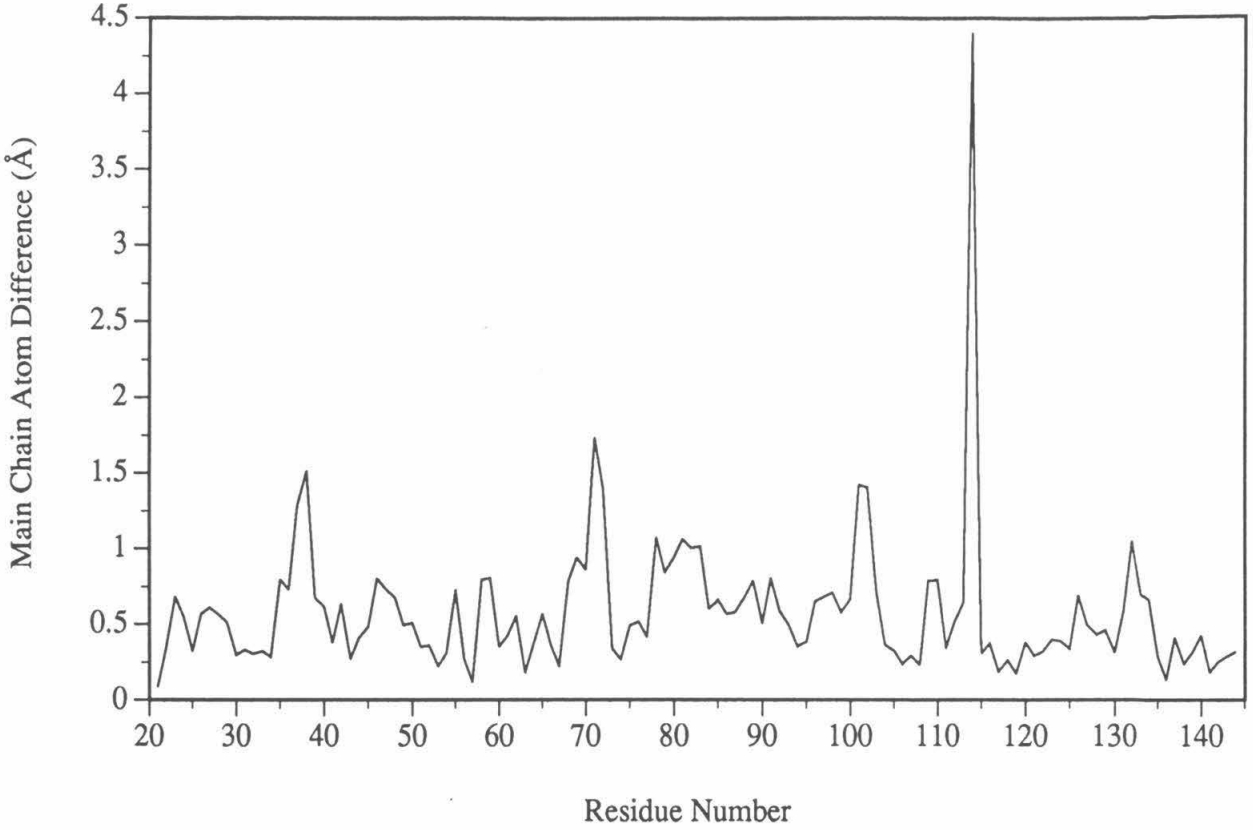

Figure 3.9. Difference in Cα position after superposition of aFGF and bFGF structures.

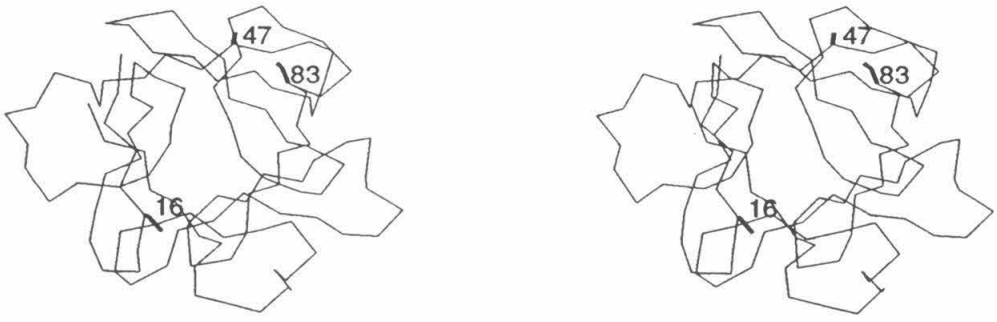

Figure 3.10. Locations of the three cysteines (residues 16, 47 and 83) present in the aFGF structure.

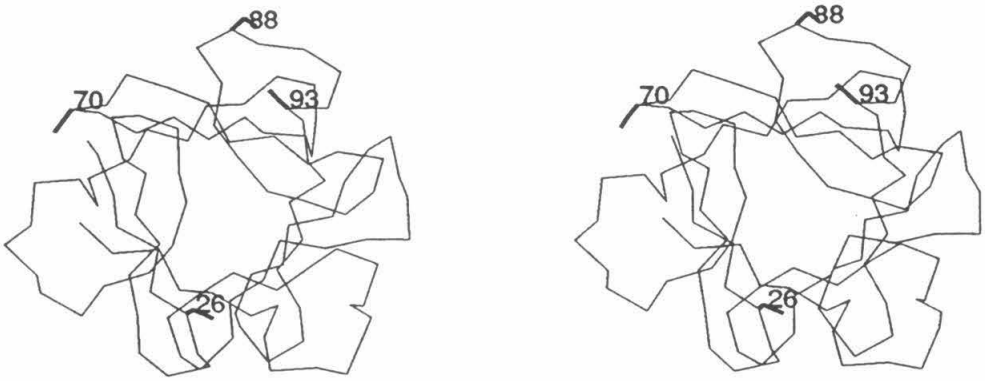

Figure 3.11. Cysteine locations in the bFGF structure (shown with the same orientation of aFGF in Figure 3.10).

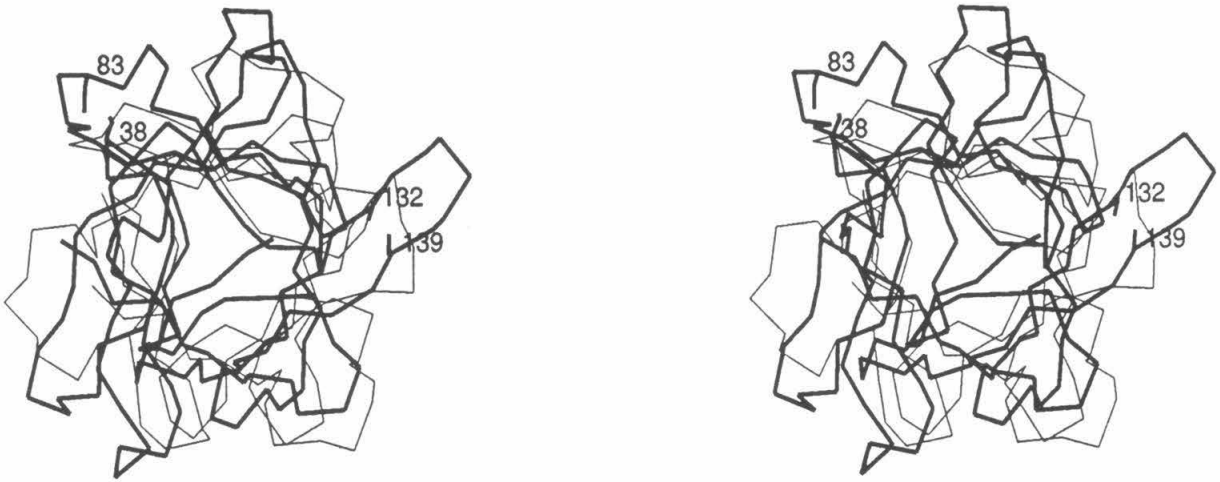

Figure 3.12. Superposition of ETI (thicker lines) and bFGF (thin lines) based on the core hydrophobic residues. The bFGF Cα trace has the same orientation as shown in Figure 3.11 where the four cysteines are marked. In ETI, two disulfide bonds are formed between the residues of 39-83 and 131-139.

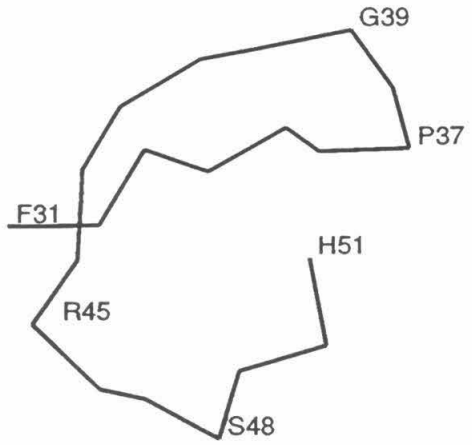

Figure 3.13. Backbone conformation of bFGF-(31-51), the N-terminal putative receptor binding site.

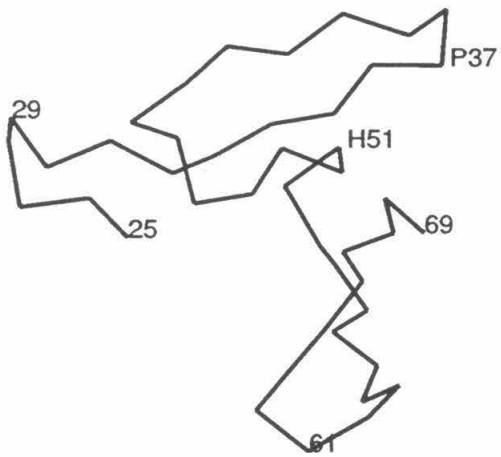

Figure 3.14. Backbone conformation of bFGF-(25-69).

```
          21.....31.....41
aFGF      Y F L R I L P D G T V D G T K D R S D Q H
bFGF      F F L R I H P D G R V D G V R E K S D P H
          31.....41.....51
```

(A)

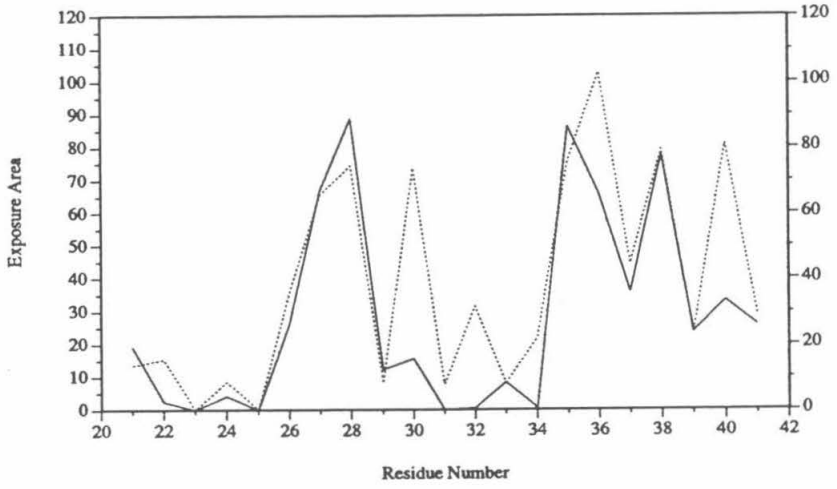

(B)

Figure 3.15. (**A**) Sequence alignment and (**B**) solvent accessible surface area of the N-terminal putative receptor binding regions in aFGF (solid line) and bFGF (dash line).

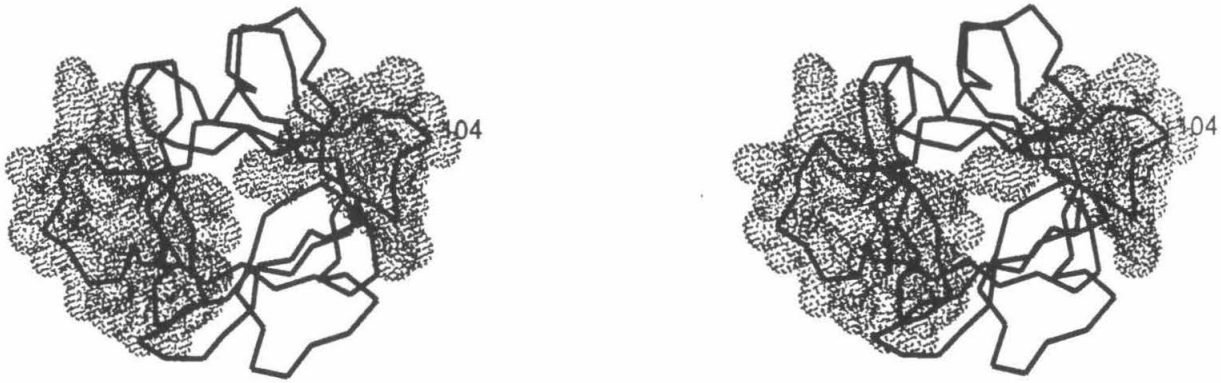

Figure 3.16. Location of the two aFGF functional domains implicated in receptor binding (shown with van der Waals surface).

```
KGF   NTYASAKWTHNGGE..............MFVALNQ
      95
AFGF  NTYISKKHA....EKH..............WFVGLKK
     104
BFGF  NTYRSRKYT....S................WYVALKR

INT2  NTYASRLYR....TGSSGPGAQRQPGAQRPWYVSVNG

FGF5  NTYASAIHR....TEKTGRE..........WYVALNK
```

Figure 3.17. Sequence comparison of KGF, aFGF, bFGF, int2 and FGF5 in the putative receptor binding region.

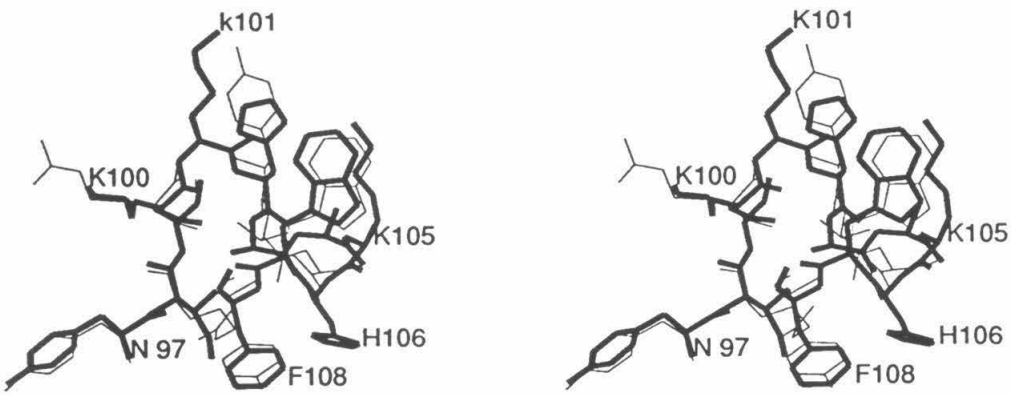

Figure 3.18. Stereoview of the putative C-terminal receptor binding site. bFGF (thin line) is superimposed to aFGF (thick line), based on the twelve β strands.

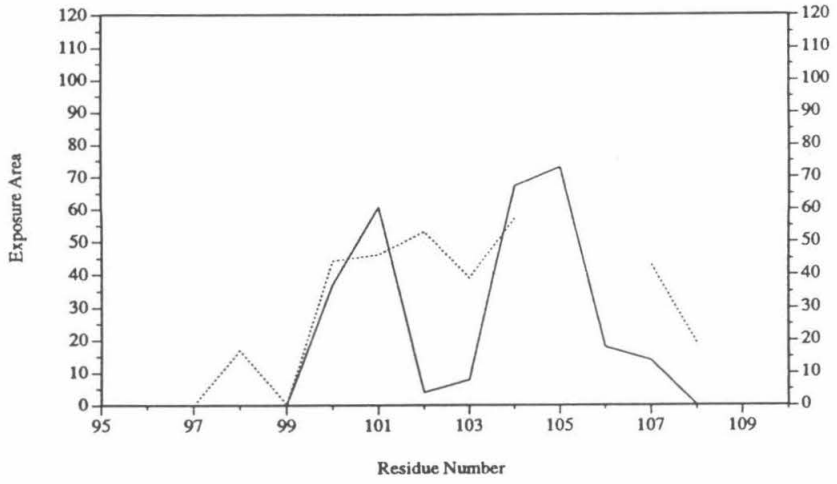

(A)

	97											108
aFGF	Y	I	S	K	K	H	A	E	K	H	W	F
bFGF	Y	R	S	R	K	Y	T	S	.	.	W	Y
	107											116

(B)

Figure 3.19. (**A**) Solvent accessibility comparison between aFGF and bFGF in the C-terminal putative receptor binding site. Interestingly, although aFGF has two more residues than bFGF at this putative receptor binding site, bFGF has a slightly larger solvent accessible area (318 $Å^2$) than aFGF (281 $Å^2$). (**B**) Sequence alignment of aFGF and bFGF at the C-terminal putative receptor binding site.

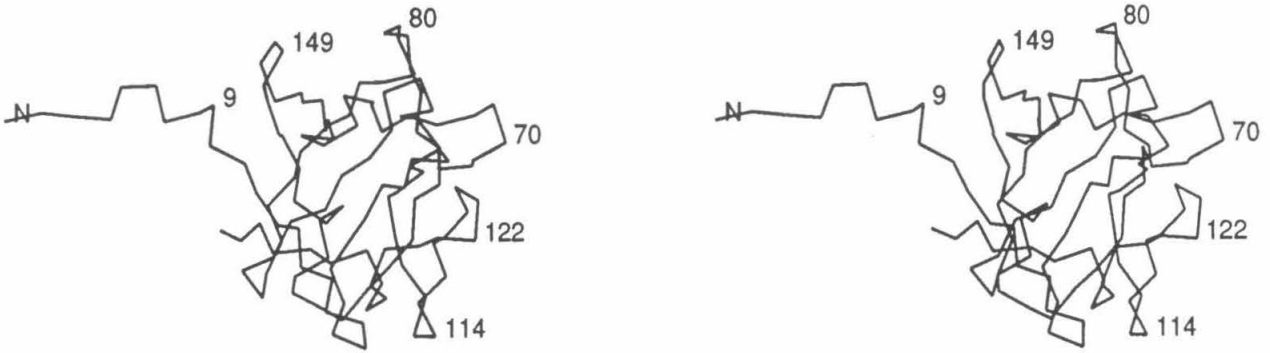

Figure 3.20. Stereoview of the Cα trace of residues 1-137, viewed with the internal threefold symmetry axis in the vertical plane.

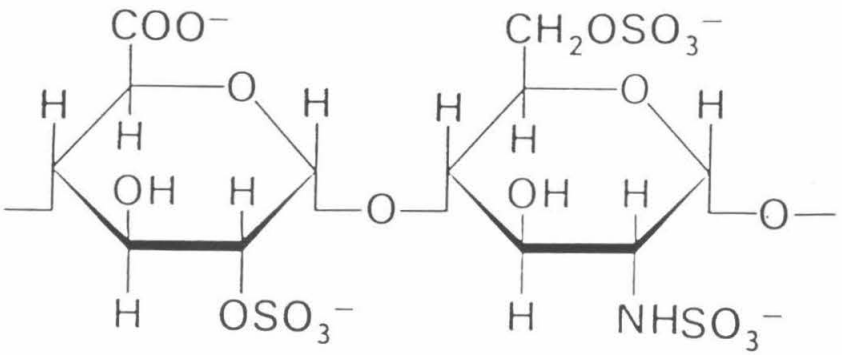

Figure 3.21. The major repeating unit of heparin.

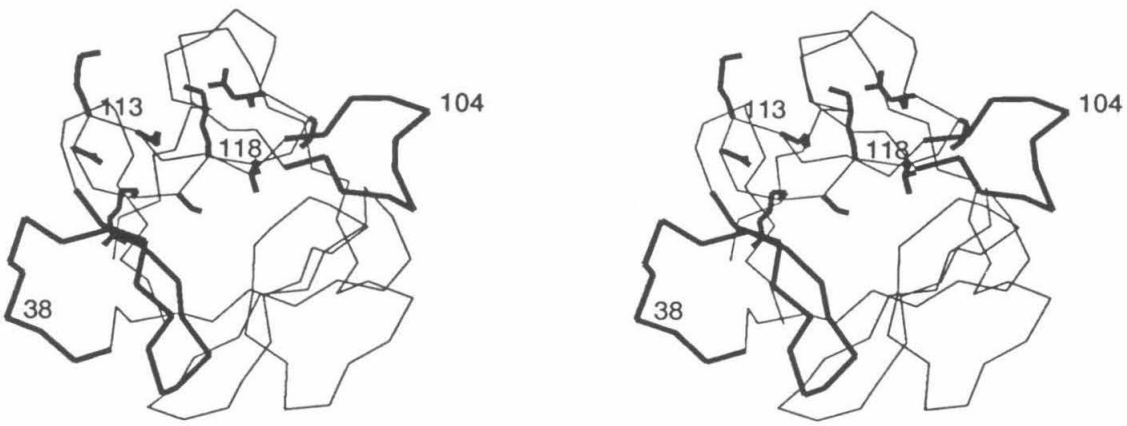

Figure 3.22. The putative heparin binding site (shown with side chains in the region from residue 112 to residue 122) and receptor binding sites (thick lines) mapped onto the aFGF structure.

References

1. J. P. Priestle, H-P. Schar, M. G. Grutter, *EMBO J.* **7,** 339 (1988).

2. B. C. Finzel, L. L. Clancy, D. R. Holland, S. W. Muchmore, K. D. Watenpaugh, H. M. Einspahr, *J. Mol. Biol.* **209,** 779 (1989).

3. B. J. Graves, M. H. Hatada, W. A. Hendrickson, J. K. Miller, V. S. Madison, Y. Satow, *Biochemistry* **29,** 2679 (1990).

4. E. Labriolatompkins, C. Chandran, K. L. Kaffka, D. Biondi, B. J. Graves, *Proc. Natl. Acad. Sci. USA* **88,** 1182 (1991).

5. J. Habazettl, D. Gondol, R. Wiltscheck, J. Otlewski, M. Schleicher, *Nature* **359,** 855 (1992).

6. S. Onesti, P. Brick, D. M. Blow, *J. Mol. Biol.* **217,** 153 (1991).

7. D. M. Blow, J. Janin, R. M. Sewell, *Nature* **249,** 52 (1974).

8. A. D. McLachlan, *J. Mol. Biol.* **133,** 557 (1979).

9. X. Zhu, H. Komiya, A. Chirino, S. Faham, G. M. Fox, T. Arakawa, B. T. Hsu, D. C. Rees, *Science* **251,** 90 (1991).

10. A. E. Eriksson, L. S. Cousens, L. H. Weaver, B. W. Matthews, *Proc. Natl. Acad. Sci. USA* **88,** 3441 (1991).

11. J. Zhang, L. S. Cousens, P. J. Barr, S. R. Sprang, *Proc. Natl. Acad. Sci. USA* **88,** 3441 (1991).

12. H. Ago, Y. Kitagawa, A. Fujishima, Y. Matsuura, Y. Katsube, *Biochemistry J.* **110,** 360 (1991).

13. F. Esch *et al., Biochem. Biophys. Res. Commun.* **133,** 554 (1985).

14. J. W. Harper, D. J. Strydom, R. R. Lobb, *Biochemistry* **25,** 4097 (1986).

15. T. Arakawa, Y-R. Hsu, S. G. Schiffer, L. B. Tsai, C. Curless, G. M. Fox, *Biochem. Biophys. Res. Commun.* **161,** 335 (1989).

16. G. M. Fox, S. G. Schiffer, M. F. Rohde, L. B. Tsai, A. R. Banks, T. Arakawa, *J. Biol. Chem.* **263,** 18452 (1988).

17. M. Seno, R. Sasada, M. Iwane, K. Sudo, T. Kurokawa, K. Ito, K. Igarashi, *Biochem. Biophys. Res. Commun.* **151,** 701 (1988).

18. T. Arakawa, T. P. Horan, L. O. Nahri, D. C. Rees, S. G. Schiffer, P. L. Holst, S. J. Prestrelski, L. b. Tsai, G. M. Fox (submitted).

19. A. Miyajima, T. Kotamura, N. haraka, T. Yokota, K. Arai, *Annual Review Immunology* **10**, 295 (1992).

20. A. Ullrich, J. Schiessinger, *Cell* **61,** 203 (1990).

21. A. M. De Vos, M. Ultsch, A. A. Kossiakoff, *Science* **255,** 306 (1992).

22. N. Q. McDonald, R. Lapatto, J. Murray-Rust, J. Gunning, A. Wlodawer, T. L. Blundell, *Nature* **354,** 411 (1991).

23. S. Daopin, K. A. Piez, Y. Ogawa, D. R. Davies, *Science* **257,** 369 (1992), and M. P. Schlunegger and M. G. Grutter, *Nature* **358,** 430 (1992).

24. J. Pandit, A. Bohm, J. Jancarik, R. Halenbeck, K.Koths, S-H. Kim, *Science* **258,** 1358 (1992).

25. P. L. Lee, D. E. Johnson, L. S. Cousens, V. A. Fried, L. T. Williams, *Science* **245,** 57 (1989).

26. M. Ruta *et al., Oncogen* **3,** 9 (1988).

27. T. Miki *et al., Proc. Natl. Acad. Sci. USA* **89,** 246 (1992).

28. A. Yayon, Y. Zimmer, G-H. Shen, A. Avivi, Y. Yarden, D. Givol, *EMBO J.* **11,** 1885 (1992).

29. S. Kornbluth, K. E. Paulson, H. Hanafusa, *Mol. Cell. Biol.* **8,** 5541 (1988).

30. E. B. Pasquale, S. J. Singer, *Proc. Natl. Acad. Sci. USA* **86,** 5449 (1989).

31. C. A. Dionne *et al., EMBO J.* **9,** 2685 (1990).

32. A. Avivi, Y. Zimmer, A. Yayon, Y. Yarden, D. Givol, *Oncogene* **6,** 1089 (1991).

33. K. Keegan, D. E. Johnson, L. T. Williams, M. J. Hayman, *Proc. Natl. Acad. Sci. USA* **88,** 1095 (1991).

34. J. Partanen, T. P. Makela, E. Eerola, J. Korhonen, H. Hirvonen, L. Claesson-Wilsh, K. Alitalo, *EMBO J.* **10,** 1347 (1991).

35. V. Raz, Z. Kelman, A. Avivi, G. Neufeld, D. Givol, Y. Yarden, *Oncogene* **6,** 753 (1991).

36. H. H. Reid, A. F. Wilks, O. Bernard, *Proc. Natl. Acad. Sci. USA* **87,** 1596 (1990).

37. J. Hou, M. Kan, K. McKeehan, G. McBride, P. Adams, W. L. McKeehan, *Science* **251,** 665 (1991).

38. A. Baird, D. Schubert, N. Ling, R. Guillemin, *Proc. Natl. Acad. Sci. USA* **85,** 2324 (1988).

39. J-T. Feige and A. Baird, *Proc. Natl. Acad. Sci. USA* **86,** 3174 (1989).

40. R. Friesel and T. Maciag, *Biochem. Biophys. Res. Comm.* **151,** 957 (1988).

41. D. Moscatelli, *J. Cell Biol.* **107,** 753 (1988).

42. H. Sano *et al.*, *J. Cell Biol.* **110,** 1417 (1990).

43. C. Dingwall and R. A. Laskey, *Annu. Rev. Cell Biol.* **2,** 367 (1986).

44. T. Imamura *et al.*, *Science* **249,** 1567 (1990).

45. Y. Nakanishi, K. Kihara, K. Mizuno, Y. Masamune, Y. Yoshitake, K. Nishikawa, *Proc. Natl. Acad. Sci. USA* **85,** (1992).

46. K. Sakaguchi, M. Yanagishita, Y. Takeuchi, G. D. Aurbach, *J. Biol. Chem.* **266,** 7270 (1991).

47. A. Yayon, M. Klagsbrun, J. D. Esko, P. Leder, D. M. Ornitz, *Cell* **64,** 841 (1991).

48. A. C. Rapraeger, A. Krufka, B. B. Olwin, *Science* **252,** 1705 (1991).

49. E. Ruoslahti and Y. Yamaguchi, *Cell* **64,** 867 (1991).

50. D. Gospodarowicz and J. Chen, *J. Cell Physiol.* **128,** 475 (1886).

51. O. Saksela, D. Moscatelli, A. Sommer, D. B. Rifkin, *J Cell Biol.* **107,** 743 (1988).

52. R. Ishai-Michaeli, A. Eldor, I. Vlodavsky, *Cell Regul.* **1,** 833 (1990).

53. R. Ishai-Michaeli *et al., Biochemistry* **31,** 2080 (1992).

54. J. Sudhalter, J. Flokman, C. M. Svahn, K. Bergenda, P. A. D'Amore, *J. Biol. Chem.* **264 ,** 6892 (1990).

55. D. M. Ornitz, A. Yayon, J. G. Flanagan, C. M. Svahn, E. Levi, P. Leder, *Mol.& Cell. Biol.* **12,** 240 (1992).

56. M. Seno, R. Sasada, T. Kurokawa, K. Igarashi, *Eur. J. Biochem.* **188,** 239 (1990).

57. J. W. Harper and R. R. Lobb, *Biochemistry* **27,** 671 (1988).

58. R. R. Lobb, *Biochemistry* **27,** 2572 (1988).

59. W. H. Burgess, A. M. Shaheen, M. Ravera, M. Jaye, P. J. Donohue, U. A. Winkes, *J. Cell Biol.* **111,** 2129 (1990).

Chapter 4

Interactions of FGF with Sucrose Octasulfate and an Implied Receptor Binding Mechanism

4.1. Introduction

Although sucrose octasulfate has long been known to promote tissue repair, its therapeutical mechanism is unclear. Used in the treatment of stomach ulcers, sucrose octasulfate is unique in that the effectiveness appears not to involve an adjustment of the stomach pH (1). Based on its polyanionic property and its structural similarity to heparin disaccharide, Folkman *et al.* tested the binding affinity of FGF to sucrose octasulfate and found that it can bind sucrose octasulfate more tightly than it binds heparin (2). As with the FGF and heparin complex, bFGF bound to sucrose octasulfate remains stable even at low pH and exhibits enhanced mitogenic activity to various tissue ulcers (2). Recently sucrose octasulfate has been shown to induce the same small but highly reproducible spectroscopic changes in bFGF as heparin does, further suggesting that heparin and sucrose octasulfate interact similarly with bFGF (3). To better characterize the specific interaction between sucrose octasulfate and FGF, crystallographic studies of the FGF and sucrose octasulfate complex have been performed. In addition, the three-dimensional structure of sucrose octasulfate bound to FGF may provide a structural basis for understanding the binding of FGF to heparin as well as to its receptor in the presence of heparin.

4.2. Structure determination of the aFGF and sucrose octasulfate complex

Both the single (Ala47Cys) and double (Ala47Cys, Gly93His) mutant aFGF samples exhibit comparable mitogenic activity to the wild type and were used in cocrystallization trials. Low ionic strength precipitant solutions in the presence of 3.3 mM sucrose octasulfate were used in the factorial screening (4). Cocrystals were obtained with both aFGF mutants by the vapor diffusion method. Hanging drops contained equal volumes of a 10 mg/ml protein solution and reservoir buffer (0.1 M $MgCl_2$, 27.5% PEG8K, 0.1 M ADA, pH 6.5 and 3.3 mM sucrose octasulfate). While only small crystals of the [Ala^{47}, Gly^{93}] aFGF analog were obtained using this

condition, the [Ala^{47}] aFGF analog yielded crystals approximately 0.5 x 0.5 x 0.5 mm^3 in size with a trigonal morphology. The crystals of the [Ala^{47}] aFGF analog were therefore used in the following structural studies. Precession photographs revealed that these crystals belong to the space group $P3_121$ or $P3_221$ with unit dimensions of a = b = 55.3 Å and c = 86.1 Å.

Intensity data were collected on a Siemens multiwire area detector mounted on an 18-kW rotating anode generator and were indexed with the XENGEN programs (5). The cell constants provided by the autoindexing program were a = b = 110.6 Å and c = 172.2 Å, which were exactly twice of those obtained from precession photographs. Attempts to index the data using the initial small cell constants (a = b = 55.3 Å and c = 86.1 Å) failed to index a large fraction of the data, supporting the correctness of the XENGEN cell constants. Due to the larger dimensions of cell constants, the structure determination became more difficult. While the smaller unit cell contains only one protein molecule in one asymmetric unit, the larger unit cell contains eight molecules per asymmetric unit.

Nevertheless, when the intensities of reflections were examined, the processed data showed a general pattern at low resolution of large intensities for reflections with even indices and small intensities for reflections with odd index (Table 4.1). Together with the observation that only the smaller cell constants were found on the precession photographs, it appeared that the crystal form with the larger unit cell could be thought of as containing the equivalent of eight smaller unit cells related approximately by translations of one half along the a, b, and c axes in the larger unit cell. Yet these are not exact relationships, otherwise all reflections with any odd index would have intensities exactly equal to zero.

Because the reflections with odd index are much weaker than those with even indices, the molecular replacement search was first attempted in the smaller unit cell where there is only one molecule per asymmetric unit. A new data set was generated

by removing all reflections with odd h, k or l, and dividing by a factor of two the even indices of the remaining reflections. The search model used in the molecular replacement was the 2.7 Å resolution aFGF structure (Ala47Cys, Gly93His) previously determined in Rees' laboratory [Chapter 3 and (6)]. By using the reflections within the resolution of 5 - 8 Å, a rotation function solution was obtained with the Patterson correlation refinement program (7). After the aFGF model was properly oriented, the translation search was carried out in both $P3_221$ and $P3_121$ because of the enantimorph ambiguity. The translation search in $P3_121$ yielded a solution with an R-factor of 44% (7.2 σ peak height), while for $P3_221$ the best R-factor obtained was 51% (4.6 σ peak height). The correct molecular replacement solutions were later confirmed by the binding sites of heavy atom derivatives (see below). The Hg binding site of EMTS is just near the only exposed cysteine in the [Ala^{47}] aFGF analog, whereas K_2PtCl_4 was found to bind to His 124, His 106, and Arg 122. Furthermore, the heavy atom binding sites calculated in a difference Fourier map using the molecular replacement phases gave peaks that were consistent with the difference Patterson map.

Although the difference Fourier electron density map calculated with the molecular replacement phases showed the heavy atom binding sites on aFGF, no obvious difference peaks corresponding to the bound sucrose octasulfate molecule were found. In addition, there was little density for the side chain of His 93, suggesting that the averaged structure in the smaller unit cell, though close enough to simplify the initial molecular replacement search, was not accurate for high resolution analysis. Therefore the whole cell was generated by translating the molecular replacement model along a, b and c by one half of the larger cell constants so that one asymmetric unit contained eight molecules. The space group also changed from $P3_121$ to $P3_221$ when the c axis was doubled. Real space rigid body refinement against the EMTS single isomorphous replacement phases was then carried out using

TNT (8), which lowered the R-factor to 34.9% at 3.5 Å resolution. Several more cycles of positional refinement further lowered the R-factor to 27.1%. Using the phases from this model, an F_o-F_c map was calculated. Encouragingly, a large difference peak was found near Lys 118, possibly corresponding to the bound sucrose octasulfate. However the density was still not sufficiently resolved to unambiguously model the sucrose octasulfate. Therefore, to further improve the electron density, a second heavy atom derivative data set (K_2PtCl_4) was collected. The K_2PtCl_4 binding sites were located in a difference Fourier map using the refined model phases. The MIR phases were subsequently calculated with HEAVY (9) by refining the heavy atom sites against the difference Patterson map (Table 4.2). These phases were then combined with the molecular replacement phases. Although the overall map quality improved slightly after phase combination, the regions near the His 93 side chain and sucrose octasulfate remained unchanged, probably due to the poor quality of the MIR phases. The figure of merit for the MIR phases was only 0.33 to 3.0 Å (See Table 4.2).

To further improve the phases, eight-fold molecular averaging was carried out (10). The general noncrystallographic symmetry relations between the eight molecules in the asymmetric unit were obtained from the refined model. After a sucrose octasulfate molecule was roughly positioned according to the difference map, a molecular envelope was generated by placing 4.0 Å spheres at each atomic position of sucrose octasulfate and 2.4 Å spheres around each protein atom except those in residue 93. Since the search model has a glycine at position 93 (6), 6 Å spheres were used for this residue. Phases were then iteratively refined by molecular averaging by starting from the MIR phases. Averaging at 3 Å resolution converged to a final R-factor of 22.5% between the F_{obs}s and F_{calc}s. The quality of the electron density map after averaging was greatly improved. This is exemplified by a region near His 93 where no side chain density was evident before averaging (Figure 4.1).

In the averaged map, the six-membered ring of sucrose octasulfate has relatively well-defined density, while the five-membered ring is partially disordered. After a model of glucose tetrasulfate was fitted into the averaged map, iterative manual adjustments and positional refinement were performed. The electron density map phased by the combined model and averaged phases revealed improved density for the five-membered ring and some of the sulfate groups. After gradual addition of more sulfate groups and more cycles of positional and temperature factor refinement, the entire sucrose octasulfate was successfully modeled (Figure 4.2). The present model without solvent molecules has an R-factor of 20.4% using all the data to 2.7 Å resolution. The r.m.s. deviations from ideal bond distances and angles are 0.016 Å and 2.7°, respectively.

4.3. Structure of the aFGF and sucrose octasulfate complex.

Sucrose octasulfate binds aFGF in the region around Lys 118 (Figure 4.3), which is the largest region rich in positively charged residues in both the acidic and basic FGF crystal structures (6,11-13). The region of aFGF involved in sucrose octasulfate binding spans the residues from Lys 112 to Gln 127. In addition, one N-terminal residue, Asn 18, also interacts with the bound ligand. Overall, aFGF bound to sucrose octasulfate has a very similar backbone conformation to that of aFGF alone. Superposition of 126 α-carbons from the structures of aFGF and aFGF bound to sucrose octasulfate shows an r.m.s. difference of only 0.50 Å. There are, however, some large side chain conformational changes in the sucrose octasulfate binding region. Arg 116 and His 124 are two such examples of residues whose side chains are moved for interacting with the bound sucrose octasulfate (Figure 4.4).

The detailed interactions between aFGF and sucrose octasulfate are shown in Figure 4.5. Lysine 118 has the most intensive interactions with sucrose octasulfate, forming hydrogen bonds with two sulfate groups from the six-membered ring and

also form salt bridges to two more sulfate groups from the five-membered ring. In addition to Lys 118, Lys 112 is also hydrogen bonded with two sulfates from each sugar ring and interacts electrostatically with another sulfate. Surprisingly, the side chain of the adjacent residue, Lys 113, is disordered in the complex structure and does not seem to interact specifically with sucrose octasulfate. However, its main chain amide is hydrogen bonded to sucrose octasulfate. Another amino acid interacting with more than one sulfate group is Arg 122, which binds sucrose octasulfate through the two sulfate groups from the five-membered ring. Furthermore, in addition to these positively charged residues, amino acids Asn 18, Arg 116 and Gln 127 are also involved in interactions with sucrose octasulfate.

The overall structures of the eight protein molecules in the asymmetric unit are very similar. Each of the eight aFGFs binds to a single sucrose octasulfate except one which also has weak interactions with a neighboring aFGF. On the other hand, the eight sucrose octasulfate molecules bound to the eight aFGF molecules are however more diverse. Comparison of the eight sucrose octasulfate molecules based on the superposition of aFGF α-carbons shows that both the sulfate groups and the sugar rings, especially the five-membered ring, can adopt different conformations. Additionally, the orientation and position of sucrose octasulfate bound to aFGF also shows slight variation in the superposition (Figure 4.6). In spite of the differences discussed above, the protein residues and the sulfate groups of sucrose octasulfate that are involved in binding are in general similar in all the eight complexes, although some details of the hydrogen bonds and electrostatic interactions vary in different complexes of aFGF and sucrose octasulfate.

Based on the sequence alignment of acidic and basic FGF, most residues of aFGF that are involved in binding to sucrose octasulfate are also likely to be involved in bFGF binding to sucrose octasulfate (Figure 4.7). The three aFGF basic residues that play critical roles in binding sucrose octasulfate are Lys 112, Lys 118, and Arg 122.

The analogous residues in bFGF are Lys 120, Lys 126 and Lys 130, respectively. Residues Asn 18 and Gln 127, which also contribute to sucrose octasulfate binding, are conserved in bFGF as well. The only nonconserved amino acid in aFGF binding to sucrose octasulfate is Arg 116, which is a glutamine in bFGF. Nevertheless, superposition of acidic and basic FGF suggests that the side chain amide groups of Gln 124 in bFGF and Arg 116 in aFGF could play an equivalent role in interacting with sucrose octasulfate.

The crystal structure of the complex between aFGF and sucrose octasulfate described here is consistent with biochemical studies of FGF binding to heparin. The biological importance of the two basic residues Lys 118 and Arg 122, which are shown in the complex structure to be critical in interacting with sucrose octasulfate, have been previously reported. Reductive methylation of aFGF occurs mainly on Lys 118 and yields 90% modification of this residue. The methylated aFGF exhibits a reduced binding capacity to heparin as well as a lower mitogenic activity to Balb/C3TL cells (14). Similar results were obtained by site directed mutagenesis when lysine 118 was replaced by a glutamate (15). Arginine 122, which is adjacent to Lys 118 in the tertiary structure, has been shown to be a thrombin cleavage site and its digestion can be blocked by the presence of heparin (16). By modeling in the major repeating unit of heparin to mimic sucrose octasulfate binding to aFGF, Glc(6-OSO_3) and Ido(5-CO_2) of heparin, but not Ido(2-OSO_3), appear to be able to make contacts with aFGF similar to those made by sucrose octasulfate. In addition, Glc(2-NSO_3) is very likely to interact with more than two residues of aFGF simultaneously. This is consistent with the observation that N-sulfate groups are critical for heparin binding to FGF by using a series of depolymerized and size-homogeneous heparin oligomers (17). The evidence of the structural and biochemical similarity of FGF binding to heparin and to sucrose octasulfate shown here strongly suggests that the interactions between aFGF and sucrose octasulfate are likely to be applicable to the

understanding of the interactions between the heparin polysaccharide and FGF. Because of the different molecular size and degree of sulfation between heparin and sucrose octasulfate, additional heparin binding sites are likely to be present on aFGF and will be discussed further in the following sections.

4.4. FGF binding to heparin polysaccharide

The minimum size of heparin required for FGF binding has been extensively studied by many groups (17-19). Octasaccharides (i. e., eight sugar units) have been demonstrated to be the shortest fragment that can bind FGF and facilitate FGF binding to its receptor. Furthermore, it has been recently reported that bFGF can be cross-linked as a dimer with the addition of heparin oligosaccharides, suggesting dimerization of bFGF may occur in the presence of heparin (19).

From fiber diffraction studies, heparin forms a helical structure with a repeat distance of approximately 17 Å and four sugar rings per turn (20). Therefore a heparin octasaccharide bound to two FGF molecules should span a linear distance of about 34 Å. In the cocrystals of the aFGF and sucrose octasulfate complex, there is only one type of aFGF dimer found in the crystal packing, where the bound sucrose octasulfate molecules could be replaced by a linear heparin helix without penetrating the protein molecules (Figure 4.9). The distance between the two bound sucrose octasulfates is 18 Å, which suggests that four more sugar units of heparin could be accommodated between them. Including the two independently bound sucrose octasulfate, this results in a polysaccharide with eight sugar units, which is exactly the smallest size of heparin fragment required to bind two FGFs (19). Indeed, when an octasaccharide (without any sulfate groups) was built so as to have a helical heparin conformation and moved into the aFGF dimer to replace the two bound sucrose octasulfates, a reasonable fit was observed (Figure 4.10). Further, this hypothetical structure shows that Lys 35 from each of the aFGF monomers has its side chain

pointing towards the center of the octasaccharide and are likely to interact with heparin.

The two monomers of this aFGF dimer that may bind heparin octasaccharide (Figure 4.10) are related by a non-crystallographic two fold axis. They are brought together mainly by interactions at the two ends of the molecular interface. Arg 116, which displays large side chain conformational change compared to the native aFGF structure, forms three hydrogen bonds with Asp 36 and Ser 38 of the neighboring aFGF molecule. In addition, salt bridges are formed between Arg 24 (molecule 1) and Asp 32 (molecule 2), and also possibly between Asn 114 (molecule 1), Lys 35 and Asp 37 (molecule 2) from two different aFGF monomers. Due to the approximate two fold symmetry relationship of the monomers, this interaction pattern is repeated at the other end of the dimer which thereby multiplies the intermolecular association affinity.

In this dimer structure, a single sucrose octasulfate does not bind two aFGFs simultaneously to directly cause the dimerization. Instead, the conformational change at Arg 116 leads to six new hydrogen bonds and several salt bridges, which could be the major driving force for the dimerization. Based on this observation, as well as the fact that intermolecular interactions shown in this aFGF dimer have never been observed in the crystal forms without sucrose octasulfate (6, 9-11), it is probable that sucrose octasulfate can dimerize FGF in solution and that the dimerization interaction observed here could be physiologically relevant. This idea is supported by our recent observation that bFGF can be cross-linked in the presence of sucrose octasulfate (see Appendix).

4.5. Possible mechanism of FGF binding to the receptor

While the stoichiometry of FGF binding to its receptor is still unclear, it has been shown that cross-linking of FGF to its receptor results in a complex with a molecular

weight equivalent to one FGF plus one receptor, suggesting that each FGF possibly binds only one receptor (21, 22). This contradicts the possibility that two structurally distinct sites on a single FGF molecule may interact with two FGF receptor simultaneously (6, 9, 10, 11, 29). Recently, the binding mechanism of FGF to its receptor became even more complicated by the discovery that FGF binding to the receptor can occur only in the presence of heparin (23). Based upon this observation, as well as the identification of different putative receptor and heparin binding sites on FGF (Figure 4.8), it has been proposed that binding to heparin may result in significant conformational changes in FGF to induce the subsequent high affinity binding of FGF to its receptor (23). However the structure of aFGF in complex with the heparin analog sucrose octasulfate does not appear to support this hypothesis. Since no striking conformational change is observed in aFGF when it is bound to sucrose octasulfate, it is unlikely that large conformation changes in aFGF are prerequisite to receptor binding.

Unlike dimeric peptide growth factors, such as PDGF and NGF, which can simultaneously bind two receptors to induce autophosphorylation of the receptor tyrosine kinase (24), FGF is a monomer and the attempts to trap FGF dimers in solution have so far been unsuccessful (T. Arakawa, personal communication). Recently, the observation of bFGF dimers in solution following the addition of heparin was reported (19). The transformation of FGF from a monomeric ligand to a dimeric ligand in the presence of heparin provides the possibility that FGF may interact with its receptor as a dimer, and hence cause the dimerization of two FGF receptors. While the FGF dimer structure formed in the presence of heparin is not known, the structure of aFGF and sucrose octasulfate complex may provide a reasonably analogous model (Figure 4.9 and 4.10).

In this hypothetical model of the dimeric aFGF bound to a heparin octasaccharide, the two FGF monomers are related by a non-crystallographic two-fold symmetry axis.

Examples of other dimeric growth factors with a two-fold axis relating each monomer have been demonstrated in the crystal structures of NGF, TGF-β and M-CSF (25-28), The interface of this aFGF dimer consists mainly of the region containing aFGF-(21-41), a peptide which has been reported to be important for receptor binding (29). On the other hand, the second putative receptor binding site, aFGF-(97-108), is located at the two ends of the dimer (Figure 4.11). Several lines of evidence suggest that the region of aFGF-(97-108) is important for FGF binding to its receptor. For example, bFGF Thr 113 (corresponding to aFGF Ser 103), which is located in this region, can be phosphorylated by protein kinase A. The phosphorylated bFGF exhibits an enhanced binding affinity to the FGF receptor (30). Although, in general FGF is a highly homologous protein family with infrequent sequence insertions, the area between aFGF-(97-108) is an exception. KGF and aFGF have four and two residue than bFGF respectively at this site while the two oncogenes int2 and FGF5 have an addition of 7 to 14 amino acids compared to bFGF. The high frequency of sequence insertions here suggests the functional importance of this site. Indeed while aFGF and KGF can interact with the same type of receptors, bFGF is shown to be unable to bind KGF receptors (31), which further supports the idea that receptor binding specificity is probably defined in this region.

aFGF-(97-108) has a similar solvent accessible surface area in the aFGF dimer as compared to its monomeric state. Each of these two identical sites located on the two faces of the dimer could bind one FGF receptor respectively, thereby dimerizing two FGF receptors (Figure 4.11). On the other hand, aFGF-(21-41) is fairly buried in the dimer interface and would be shielded from interaction with the FGF receptors. In fact, after dimerization, about 300 $Å^2$ is buried at the interface of the aFGF dimer. Based on this hypothetical dimer structure, aFGF-(21-41) may not contain the real receptor binding region. Instead, it may be required to form the intermolecular interface of the dimer which can then subsequently bind two FGF receptors (Figure

4.11). This model may explain why the peptides aFGF-(21-41) and aFGF-(97-108) are both able to inhibit FGF from interacting with its receptor. While the peptide aFGF-(21-41) may block FGF from binding to the receptor by disrupting formation of an FGF dimer which is required for FGF receptor binding, the peptide aFGF-(97-108) could have direct interaction with the receptor and compete with FGF for binding to the receptor.

Appendix

FGF dimerization facilitated by sucrose octasulfate

Since bFGF has been shown to cross-link as a dimer in the presence of heparin oligosaccharides (19), we attempted an analogous experiment in the presence of sucrose octasulfate. A similar cross-linking experiment procedure was followed, except that non-radiolabeled bFGF was used. FGF cross-linking experiments were carried out at room temperature in 0.5 ml microcentrifuge tubes. FGF and sucrose octasulfate were mixed to a final concentration of 1.6 mg/ml and 0.045 mg/ml, respectively, in a volume of 40 μl. The mixture, also containing 140 mM NaCl, 20 mM $NaPO_4$ (pH 7.4) and 0.025 mM β-mercaptoethanol, was incubated for half an hour. 1.5 μl disuccinimidyl suberate, dissolved in DMSO to a concentration of 20 mM, was then added to the mixture. After another 30 minutes, the reaction was quenched with 10 μl ethanolamine-HCl (3.85 M and pH 8.0). The final mixture was incubated for an additional 30 minutes and subjected to 12.5% SDS-PAGE. The polypeptide bands were visualized by Coomassie stain.

The analog of [Ser^{70}, Ser^{88}] bFGF, which exhibits equal activity to the native bFGF, was used in the cross-linking experiment. Because a fraction of the protein sample has been dimerized through intermolecular disulfide bonds, β-mercaptoethanol was added to the reaction solution in order to fully reduce the disulfide bridges. In the absence of sucrose octasulfate, no significant bFGF dimers was detected after addition of the cross-linking reagent DSS (Figure 4.12, lane 4). However, bFGF dimerization was observed to occur when sucrose octasulfate was added (Figure 4.12, lane 3). Sucrose octasulfate has been demonstrated to be functionally similar to heparin before. This cross-linking experiment further demonstrates the functional similarity of sucrose octasulfate to heparin.

A similar experimental procedure was also applied to aFGF, except that the concentration of aFGF used was about 1.3 mg/ml. No cross-linked aFGF was

observed (Figure 4.12, lane 1 and 2), even after the sucrose octasulfate concentration was much increased (data not shown here). One possibility for aFGF not to cross-link as a dimer is that the cross-linking reagent is more efficient for basic proteins and aFGF has a much lower isoelectric point. Therefore, other cross-linking reagents are being tested.

Table 4.1. An Illustration of Intensity Distribution of the Data

H	K	L	F_{obs}	Sigma
0	2	4	82.100	0.080
0	2	5	0.080	5.840
0	2	6	34.970	0.130
-	-	-	----	---
0	2	42	15.410	0.380
0	2	43	0.000	999.0
0	2	44	3.580	1.430
0	2	45	6.230	0.820
0	2	46	27.110	0.400

TABLE 4.2. Heavy Atom Refinement Statistics

Derivative	Reso-lution	Concen-tration	measured reflection	comp-lete	R_{sym} (%)	Refined Sites	f_H/E
Native	2.7 Å	--	31,326	95%	11.8	--	--
EMTS	3.4 Å	2.5 mM	16,070	92%	12.2	8	1.26
K_2PtCl_4	2.3 Å	3.0 mM	45,881	91%	9.28	14	0.84

$$R_{sym} = \sum |I - \langle I \rangle| / \sum I$$

$$f_H / E = [\sum f_H^2 / \sum (F_{deriv,obs} - F_{deriv,calc})^2]^{\frac{1}{2}}$$

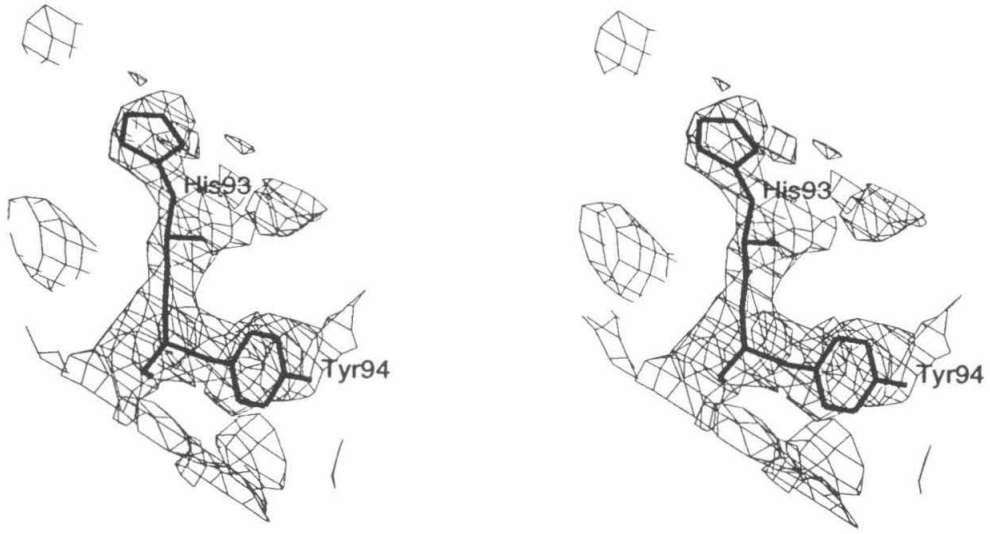

Figure 4.1. Illustration of the 8-fold averaged electron density map in the region near His 93.

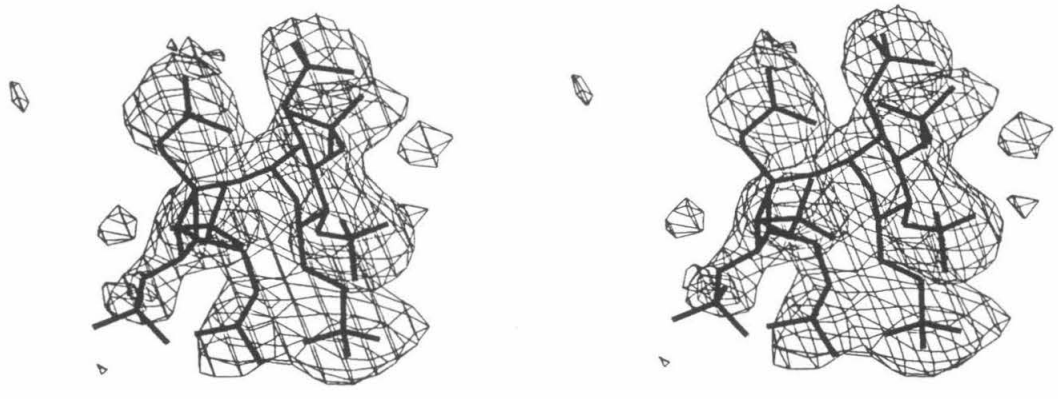

Figure 4.2. 1σ level electron density around a sucrose octasulfate molecule [$(2F_O$-$F_C)\ \alpha_{calc}$)], calculated at 2.7Å resolution.

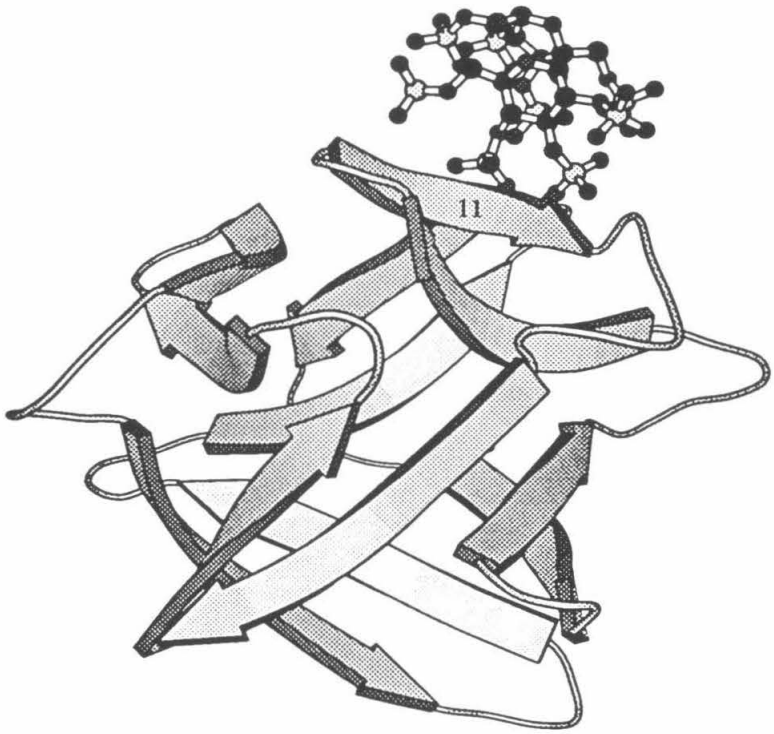

Figure 4.3. Binding of sucrose octasulfate to aFGF. The β strand that is involved in sucrose octasulfate binding is labeled.

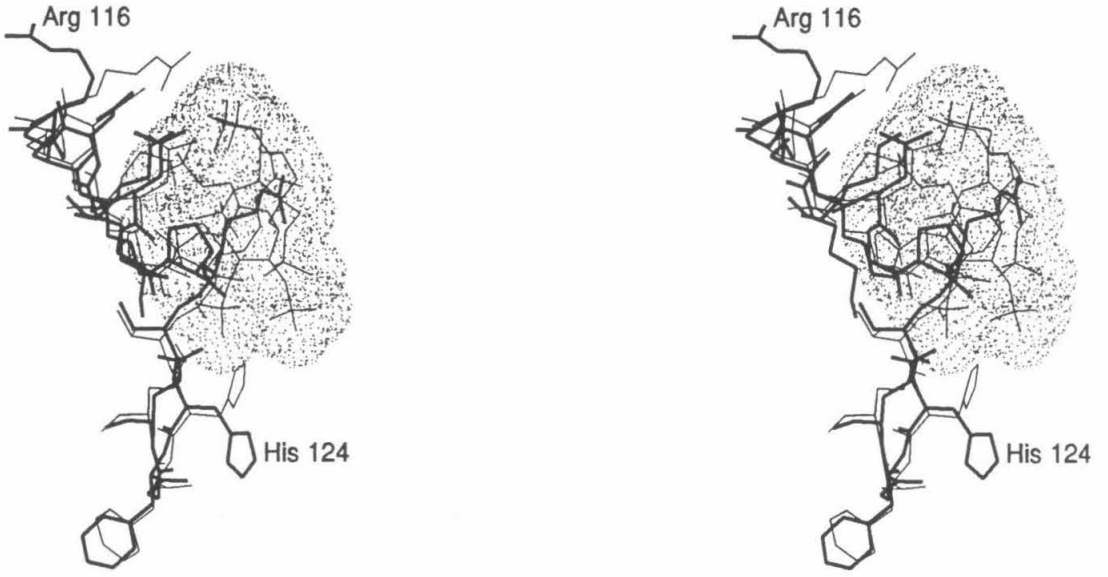

Figure 4.4. An example of the local conformational difference in the aFGF structures with (thick line) and without (thin line) sucrose octasulfate. The van der Waals surface of the bound sucrose octasulfate is shown with dots.

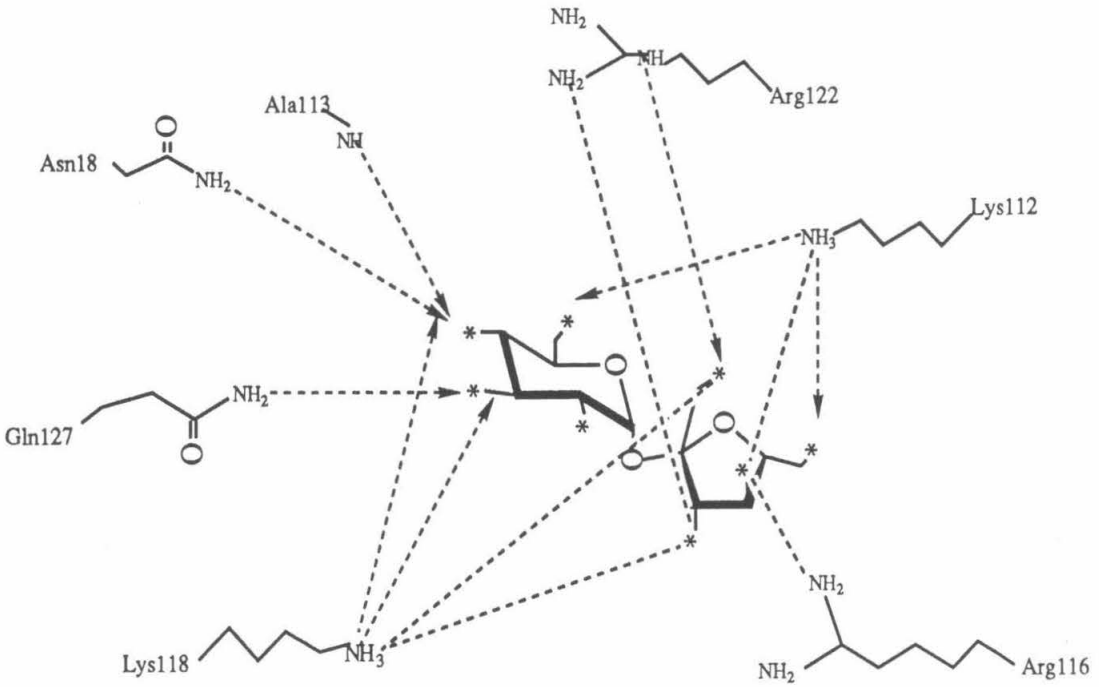

Figure 4.5. Schematic representation of sucrose octasulfate binding to aFGF.

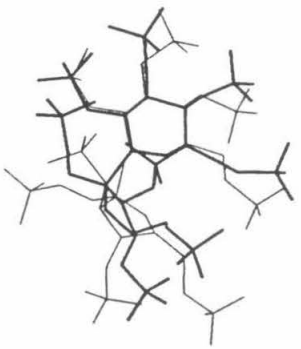

(1)

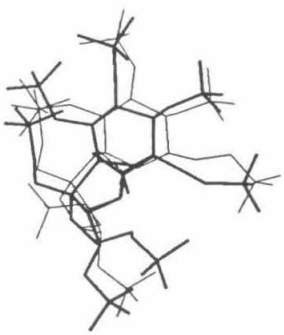

(2)

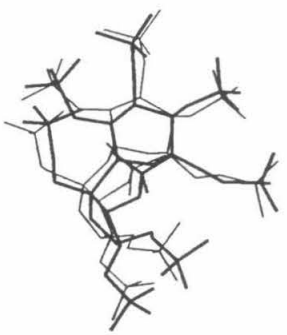

(3)

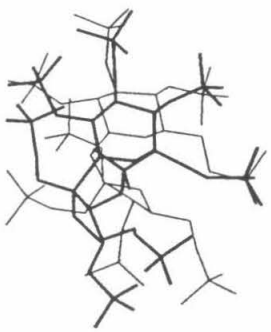

(4)

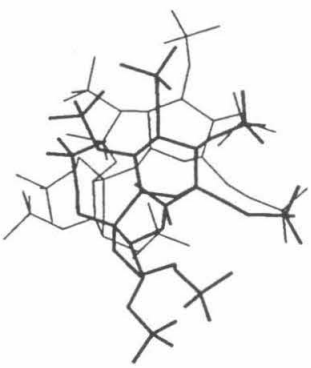

(5)

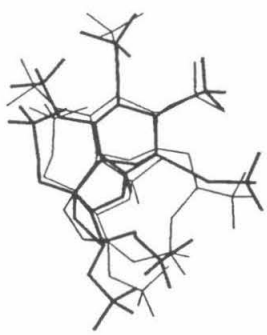

(6)

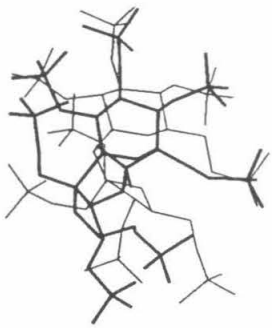

(7)

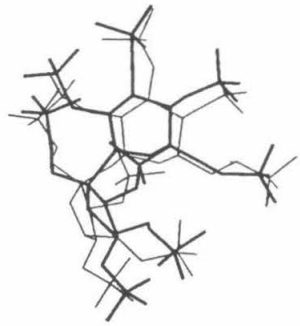

(8)

Figure 4.6. Superposition of the eight sucrose octasulfate molecules that are related by noncrystallographic symmetry. Figure 4.6 (2) to (8) reveal the sucrose octasulfate structures of #2 to #8 (thin line) superimposed to sucrose octasulfate #1, based on the corresponding aFGF molecules. Sucrose octasulfate #1 is shown in the thick line. Figure 4.6 (1): Superposition of the sucrose octasulfate bound to aFGF determined by us (#1, shown with thick line) and the free sucrose octasulfate determined by small molecule crystallography (32).

aFGF 112	K K N G R S K L G P R T H F G Q
bFGF 120	K R T G Q Y K L G P K T G P G Q

Figure 4.7. Sequence alignment of acidic and basic FGF in the sucrose octasulfate binding region.

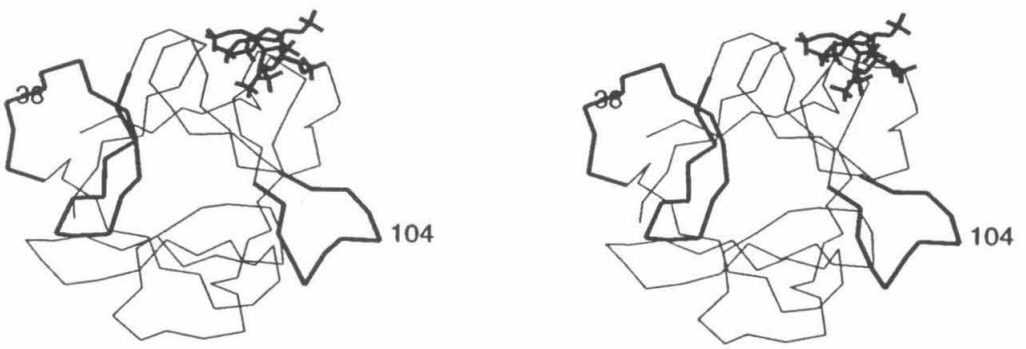

Figure 4.8. The structure of aFGF bound to sucrose octasulfate. The two putative receptor binding sites, which are near residues 38 and 104 respectively, are shown with thick line.

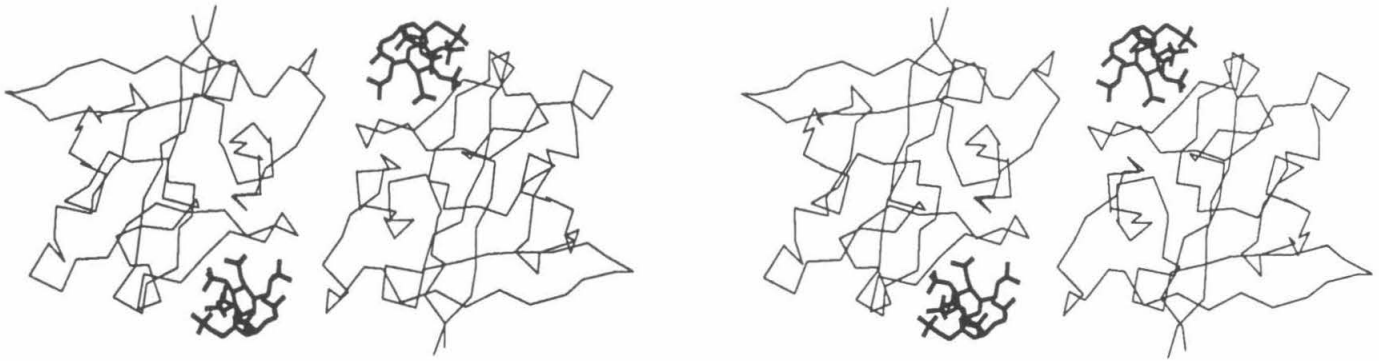

Figure 4.9. The aFGF dimer that is observed in the crystal packing.

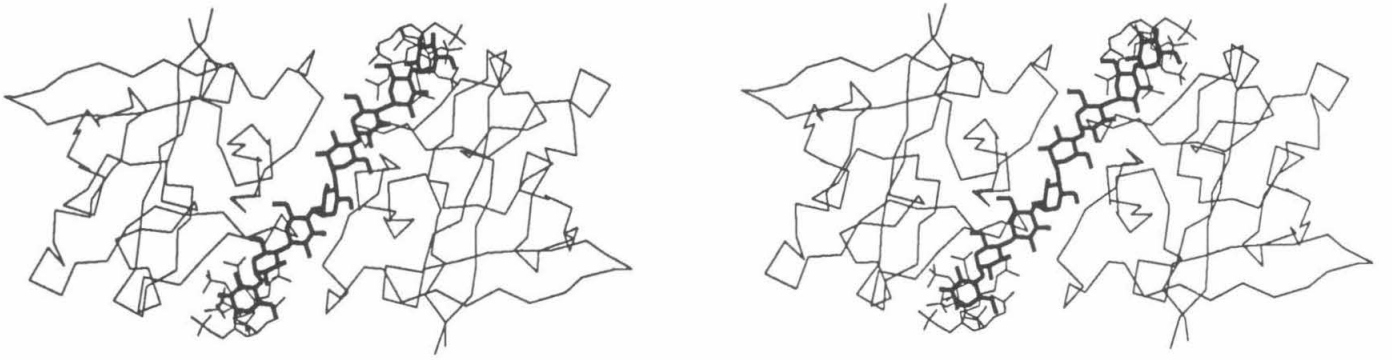

Figure 4.10. Computer docking of an octasaccharide model to an aFGF dimer. The octasaccharide (thick line) has the conformation of heparin and was modeled to fit the binding of sucrose octasulfate (thin line) to aFGF (thin line).

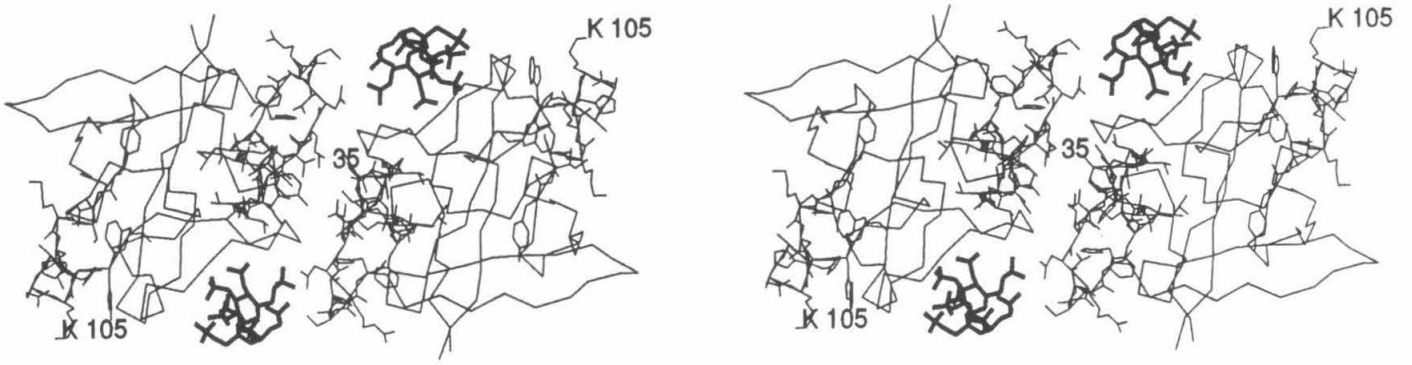

Figure 4.11. An FGF dimer observed in the crystal packing could possibly bind two FGF receptors simultaneously. One of the putative receptor binding sites (shown with the side chains near K 105) is located at the two ends of the dimer. The other region reported to be important for receptor binding (also shown with the side chains but near K 35) is located at the interface of the dimer. The two bound sucrose octasulfate molecules are shown with bold lines.

Figure 4.12. Dimerization of FGF. Lane 1, cross-linking of aFGF in the absence of sucrose octasulfate; Lane 2, cross-linking of aFGF in the presence of sucrose octasulfate; Lane 3, cross-linking of bFGF in the absence of sucrose octasulfate; Lane 4, cross-linking of bFGF in the presence of sucrose octasulfate.

References

1. J. F. Megyesi, *et al., J. Cell. Biochem.* (20th Annual Meetings, 1991).

2. J. Folkman, S. Szabo, M. Stovroff, P. McNeil, W. Li, Y. Shing, *Annals of Surgery* **214,** 414 (1991).

3. S. J. Prestrelski, G. M. Fox, T. Arakawa, *Arch. of Biochem. and Biophys.* **293,** 314 (1992).

4. J. Jancarik and S-H. Kim, *J. Appl. Cryst.* **24,** 409 (1991).

5. A. J. Howard *et al., J. Appl. Cryst.* **20**, 383 (1987).

6. X. Zhu, H. Komiya, A. Chirino, S. Faham, G. M. Fox, T. Arakawa, B. T. Hsu, D. C. Rees, *Science* **251,** 90 (1991).

7. A.T. Brunger, *J. Mol. Biol.* **203**, 803 (1988).

8. D. E. Tronrud, L. F. Ten Eyck, B. W. Mattews, *Acta Cryst.* **A43,** 489 (1987).

9. T. C. Terwilliger and D. Eisenberg, *Acta Cryst.* **A39,** 813 (1983).

10. G. Bricogne, *Acta Cryst.* **32**, 832 (1976).

11. A. E. Eriksson, L. S. Cousens, L. H. Weaver, B. W. Matthews, *Proc. Natl. Acad. Sci. USA* **88,** 3441 (1991).

12. J. Zhang, L. S. Cousens, P. J. Barr, S. R. Sprang, *Proc. Natl. Acad. Sci. USA* **88,** 3441 (1991).

13. H. Ago, Y. Kitagawa, A. Fujishima, Y. Matsuura, Y. Katsube, *Biochemistry J.* **110,** 360 (1991).

14. J. W. Harper and R. R. Lobb, *Biochemistry* **27,** 671 (1988).

15. W. H. Burgess, A. M, Shaheen, M. Ravera, M. Jaye, P. J. Donohue, J. A. Winkles, *J. Cell Biology* **111,** 2129 (1990).

16. R. R. Lobb, *Biochemistry* **27,** 2572 (1988).

17. R. Ishai-Michaeli *et al., Biochemistry* **31,** 2080 (1992).

18. J. Sudhalter, J. Folkman, C. M. Svahn, K. Bergendal, P. A. D' Amore, *J. Biol. Chem* **264,** 6892 (1989).

19. D. M. Ornitz, A. Yayon, J. G. Flanagan, C. M. Svahn, E. Levi, P. Leder, *Mol.& Cell. Biol.* **12,** 240 (1992).

20. I. A. Nieduszynski, K. H. Gardner, E. D. T. Atkins, *Cellulose Chemistry and Technology,* pp. 73-91,

21. H. Ueno, M. Gunn, D, Dell, A. Tseng, L. Williams, *J. Biol. Chem.* **267,** 1470 (1992).

22. W. H. Burgess and T. Maciag, *Annu. Rev. Biochem.* **58,** 575 (1989).

23. A. Yayon, M. Klagsbrun, J. D. Esko, P. Leder, D. M. Ornitz, *Cell* **64,** 841 (1991).

24. A. Ullrich and J. Schlessinger, *Cell* **61,** 203 (1990).

25. N. Q. McDonald, R. Lapatto, J. Murray-Rust, J. Gunning, A. Wlodawer, T. L. Blundell, *Nature* **354,** 411 (1991).

26. S. Daopin, K. A. Piez, Y. Ogawa, D. R. Davies, *Science* **257,** 369 (1992),

27. M. P. Schlunegger and M. G. Grutter, *Nature* **358,** 430 (1992).

28. J. Pandit, A. Bohm, J. Jancarik, R. Halenbeck, K.Koths, S-H. Kim, *Science* **258,** 1358 (1992).

29. A. Baird, D. Schubert, N. Ling, R. Guillemin, *Proc. Natl. Acad. Sci. USA* **85,** 2324 (1988).

30. J-T. Feige and A. Baird, *Proc. Natl. Acad. Sci. USA* **85,** 3174 (1989).

31. D. P. Bottaro, J. S. Rubin, D. Ron, P. W. Finch, C. Florio, S. A. Aaronson, *J. Biol. Chem.* **266,** 12767 (1990).

32. Y. Nawata, K. Ochi, M. Shiba, K. Morita, *Acta Cryst.* **B37,** 246 (1981).

Chapter 5

FGF Stability and Activity Revealed by the Mutant and FGF-ligand Complex Structures

5.1. Introduction

Since FGFs can induce mitogenic, chemotactic and angiogenic activity in a variety of cells of epithelial, mesenchymal and neural origins (1), FGF is a very attractively therapeutic target. With the ability to promote tissue repair (2), FGF has been considered as a potential drug for wound healing. On the other hand, some members of the family are highly expressed in many malignantly transformed cells (3). Therefore, inhibition of FGF activity in these cells may be useful. To use FGF as a tissue growth promoting drug, high therapeutic efficiency is usually connected with the high stability of the protein. One potential way of enhancing FGF stability is to introduce specific mutations into FGF. To investigate how mutations can change FGF stability, two mutant structures have been determined and will be discussed in this chapter. Furthermore, to be used as a routine therapy, high yield and efficiency of protein purification is required to prepare large quantities of FGF. Copper and heparin biaffinity columns have been demonstrated to have increased FGF binding affinity (4). The structure of FGF and copper complex has been studied. Finally, the structure of an FGF-inhibitor analog complex is analyzed to provide a structural basis for rational design of drugs to either enhance or inhibit FGF activity.

5.2. The mutant Gly93His aFGF structure

While the mutant Ala47Cys aFGF exhibits comparable activity to the native aFGF, the substitution of glycine for histidine 93 in aFGF has been shown to increase aFGF stability (5). The thermal denaturation temperature of Ala47Cys/Gly93His aFGF is about 10 ^{o}C higher than Ala 47 aFGF. This is consistent with the observation that while [Ala^{47}] aFGF rapidly loses mitogenic activity in the absence of heparin (with a half-life of approximately 13 hours (5)), [Ala^{47}, Gly^{93}] aFGF exhibits no loss of activity over 250 hours in the same conditions. In addition, [Ala^{47}, Gly^{93}] aFGF appears to have slightly higher activity because it can produce the same mitogenic

effect as the [Ala^{47}] aFGF analog or the native aFGF but at lower concentrations. Furthermore, because [Ala^{47}, Gly^{93}] aFGF can be eluted from a heparin column at an identical concentration of NaCl required for [Ala^{47}] aFGF, the stability of [Ala^{47}, Gly^{93}] aFGF does not seem to be due to its increased binding affinity for heparin. In order to provide a structural basis for comparing the stability of the [Ala^{47}] and [Ala^{47}, Gly^{93}] aFGF analogs, their crystal structures were determined.

In the [Ala^{47}, Gly^{93}] aFGF structure (6), it is shown that residues 90 to 94 have a sequence of Glu Glu Asn Gly Tyr and form a 3:5 β-hairpin as defined by Sibanda, *et al.* (7). A 3:5 β-hairpin consists of two terminal amino acids from two adjacent β strands with three intermediate residues forming a tight β turn. This hairpin structure is a combination of a classic type I β turn and a G1 β-bulge (8, 9) which possesses a conformation of $\beta\alpha_R\alpha_R\alpha_L\beta$, where α_L stands for left-handed alpha helix and α_R for right-handed alpha helix. Since the main chain torsion angles for the fourth residue of the loop are in the left hand alpha helical region of the Ramachandran plot, glycine is the most easily accommodated amino acid at this position. The most common amino acids observed to replace glycine in the 3:5 β-hairpin are asparagine and aspartic acid (10), although asparagine is seen more frequently (9). Indeed, basic FGF, which has a similar main chain conformation as aFGF in this region (Figure 5.1), has an asparagine at the fourth position of the hairpin.

Although the structure of [Ala^{47}, Gly^{93}] aFGF suggests that glycine should be the most energy-favored amino acid at position 93, it could be interesting to determine the [Ala^{47}] aFGF structure and compare the structures of the naturally occurring [His^{93}] aFGF with the [Gly^{93}] aFGF analog. Thin plates of hexagonal crystals of [Ala^{47}] aFGF were obtained by using the similar crystallization conditions for [Ala^{47}, Gly^{93}] aFGF (6), but they only diffracted to about 4 Å resolution. Conditions for better quality crystals were then screened with a factorial method (11) in the presence of sucrose octasulfate which can generally stabilize FGF (2). The details of

crystallization and structure determination are described in Chapter 4.

The crystal structure of the [Ala^{47}] aFGF-sucrose octasulfate complex reveals the well defined side chain position of His 93 (Figure 4.1). Further, the side chain of His 93 is highly exposed to solvent and is not in contact with the rest of the aFGF molecule. The overall geometry of the 3:5 hairpin around position 93 in [Ala^{47}] aFGF is quite similar to that in [Ala^{47}, Gly^{93}] aFGF (Figure 5.2). In addition, the main chain torsion angles of histidine 93 are observed to be maintained in a left-handed alpha helix conformation. Therefore, as demonstrated by this structure, in addition to asparagine and aspartate, histidine can also be accommodated at the 4th position of a typical 3:5 hairpin and adopt a left-handed alpha helix conformation. However, relative to glycine, a histidine in the fourth position of a 3:5 hairpin is less favorable and hence leads to decreased stability of aFGF.

5.3. The mutant Asp40Arg bFGF structure

Another mutant FGF that was studied was the Asp40Arg bFGF analog. Arginine 40 is one of the positively charged residues located in the region of bFGF-(31-51) which has been reported to be important in receptor binding and probably also in heparin binding (9). Surprisingly, mutation of arginine 40 to an aspartic acid resulted in an active bFGF, although it appears to be less stable at low ionic strength (10). To further investigate the property of the mutant, the structural determination of Asp40Arg bFGF has been carried out.

Crystallization trials with the low ionic precipitant solution PEG8K, from which the [Arg^{40}]bFGF crystals have been obtained (4), failed to produce any [Asp^{40}] bFGF crystals. Instead, screening with factorial conditions (7) yielded crystals of 0.5 x 0.5 x 0.5 mm^3 in size that diffracted to about 1.7 Å resolution. Each droplet contains equal volumes of the [Asp^{40}] bFGF sample at a concentration of 10 mg/ml and the reservoir solution of 2.0 M $(NH_4)_2SO_4$ and 0.2 M Na Citrate at pH 5.6. These crystals belong

to the space group $P2_12_12_1$ and have cell dimensions of 31.8 Å, 42.1 Å and 86.1 Å. At about the same time as the [Asp^{40}] bFGF crystals were obtained, the same crystal form of the native bFGF crystals was reported to be crystallized in 60% saturated ammonium sulfate and 0.2 M sodium succinate (pH 5.3) (12).

The mutant structure of Asp40Arg bFGF was determined by a combination of molecular replacement and single isomorphous replacement (SIR) method. Using the determined bFGF structure (4), a clear molecular replacement solution with an R-factor of 38.0% was obtained by using the Crowther fast rotation function (13) and the brute-force translation search (14) when diffraction data within 4 to 8 Å resolution were used. In addition, rigid body refinement of the molecular replacement model with TNT (15) lowered the R-factor down to 36.7% using the same reflections. The difference Fourier (F_o - F_c) map calculated with the model phases, however, displayed no density for the aspartic acid side chain. To improve the model phases, several cycles of positional refinement with TNT to 3 Å resolution was carried out. A model with an R-factor of 26.1% and r.m.s. deviations from the ideal bond distances and bond angles of 0.023 Å and 3.6°, respectively, was obtained. The difference map phased with this model still did not reveal side chain density for Asp 40.

An ETMS derivative data set was then collected in order to further improve the phases. The heavy atom binding site, located from a difference Patterson map (Figure 5.3), was consistent with that located from a difference Fourier map using the molecular replacement phases. In addition, the mercury binding site was near the solvent exposed cysteine 93 residue, which further supported the correctness of the molecular replacement. The single isomorphous replacement phases were subsequently calculated by refining the Hg binding site against the difference Patterson with HEAVY (16) (Table 5.1). After the SIR phases were combined with the molecular replacement phases, the density of the C_β atom of Asp 40 was found in the electron density map calculated with the combined phases. Building in an alanine

at position 40 followed by several cycles of refinement, manual adjustment of the model and phase combination finally made it possible to model in an aspartic acid. Refinement of the [Asp^{40}] bFGF model to 1.7 Å proceeded to an R factor of 18.4%, with the root-mean-square deviations from the ideal bond distances and angles of 0.016 Å and 2.7°, respectively (Figure 5.4).

The overall structure of [Asp^{40}] bFGF is very similar to the model of [Arg^{40}] bFGF which was used during the molecular replacement solution. The root-mean-square difference of the 124 corresponding α-carbons is only 0.61 Å. Surprisingly, the change of arginine to aspartic acid at residue 40 does not cause any large structural disturbance in this region (Figure 5.5). The positional deviation between the Cαs of amino acid 40 in the two structures is only 0.14 Å. Yet, in spite of the similar backbone structures around residue 40, the side chains of Arg 40 and Asp 40 exhibit quite different conformations (Figure 5.6). In the crystal structure, Arg 40 is localized at the beginning of β-strand 3 and its side chain is mainly stabilized by forming two hydrogen bonds with an adjacent amino acid, Asp 38. In addition, Arg 40 is involved in a lattice contact and is further stabilized by interacting with two asparagines of a neighboring molecule. It is hence expected that the substitution of the arginine to aspartic acid would lead to the disruption of all the interactions that Arg 40 is involved in, and would result in an altered structure. Indeed, the mutant Asp 40 structure shows that the Asp 40 side chain does not interact with Asp 38. Nor is it in contact with the neighboring molecule. Nevertheless, the mutant structure reveals that Asp 40 bFGF appears to remain a stable structure. Instead of forming the interactions observed in [Arg^{40}] bFGF, Asp 40 is stabilized by interacting with the neighboring amino acid histidine 36. His 36 is observed to display a large conformational change in the D40 mutant structure (Figure 5.6). By moving closer to Asp 40, His 36 is able to be hydrogen bonded to Asp 40. In addition, a new hydrogen bond is formed between Asp 42 and the repositioned His 36. Therefore, according to this structure, it

seems that [Asp^{40}] and [Arg^{40}] bFGF may have comparable stabilities. Indeed, this is confirmed by other biochemical studies after the structure was solved (T. Arakawa, personal communication).

While the [Asp^{40}] bFGF Cα backbone is shown to remain a similar configuration to that of [Arg^{40}] bFGF, considerably larger conformational differences are observed in the regions far away from amino acid 40. For instance, the Cα positional differences of residues 101, 102 and 103 in the two structures are as large as 2.6 Å, 3.3 Å and 2.2 Å, respectively (Figure 5.7). The structural analysis shows that the conformational divergence is mainly caused by a lattice contact. Amino acids 101, 102 and 103 are three continuous negatively charged residues localized in the loop between the β strands 8 and 9, which is extensively involved in the interactions with the neighboring molecules. In the [Asp^{40}] bFGF crystal form, the main chain carbonyl group and the side chain of Asn 102 form hydrogen bonds with Arg 45 and Glu 46 of a neighboring bFGF. In addition, the same Arg 45 also interacts with Asn 103. In the [Arg^{40}] bFGF crystal form, however, Asn 102 is not involved in lattice contacts, while Asn 103 is hydrogen bonded to Arg 40 from an adjacent bFGF. Therefore, the dramatic structural difference demonstrated here is probably not an intrinsic characteristic of this loop. Instead, it is mainly caused by a lattice contact in the crystal. This idea is further supported by the structural similarity of the Asn 102 region in this [Arg^{40}] bFGF structure to another [Arg^{40}] bFGF structure, which was independently determined in a new crystal form (17). Furthermore, interactions between neighboring molecules are also responsible for the second largest structural variance revealed in these two structures (Figure 5.5). Located in a β turn, Arg 61 forms a hydrogen bond to Glu 79 of an adjacent bFGF in the D40 crystal form, whereas the same residue in the [Arg^{40}] crystal (6) is not involved in any lattice contact.

Because of the lattice contact effect, it is often asked how reliable protein crystal

structures are. A further related question is to ask whether water molecules located in crystal structures are physiologically relevant. The two high resolution bFGF structures determined by us as well as other independently determined bFGF structures provide an excellent example for this kind of analysis.

At least three different bFGF crystal forms that diffract beyond 2.0 Å have been reported (6, 12,17) using both high and low ionic strength precipitant solutions. This includes two different triclinic P1 forms, crystallized in PEG or ammonium sulfate (6, 17), and an orthorhombic crystal form obtained with ammonium sulfate (12). Interestingly, the two bFGF structures determined in P1 space group (1BAS_BFGF.PDB and 3FGF.PDB) have more similar conformations despite very different ionic strength precipitant solutions were used. The root-mean-square difference of the 124 corresponding α-carbons is only 0.25 Å. This is almost within experimental error because the two independently determined bFGF structures by us and others using the same crystal form and similar crystallization conditions also reveal an r.m.s. difference of 0.25 Å for the Cα atoms. On the other hand, the bFGF structures determined in the orthorhombic form show more structural divergence compared to the ones determined in the triclinic forms, with an r.m.s. difference of approximately 0.6 - 0.7 Å. This suggests that different lattice contacts associated with changes in space group could cause more conformational differences than different crystallization conditions.

In the three different bFGF crystal forms, forty (6), seventy (17) and eighty (D40 structure) water molecules were located. While nineteen water molecules are found at similar positions in the two P1 bFGF crystal forms, fifteen of these are common in all three crystal forms. In addition, eleven common water molecules are located on the protein surface and most of them are bound to main chain amide and carbonyl groups. Therefore, it may be concluded that although some of the solvent molecules binding to proteins appear to have ordered structures due to the crystal packing effect, others

are physiologically relevant and could play important roles in mediating protein function.

5.4. Inhibition of FGF activity by suramin

Although it has been shown that polysulfated glucosaminoglycans are required for FGF binding to its high affinity receptor (18-20), other polysulfated compounds inhibit interaction between FGF and its receptor (21, 22). One of the polyanionic FGF inhibitors which has therapeutic potential against tumor cell growth is suramin (23).

Suramin is a symmetrical polysulfonated naphthylurea which has been extensively used for the treatment of tryposnosomiasis and onchocerciasis (24) (Figure 5.8). In addition, suramin has been known to possess anti-proliferative activities possibly by inhibiting the binding of various growth factors with their receptors (25, 26). Experimental evidence for direct interaction of suramin with growth factors has recently been reported (27) by the observations that 1) the fluorescence of suramin is significantly enhanced in the presence of aFGF; 2) heparin effectively competes with suramin binding to aFGF; 3) the presence of suramin stabilizes aFGF from thermal denaturation and also prevents formation of aFGF intermolecular disulfide bonds. In addition, based on the observation that the molecular weight of aFGF is six times higher after suramin is added in a molar ratio of 2:1, one of the possible inhibitory mechanisms of suramin on FGF activity may be that suramin can cause FGF microaggregation.

To further understand the detailed interactions between suramin and FGF, as well as to obtain a structural basis for rational drug designs of better anti-tumor agents, crystallographic studies of the FGF and suramin complex were attempted. The importance of FGF in carcinogenesis has previously been suggested by the observed high concentration of FGF in various tumor cell lines. Recently, direct cellular malignant transformation by FGF oncogenes or by bFGF fused with a signal peptide

sequence has been demonstrated (21). Furthermore, it is shown that the autocrine transformation process induced by the chimeric bFGF can be blocked with the addition of suramin (21). Therefore, the use of suramin or suramin analogs has been suggested to be a potentially powerful therapy against autonomous cell growth and tumorgenesis.

Attempts to cocrystallize either aFGF or bFGF with suramin have not been successful, mainly due to the problem of FGF precipitation in the presence of suramin. However, when 1,3,6-naphthalene trisulfonate, which is a close analog of half of a suramin molecule in structure, was diffused into an aFGF crystal (6), it was found to bind an aFGF dimer with high occupancy. The bound 1,3,6-naphthalene trisulfonate was located in the difference Fourier map (F_o - F_c), calculated with the phases from the aFGF structure (6). After manually fitting of 1,3,6-naphthalene trisulfonate into the difference density, the complex structure was refined to 3 Å using the XPLOR package (28) The refinement has progressed to a current R-factor of 16.2% with 0.013 Å for the r.m.s. bond length deviation and 2.3° for the r.m.s. bond angle deviation.

The refined structure of aFGF and 1,3,6-naphthalene trisulfonate complex demonstrates that one 1,3,6-naphthalene trisulfonate binds two aFGF molecules simultaneously around the regions of Arg 24 on one aFGF and Lys 128 on the other (Figure 5.10). Two lysines around the sucrose octasulfate binding region, Lys 113 and Lys 128, form hydrogen bonds to two sulfate groups of 1,3,6-naphthalene trisulfonate. 1,3,6-naphthalene trisulfonate also binds another neighboring molecule through hydrogen bonds with the side chain of Arg 24 and the main chain amide of Asp 28. In addition, the binding is strengthened by hydrophobic interactions. The aromatic ring of the naphthalene is sandwiched between Leu 26 from one aFGF and carbon atoms of the Lys 113 side chain from the other (Figure 5.11).

Since the growth factors inhibited by suramin are primarily heparin binding

proteins (29), direct interaction of the proteins with suramine in a similar manner as heparin has been speculated. This similarity is further supported by the recent report that heparin competes with suramin to bind FGF and *vice versa* (27). The structure of the aFGF-1,3,6-naphthalene trisulfonate complex shows that the proposed heparin binding site on aFGF is likely to be involved in interacting with suramin. Although 1,3,6-naphthalene trisulfonate binds two aFGF monomers, the major binding site is within the region near Lys 118, which has been suggested to be the heparin binding site according to the crystal structure analysis as well as other biochemical results (6, 30). Among the residues of Asn 18, Lys 112, Lys 113, Asn 114, Arg 116, Lys 118, Arg 122, Gln 127 and Lys 128 that are involved in binding to sucrose octasulfate, Asn 18, Lys 112 and Lys 113 of one aFGF form four hydrogen bonds with the bound 1,3,6-naphthalene trisulfonate (Figure 5.11), implying that the inhibitory influence of suramin upon the activity of aFGF may be at least partially due to the occupation of the heparin binding site on aFGF by suramin. Further, in addition to this binding site, the structure of the complex reveals that the region between Arg 24 and Asp 28 are also involved in 1,3,6-naphthalene trisulfonate binding. The importance of the aFGF-(21-41) region in receptor binding has been reported before (30). Furthermore, the same region has been further suggested to possibly be located at the interface of the aFGF dimer that binds the FGF receptors (Chapter 4). Therefore, it is also likely that suramin disrupts the interactions of FGF with its receptor by occupying the sites which are important for FGF binding to the receptor. Finally, since suramin is reported to induce FGF microaggregation (27), the structure of one 1,3,6-naphthalene trisulfonate binding to two aFGF molecules provides a possible model of how one suramin may bind several FGF molecules simultaneously.

5.5. The FGF Cu binding site

Copper has been known to modulate the neovascular response from angiogenic

stimuli as FGF. While some studies indicate that FGF binding to heparin requires copper (31-36), others report that FGF could interact with heparin even in the absence of copper (37). FGFs were shown to potentially possess different heparin and copper binding sites (37). Shing further showed that although a copper-Sepharose column alone is not sufficient to bind either aFGF or bFGF, the biaffinity chromatography of copper-heparin is more efficient than heparin affinity columns to resolve aFGF from bFGF as well as the multiple forms of aFGF or bFGF (37).

To confirm the direct interactions between FGF and copper, the difference Fourier method has been employed to locate the possible copper binding site on FGF. Unfortunately, soaking of bFGF crystals (6) in the synthetic mother liquor of 30% PEG8K and 0.1 M Hepes buffer (pH 7.5) in the presence of high concentration of $CuCl_2$ did not successfully incorporate copper into the crystals. Based on speculation that the $CuCl_2$ may form $Cu(OH)_2$ precipitant at the crystallization pH, the bFGF crystals (6) were soaked for about 10 hours in a solution of 30% PEG8K and 5 mM $CuCl_2$ without the buffer solution. The collected 3 Å area detector data of the soaked bFGF crystal revealed a clear difference Fourier peak between histidines 36 and 51 (Figure 5.12). It was further shown in the structure that few local conformational changes occur in this region. Both histidines 31 and 51 bind Cu^{2+} through the N_δ atoms and the angle between $N_\delta{}^{36}$, Cu and $N_\delta{}^{51}$ is about 120°. Furthermore, the copper binding site on bFGF is remotely located from the heparin binding site, with a distance of 15 Å between His 36 and Lys 118, the residue shown to intimately interact with sucrose octasulfate (Figure 5.13).

Soaking of aFGF crystals (6) with $CuCl_2$ failed to produce crystals with incorporated copper. This may be due to the chelation of copper by Na Citrate which is the buffer used in crystallization (6). Although the structure of aFGF and copper complex is not yet available, sequence alignment analysis shows that the copper binding site revealed in bFGF is not conserved in aFGF. Corresponding to bFGF His

36 is Leu 26 in aFGF. Nevertheless, despite the sequence divergence, aFGF has been reported to have a stronger binding affinity for copper than bFGF (37). Therefore, a different binding site on aFGF may be involved in binding to copper. Further structural analysis of aFGF shows that two histidines in aFGF, His 106 and His 124, are quite close to each other in the three dimensional structure. In addition, one water molecule is found to be bound between the two histidines in the refined aFGF structure. Furthermore, K_2PtCl_4, which has been used as the heavy atom derivative for the aFGF structure determination, was found to bind aFGF histidines 106 and 124 simultaneously in two different aFGF crystal forms (6) (Chapter 4). Hence it is very likely that copper binds aFGF through these two histidines. Also, as in bFGF, this putative copper binding site is separate from the heparin binding site (Figure 5.14). The distance between His 106 and Lys 112, which is involved in sucrose octasulfate binding, is more than 20 Å. This is in agreement with the biochemical studies that copper and heparin binding sites appear to be separate (37).

The distinct binding sites of copper and heparin on FGF explain why a copper and heparin biaffinity column is more efficient for FGF purification than a heparin column alone. These sites could be used to design engineered metal-binding FGF to further increase the protein purification efficiency. For example, a copper binding site similar to bFGF may be generated by changing aFGF Leu 26 to histidine so that aFGF may have two different copper binding sites around Leu 26 and His 106. Furthermore, either the present copper binding sites or engineered sites on FGF could be used to bind other metals. One of the possible therapeutic applications for FGF-metal complexes involves using radiolabled metals such as ^{57}Co for the detection or the treatment of tumor cells.

Table 5.1. EMTS SIR Phases Statistics

Resolution	6.75	4.42	3.50	2.99	2.65	2.40	2.21	2.06	TOTAL
FOM	0.55	0.47	0.44	0.38	0.36	0.33	0.31	0.29	0.37
P. P. (centric)	2.25	1.78	1.74	1.52	1.48	1.22	1.05	1.07	1.72
P. P. (acentric)	3.85	2.86	2.55	2.27	2.24	1.87	1.65	1.46	2.33

FOM: Figure of Merit

P. P.: Phasing Power

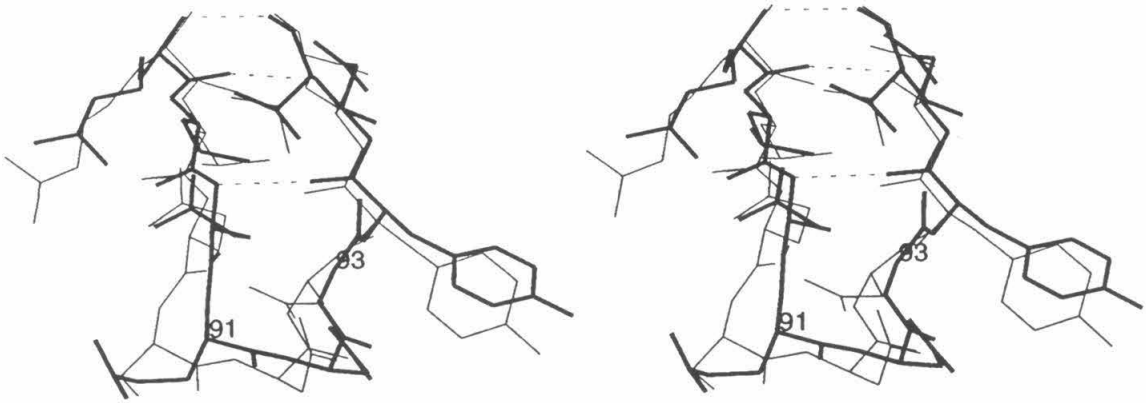

Figure 5.1. The superimposed 3:5 β-hairpin structures of [Ala^{47}, Gly^{93}] aFGF (thick line) and bFGF (thin line) near aFGF residue Gly 93. The hydrogen bonds between the strands 8 and 9 are shown with the dashed lines.

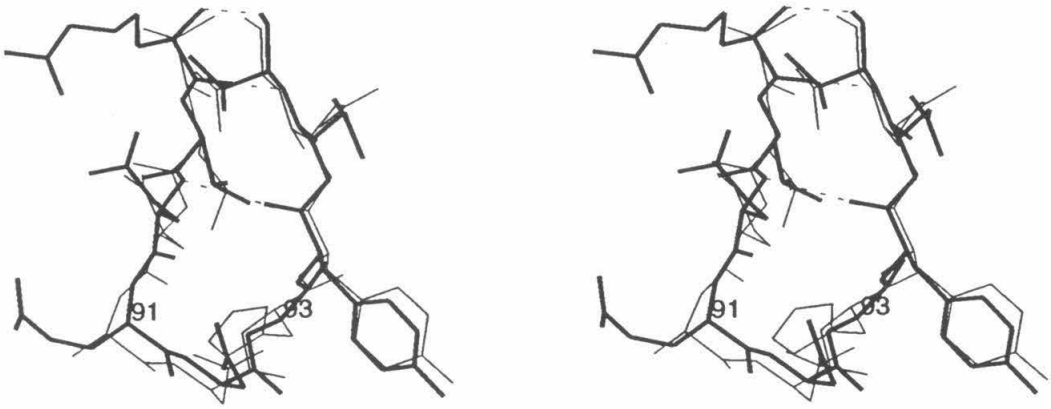

Figure 5.2. Structural superposition of [Gly^{93}] aFGF (thick line) and [His^{93}] aFGF (thin line).

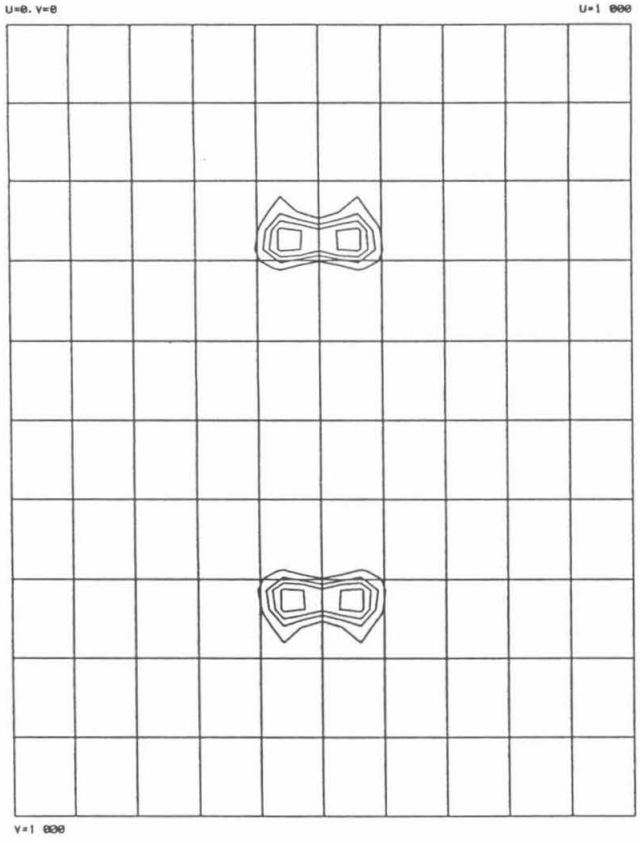

Figure 5.3. The EMTS difference Patterson map in the Harker section w = 1/2.

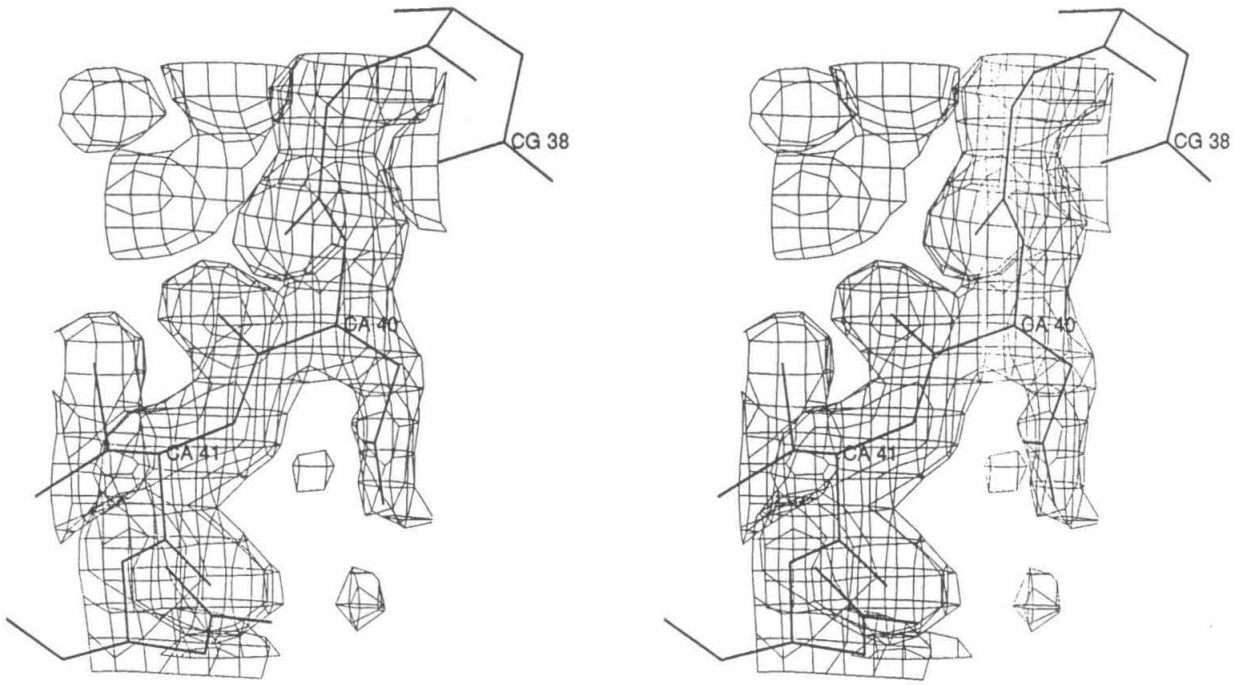

Figure 5.4. Stereoview showing the final $[2F_o\text{-}F_c]$ α_{calc} electron density map in the region near Asp 40 with a 1σ contour level .

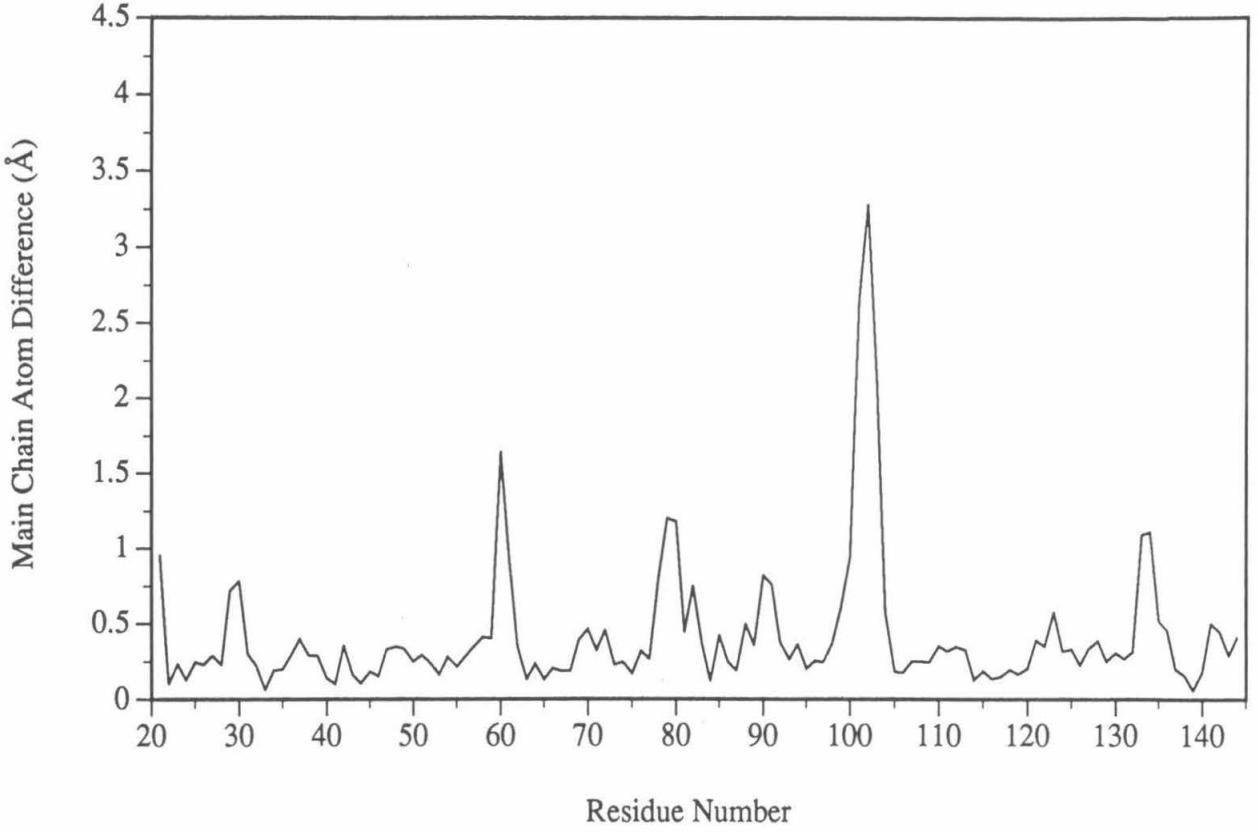

Figure 5.5. Quantitatively structural comparison of the [Asp^{40}] bFGF analog and [Arg^{40}] bFGF (the model used in the molecular replacement search).

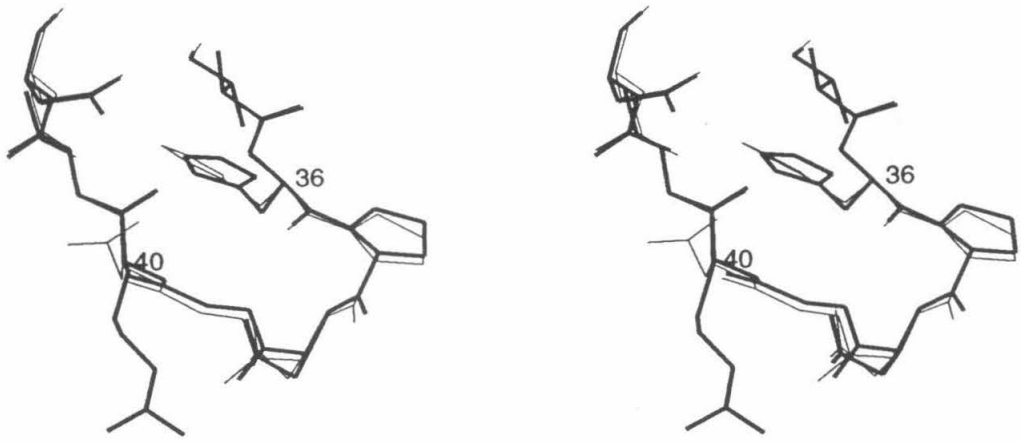

Figure 5.6. The region near residue 40 in the superimposed [Asp^{40}] (thick line) and [Arg^{40}] (thin line) bFGF crystal structures.

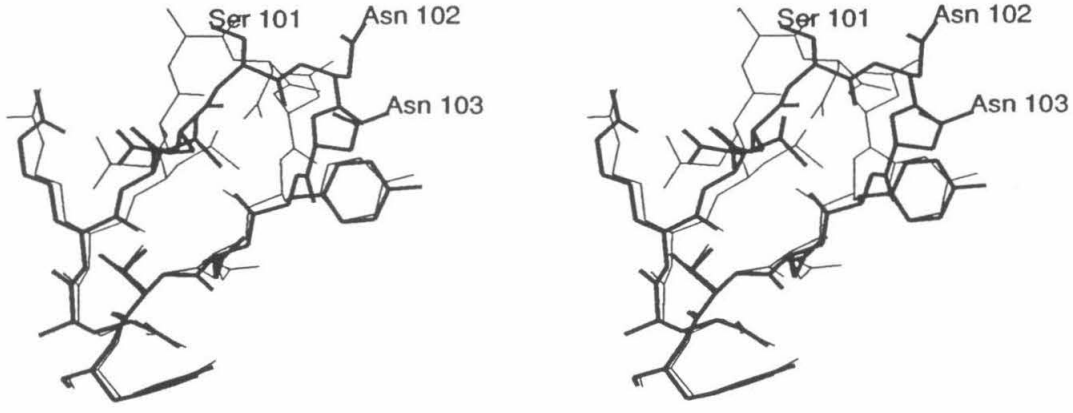

Figure 5.7. Conformational difference near Asn 102 in the two crystal forms of bFGF are caused by different lattice contacts.

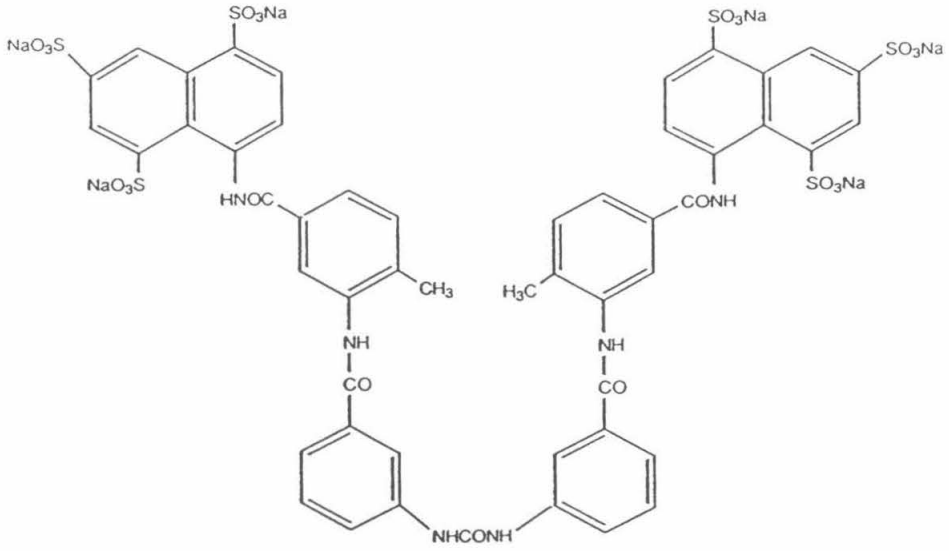

Figure 5.8. Molecular structure of suramin.

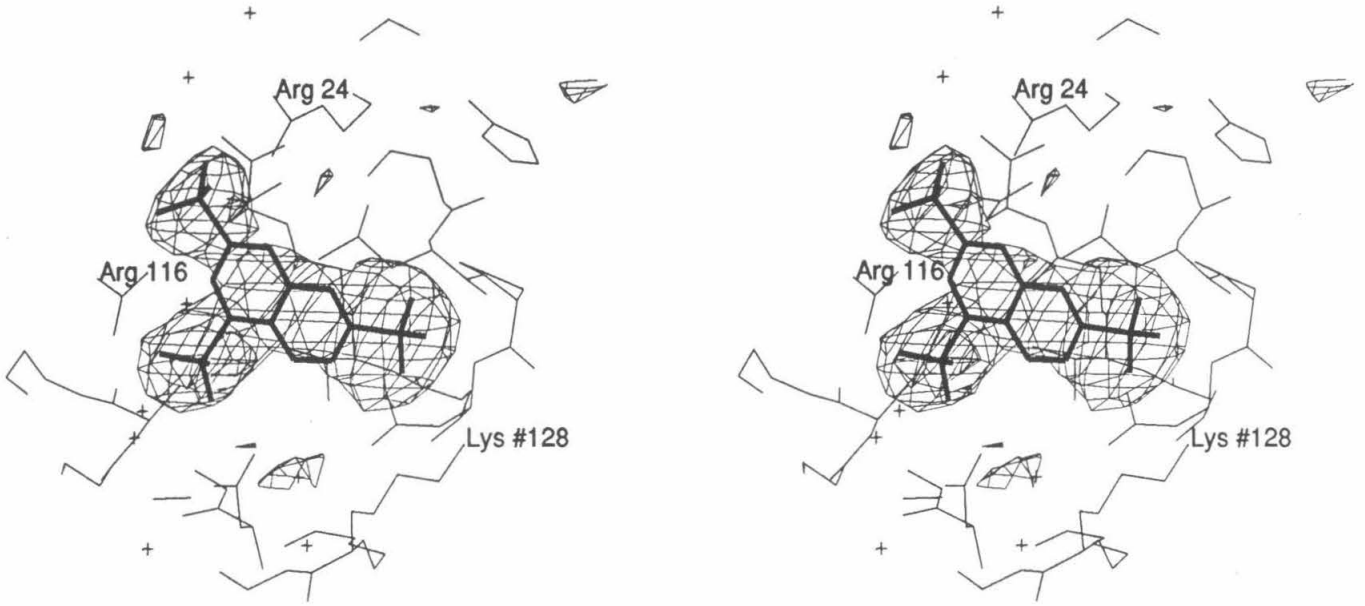

Figure 5.9. An F_o - F_c map at the 2σ contour level showing the location of 1,3,6-naphthalene trisulfonate in the aFGF crystal.

Figure 5.10. The binding of one 1,3,6-naphthalene trisulfonate molecule to an aFGF dimer. Residues of the second molecule in the asymmetric unit are numbered from 201.

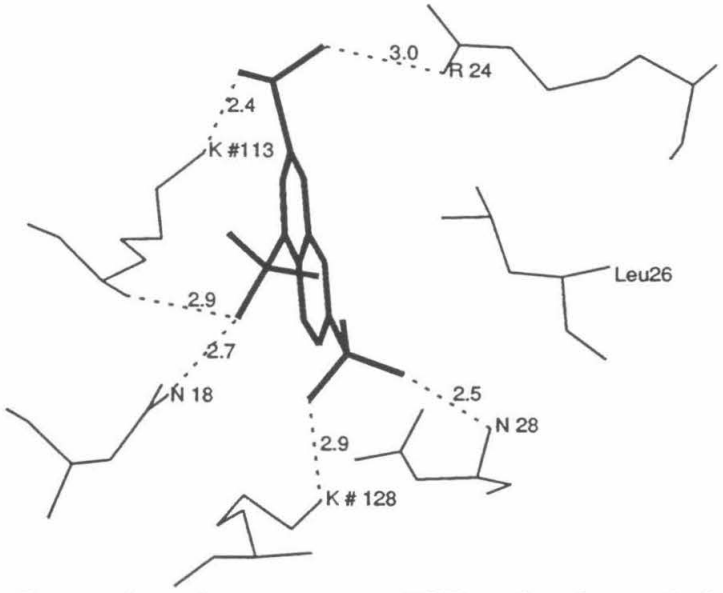

Figure 5.11. Interactions between two aFGF molecules and the bound 1,3,6-naphthalene trisulfonate. K #113 and N #128 are from a second molecule in the asymmetric unit.

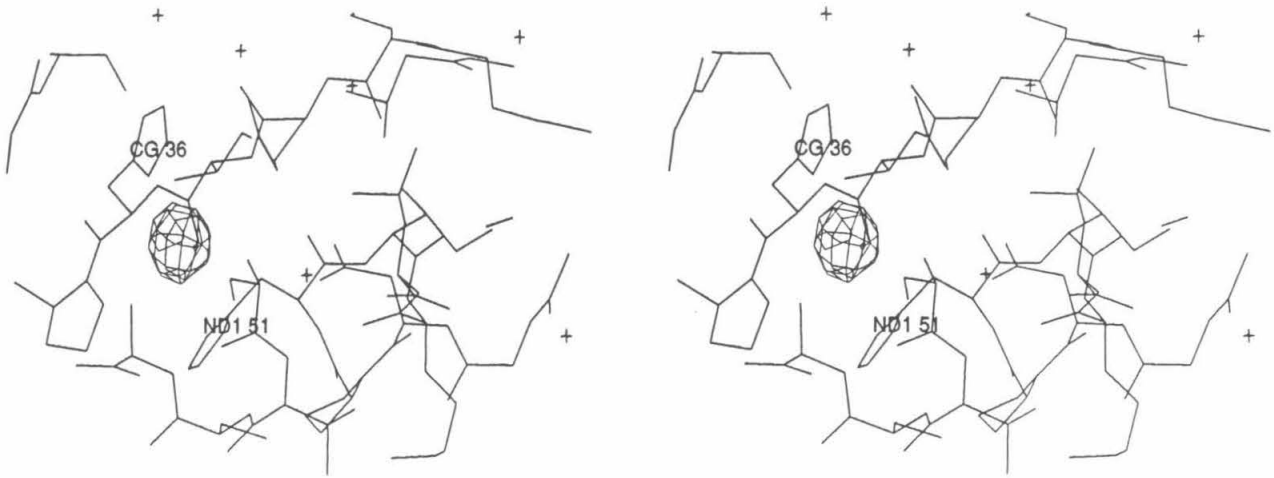

Figure 5.12. The difference Fourier electron density map (F^{Cu}_o - F^{native}_o) that reveals the copper binding site on bFGF.

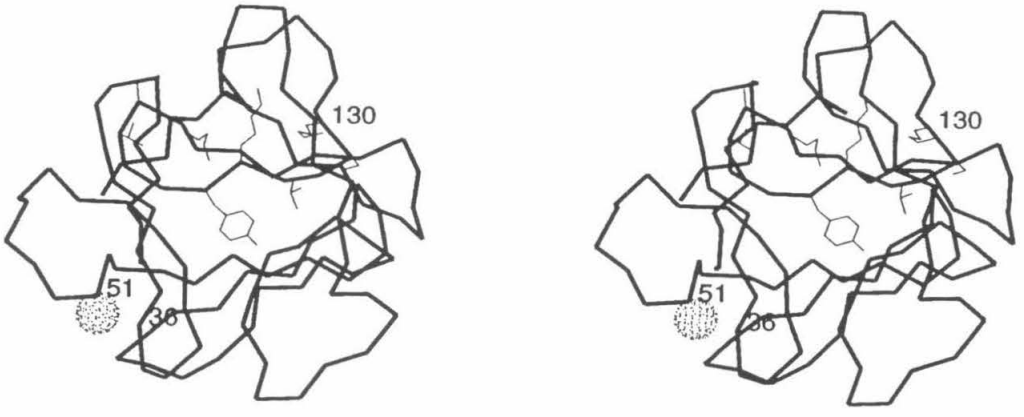

Figure 5.13. Copper (shown with van der Waals surface) and heparin binding sites on bFGF. The side chains of bFGF-(120-130), which are likely to interact with hepairn, are shown with thin lines.

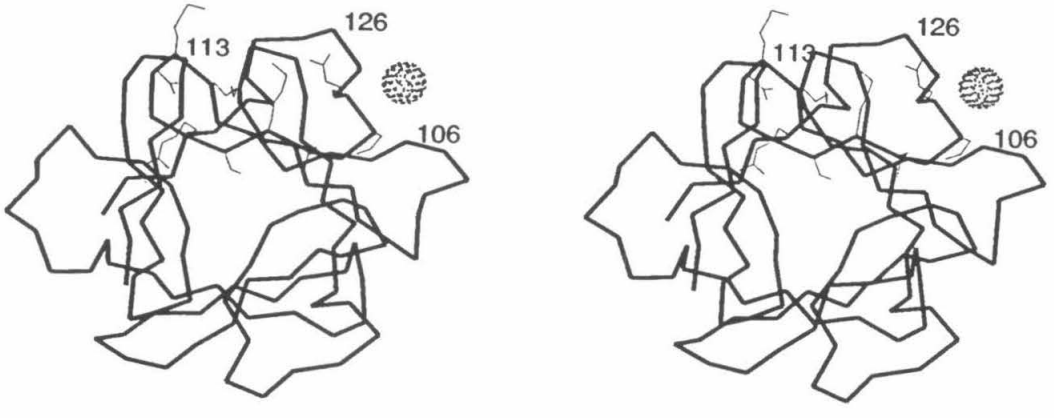

Figure 5.14. Possible copper (shown with van der Waals surface) and heparin binding sites on aFGF. The aFGF backbone has a similar orientation to bFGF shown in Figure 5.13. The side chains of aFGF-(112-122), which are likely to interact with heparin, are shown with thin lines.

References

1. W. H. Burgess and T. Maciag, *Annu. Rev. Biochem.* **58,** 575 (1989).

2. J. Marx, *Science* **249,** 1376 (1990).

3. J. Folkman, S. Szabo, M. Stovroff, P. McNeil, W. Li, Y. Shing, *Annals of Surgery* **214,** 414 (1991).

4. Y. Shing, *J. Biol. Chem.* **263,** 9059 (1988).

5. T. Arakawa, T. P. Horan, L. O. Nahri, D. C. Rees, S. G. Schiffer, P. L. Holst, S. J. Prestrelski, L. B. Tsai, G. M. Fox (submitted).

6. X. Zhu, H. Komiya, A. Chirino, S. Faham, G. M. Fox, T. Arakawa, B. T. Hsu, D. C. Rees, *Science* **251,** 90 (1991).

7. B. L. Sibanda, T. L. Blundell, J. M. Thornton, *J. Mol. Biol.* **206,** 759 (1989).

8. J. S. Richardson, E. D. Getzoff, D. C. Richardson, *Proc. Natl. Acad. Sci. USA* **75,** 2474 (1978).

9. J. S. Richardson and D. C. Richardson, Prediction of Protein Structure and the Principles of Protein Conformation (Plenum Press, New York, 1989).

10. B. L. Sibanda and J. M. Thornton, *Nature* **316,** 170 (1985).

11. J. Jancarik & S. H. Kim *J. Appl. Cryst.* **24,** 409 (1991).

12. J. Zhang, L. S. Cousens, P. J. Barr, S. R. Sprang, *Proc. Natl. Acad. Sci. USA* **88,** 3441 (1991).

13. M. G. Rossmann, *Molecular Replacement Method* (Gordon and Breach, New York, 1972).

14. A program written by Doug C. Rees.

15. D. E. Tronrud, L. F. Ten Eyck, B. W. Mattews, *Acta Cryst.* **A43,** 489 (1987).

16. T. C. Terwilliger and D. Eisenberg, *Acta Cryst.* **A39,** 813 (1983).

17. 10.A. E. Eriksson, L. S. Cousens, L. H. Weaver, B. W. Matthews, *Proc. Natl. Acad. Sci. USA* **88**, 3441 (1991).

18. K. Sakaguchi, M. Yanagishita, Y. Takeuchi, G. D. Aurbach, *J. Biol. Chem.* **266,**

7270 (1991).

19. A. Yayon, M. Klagsbrun, J. D. Esko, P. Leder, D. M. Ornitz, *Cell* **64,** 841 (1991).

20. A. C. Rapraeger, A. Krufka, B. B. Olwin, *Science* **252,** 1705 (1991).

21. A. Yayon and M. Klagsbrun, *Proc. Natl. Acad. Sci. USA* **87**, 5346 (1990).

22. S. J. Leibovich and P. J. Polverini, *J. NCI* **73,** 1337 (1984).

23. M. Nakajima, A. DeChavigny, C. E. Johnson, J. Hamada, C. A. Stein, G. L. Nicolson, *J. Biol. Chem.* **266,** 9661 (1991).

24. L. T. Webster, *Goodman and Gilman's The Pharmacological Basis of Therapeutics* (A. G. Gilman, T. W. Rall, A. S. Nies, & P. Taylor Eds.) 8th ed., pp. 1014-1017, Pergamon, New York.

25. R. J. Coffey, Jr., E. B. Leof, G. D. Shipley, H. L. Moses, *J. Cell. Physiol.* **132,** 143 (1987).

26. S. R. Coughlin, P. J. Barr, L. S. Cousens, L. J. Fretto, L. T. Williams, *J. Biol. Chem.* **263,** 988 (1988).

27. C. R. Middaugh, H. Mach, C. J. Burke, D. B. Volkin, J. M. Dabora, P. K. Tsai, M. W. Bruner, J. A. Ryan, K. E. Marfia, *Biochemistry* **31,** 9016 (1992).

28. A. T. Brunger, *J. Mol. Biol.* **203**, 803 (1988).

29 R. V. La Rocca, C. A. Stein, C. E. Myers, *Cancer Cells* 2, 106 (1990).

30. A. Baird, D. Schubert, N. Ling, R. Guillemin, *Proc. Natl. Acad. Sci. USA* **85,** 2324 (1988).

31. B. R. McAuslan and W. Reilly, *Exp. Cell Res.* **130,** 147 (1980).

32. M. Ziche, J. Jones, P. M. Gullino, *J. Natl. Cancer Inst.* **69,** 475 (1982).

33. H. Alphern-Elran and S. Brem, *Surg. Forum* **36,** 498 (1985).

34. K. S. Raju, G. Alessandri, P. M. Gullino, *Cancer Res.* **44,** 1579 (1984).

35. E. Grushka and A. S. Cohen, *Anal. Lett.* **15,** 1277 (1982).

36. S. S. Stivala, *Fed. Proc.* **36,** 83 (1977).

37. Y. Shing, *J. Biol. Chem.* **263,** 9059 (1988).